

RETURNING MATERIALS:
Place in book drop to remove this checkout from your record. FINES will be charged if book is returned after the date stamped below.

CHAPTER V

INFLUENCES OF SPECIFIC REACTANT-SOLVENT INTERACTIONS ON ELECTRON-TRANSFER KINETICS AND THERMODYNAMICS

A. The Influence of Specific Reactant-Solvent Interactions on

Intrinsic Activation Entropies for Outer-Sphere Electron Transfer

Reactions

(Accepted for publication in J. Phys. Chem.)

1. Introduction

In recent years increasingly detailed and sophisticated theories of outer-sphere electron-transfer kinetics have been formulated. 56

These enable rates and activation parameters to be calculated from reaction thermodynamics together with reactant and solvent structural information. Although treatments of inner-shell (intramolecular reactant) reorganization have reached a high degree of sophistication, 23 the important contribution to the free energy barrier arising from outer-shell (noncoordinated solvent) reorganization is usually treated in terms of the classical dielectric continuum model as originally formulated by Marcus. 13 While comparisons between theory and experiment for bimolecular outer-sphere processes show reasonable agreement in a number of cases, 10 significant and often large

discrepancies still remain (cf. Chapter VII). Among other things, such discrepancies call into question the quantitative validity of the dielectric continuum model, especially in view of the well-known failure of similar treatments to describe the thermodynamics of ion solvation.

In principle, a useful way of monitoring the influence of outershell solvation upon electron-transfer energetics is to evaluate entropic parameters since these are expected to arise chiefly from the changes in the degree of solvent polarization associated with electron transfer. The activation entropy, ΔS^* , as for other reorganization parameters, can usefully be divided into "intrinsic" and "thermodynamic" factors: 245,246

$$\Delta S^* = \Delta S_{int}^* + \alpha \Delta S^0$$
 (5.1)

where the coefficient α is predicted usually to be close to 0.5. 247 The intrinsic activation entropy, ΔS_{int}^* , is that component of ΔS_i^* that remains in the absence of the entropic driving force ΔS_i^0 . When estimating values of ΔS_i^* from Equation 5.1, it is usual to employ experimental values of ΔS_i^0 and yet also employ values of ΔS_{int}^* calculated from dielectric continuum theory. Although these calculated values of ΔS_{int}^* are often small, given that the values of ΔS_i^0 are often much larger and more variable than those calculated from the dielectric continuum model, it is reasonable to inquire if a more trustworthy method for estimating ΔS_{int}^* could be formulated.

A useful and often enlightening approach for understanding electron transfer processes both on a conceptual and an experimental basis is to examine the thermodynamics and kinetics of electrochemical reactions: 53-55,248

$$0x + e^{-}(\phi_m)$$
 Red (1.12)

where ϕ_m is the (Galvani) electrode-solution potential difference. Although absolute values of ϕ_m cannot be evaluated with useful accuracy, the temperature dependence of ϕ_m can be obtained using a nonisothermal cell arrangement. This enables the entropic change induced by reduction of a single redox center, the so-called "reaction entropy" ΔS_{rc}^0 , to be determined from the temperature dependence of the standard (or formal) potential ϕ_m^0 under these conditions. Activation parameters for such electrochemical "half reactions" can be obtained using an analogous procedure. These quantities provide insights into the structural changes accompanying electron transfer at each redox center that remain hidden for homogeneous bimolecular reactions.

The aim of this section is first to provide a simple physical picture, based on electrochemical half-reactions, of the origin of the intrinsic activation entropy in homogeneous and electrochemical redox reactions. With this background a new approach for estimating ΔS_{int}^* will be outlined based on reaction entropy data whereby the effects of specific reactant-solvent interactions can be taken into account. Despite their potential importance, such interactions have yet to be considered even in the more sophisticated theories of electron transfer.

2. Origin of the Intrinsic Activation Entropy

The actual entropic barriers, ΔS_f^* and ΔS_r^* , to electron transfer for the forward (reduction) and reverse (oxidation) electrochemical reactions at a given electrode potential have been termed "ideal" activation entropies. 53,54,248 These can be formulated as

$$\Delta S_f^* = \alpha \Delta S_{rc}^o + \Delta S_{int,e}^*$$
 (5.2a)

$$\Delta S_{r}^{*} = (\alpha - 1) \Delta S_{rc}^{o} + \Delta S_{int,e}^{*}$$
 (5.2b)

where α is the electrochemical transfer coefficient and $\Delta S_{int,e}^*$ is the so-called "real" (or intrinsic) electrochemical activation entropy, i.e. that which remains after accounting for the entropic driving force. For convenience, we shall assume that the interactions between the reactant and electrode, and between the reactant pair in homogeneous solution, are weak and nonspecific (i.e. the "weak interaction" limit). Under these circumstances $\Delta S_{int,e}^*$ is related to the intrinsic activation entropy for the corresponding self-exchange reaction by

$$\Delta S_{int}^{*} = 2\Delta S_{int,e}^{*}$$
 (5.3)

Relationships such as Equation 5.3 reflect the fact that homogeneous outer-sphere reactions can be regarded as coupled reductive and oxidative electrochemical reactions.

Equations 5.2a and 5.2b point to a key difference between homogeneous self-exchange and electrochemical exchange reactions: the latter are characterized by a net entropy driving force ΔS_{rc}^0 even when the free energy driving force is zero. This results from the inherent chemical asymmetry of the electrochemical half reactions. This entropy driving force contributes to the forward or reverse entropic barrier for each redox center to an extent determined by the difference in (hypothetical) charge between the oxidized or reduced reactant and the transition state, namely α or $(\alpha-1)$. The transition state of course never acquires a fractional charge since electron transfer occurs approximately independently of nuclear motion, but nonetheless is characterized by a polarized solvent environment appropriate to a molecule possessing such a charge. $^{13}, ^{56}$

According to the theoretical approach of Marcus, 13 solvent reorganization to form the transition state can be viewed as occurring by a hypothetical two-step process. First the charge of the reactant is slowly adjusted to a fractional charge approximately midway between the reactant and product charges, with attendant reorientation of the surrounding solvent. 250,251 Then in a rapid step (much faster than solvent motion) the transition-state charge is reset to that of the reactant. Taken together, the energies of the two steps are equivalent to the nonequilibrium solvent polarization energy. On the basis of the conventional dielectric continuum approach, the energetics of the first step are determined by the static solvent dielectric constant ε_{g} , while the optical (i.e. infinite frequency) dielectric constant ε_{g} , determines the energy of the fast second step. We shall term these two

steps the "static" and "optical" components, respectively. Generally the optical component is anticipated to provide the dominant contribution to the free energy of solvent reorganization due to the relative magnitudes of $\epsilon_{\rm op}$ and $\epsilon_{\rm s}$. However, the temperature coefficients of the two dielectric constants are such that in many solvents the optical and static components are calculated to contribute roughly equally to the entropic component of the solvent barrier.

The conventional calculation of the solvent reorganization energetics involves an application of the Born ion-solvation model to transition state theory. $^{250.251}$ The Born model predicts that entropies of ions will vary with the square of the charge number. 252 It is reasonable to suppose that the static component of the electrochemical transition-state entropy will also depend on the square of the effective charge. The differences in static entropy between the transition and ground states should be appropriately weighted fractions of the total entropy difference ΔS_{rc}^{0} between the two ground redox states. We can therefore express the static components of the forward and reverse electrochemical activation entropies as

$$\Delta S_{f}^{*}(static) = \{[(n+1)^{2} - (n+1-\alpha)^{2}]/[(n+1)^{2} - n^{2}]\} \Delta S_{rc}^{o}$$
 (5.4a)

$$\Delta S_{r}^{*}(static) = \{ [n^{2} - (n + 1 - \alpha)^{2}] / [(n + 1)^{2} - n^{2}] \} \Delta S_{rc}^{o}$$
 (5.4b)

where n and n+1 are the charge numbers of the two forms of the redox couple, and $(n+1-\alpha)$ is the effective transition-state charge.

It can be seen from Equations 5.4a and 5.4b that even for a transition state that is symmetrical with respect to charge, i.e. α = 0.5, that ΔS_f^* (static) will differ from $-\Delta S_r^*$ (static). In other words, the transition state will not lie midway in terms of entropy between the reduced and oxidized states even though it may be equally accessible in terms of free energy from either oxidation state. This mismatch of the energetics of the forward and reverse half reactions follows from the <u>linear</u> variation of driving force contributions with charge (Equation 5.2), coupled with the <u>quadratic</u> dependence of static entropy on charge.

Equations 5.2a and 5.2b can be combined to yield

$$\Delta S_{int,e}^{\star} = (1-\alpha)\Delta S_{f}^{\star} + \alpha \Delta S_{r}^{\star}$$
 (5.5)

The intrinsic activation entropy therefore is a measure of the extent of the mismatch between forward and reverse half-reaction entropic barriers after normalizing for driving force contributions. This is seen most clearly when α = 0.5 and the driving force components of ΔS_f^* and ΔS_f^* exactly cancel. The connections between the various entropic quantities are illustrated schematically in Figure 5.1. The magnitude of ΔS_{int}^* is given by the vertical displacement of the curve AB from the chord (dashed line) to this curve. The curve AB describes the dependence of ΔS_{int}^* upon the effective ionic charge.

Equations 5.4a and 5.4b can be combined with Equation 5.5 to yield an expression for the static component of $\Delta S_{int.e}^{*}$:

$$\Delta S_{int,e}^{*}(static) = [\alpha(1-\alpha)/(2n+1)]\Delta S_{rc}^{0}$$
 (5.6)

Taking α = 0.5 and inserting the Bornian expression for the reaction entropy: ²⁵³

$$\Delta S_{rc}^{o} = (Ne^{2}/2r\varepsilon_{s}^{2})(d\varepsilon_{s}/dT) [(n+1)^{2}-n^{2}]$$
 (5.7)

into Equation 5.6 yields:

$$\Delta S_{\text{int,e}}^{*}(\text{static}) = -(Ne^{2}/8r\varepsilon_{s}^{2}) (d\varepsilon_{s}/dT)$$
 (5.8)

where N is the Avogadro number, e is the electronic charge, and r is the reactant radius. Note that the apparent dependence of ΔS^* int, e (static) on reactant charge in Equation 5.6 has now been eliminated.

Equation 5.7 can be compared with the relation obtained from the temperature derivative of the usual dielectric continuum expression for the reorganization free energy: 13,54

$$\Delta S_{int,e}^{*} = [(Ne^{2}/8)(1/r-1/R)][(1/\epsilon_{op}^{2})(d\epsilon_{op}/dT)-(1/\epsilon_{s}^{2})(d\epsilon_{s}/dT)]$$
 (5.9)

Equations 5.8 and 5.9 differ in that the latter takes account of image stabilization of the ion in the vicinity of the electrode by including the ion-image separation distance R; furthermore, the optical portion of the activation entropy is included. This term is similar in form to the static term since it is assumed, based on a linear response of solvent polarization to the field of the ion, that the optical portion

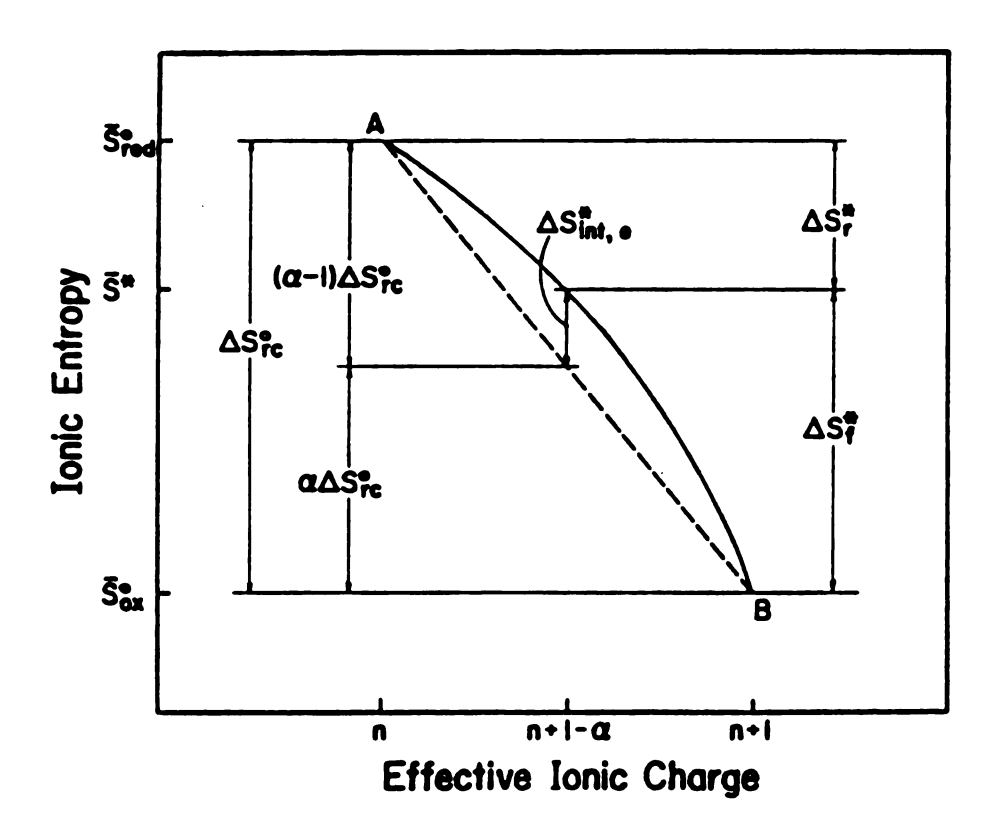


Figure 5.1. Schematic representation of the ionic entropy of an individual redox center as a function of its effective ionic charge during the electron transfer step. See text for details.

of $\Delta S_{\mbox{int,e}}^{\mbox{*}}$ also varies with the square of the effective charge of the transition state. 56b

Similarly. from Equations 5.3 and 5.6 the static portion of the intrinsic entropy for homogeneous self-exchange reactions can be expressed as

$$\Delta S_{int}^{\star}(static) = [2\alpha(1-\alpha)/(2n+1)] \Delta S_{rc}^{o}$$
 (5.10)

Again, for $\alpha = 0.5$ and on the basis of the Bornian model (Equation 5.7), this leads to

$$\Delta S_{int}^{*}(static) = (Ne^{2}/4r\varepsilon_{g}^{2}) (d\varepsilon_{g}/dT)]$$
 (5.11)

This is identical in form to the dielectric continuum expression for ΔS_{int}^{*} (cf. Equation 5.9):

$$\Delta S_{int}^{\star} = (Ne^2/4) \left(\frac{1}{r} - \frac{1}{R}\right) \left[(1/\epsilon_{op}^2) \left(d\epsilon_{op}/dT\right) - (1/\epsilon_{s}^2) \left(d\epsilon_{s}/dT\right) \right]$$
 (5.12)

allowing again for the addition of the optical term and the presence of the nearby coreactant through the internuclear distance term R.

3. Real Chemical Environments. Incorporating Specific

Reactant-Solvent Interactions in Activation Entropy Calculations.

In general, the experimental values of $^{\Delta}S^{o}_{rc}$ differ widely from the continuum predictions of Equation 5.7. In water, for example $^{\Delta}S^{o}_{rc}$ for the $\text{Cr}(\text{H}_2\text{O})^{3+/2+}_6$ couple is seven times greater than predicted,

while the experimental value of ΔS_{rc}^{o} for Fe(bpy) $_{3}^{3+/2+}$ is less than a third of the theoretical value. Furthermore, the expected variation of reaction entropies with solvent dielectric properties is not observed. $^{253-255}$ The discrepancies between theory and experiment have variously been attributed to dielectric saturation, hydrogen bonding between reactants and solvent, 55 long range solvent structuring, $^{253-256}$ and hydrophobic interactions. 257 Consequently, in view of Equation 5.10 dielectric continuum theories of solvent reorganization are not expected to provide accurate estimates of intrinsic activation entropies.

Nevertheless Equation 5.10 suggests a means of incorporating the numerous factors neglected in the dielectric continuum treatments. Rather than employing estimates of ΔS_{rc}^{O} based on Equation 5.8, experimental values of ΔS_{rc}^{O} can be used to determine the static component of ΔS_{int}^{\bullet} . Therefore instead of Equation 5.12 the intrinsic activation entropy can be expressed as

$$\Delta S_{int}^{*} = (Ne^{2}/4) \left(\frac{1}{r} - \frac{1}{R}\right) \left[(1/\epsilon_{op}^{2}) \left(d\epsilon_{op}/dT\right) \right] + \Delta S_{rc}^{o}/(4n + 2)$$
 (5.13)

The optical component of ΔS_{int}^{\star} , the first term on the r.h.s. of Equation 5.13, is unchanged from Equation 5.14; however the static component embodied in the second term is taken instead from Equation 5.10 with $\alpha = 0.5$ (As expected, α is commonly observed to be close to 0.5 for outer-sphere electrochemical reactions). Equation 5.13 is therefore anticipated to yield more reliable values of ΔS_{int}^{\star} , at least in the weak-interaction limit, since it circumvents the known severe

limitations of the Born model for calculating static entropies.

The latter model is retained for estimating the optical component in lieu of any direct experimental information to the contrary. The justification for this approach is that the Born model is likely to be much more reliable for estimating the optical rather than the static component in view of the relative insensitivity of $\epsilon_{\rm op}$ to solvent structure. Thus the extensive local perturbations in solvent structure induced around an ionic solute that are responsible for the failure of the dielectric continuum model for predicting ionic solvation thermodynamics should have a much smaller influence on the intramolecular electronic perturbations which constitute the optical component of the reorganization barrier.

A comparison between values of ΔS_{int}^* calculated from Equations 5.12 and 5.13 for some representative redox couples in aqueous media is presented in Table 5.1. Whereas the dielectric continuum model (Equation 5.12) predicts that ΔS_{int}^* will be small and nearly independent of the chemical nature of the redox couple, somewhat larger and more varying values of ΔS_{int}^* are predicted by Equation 5.13 since this takes into account specific reactant-solvent interactions via inclusion of the experimental values of ΔS_{rc}^0 . Further, the latter relation predicts markedly larger variations in ΔS_{int}^* with solvent than obtained with the former relation, resulting from the much greater sensitivity of ΔS_{rc}^0 to the solvent than predicted by the Born model. 253-255

Although the differences between Equations 5.12 and 5.13 have been emphasized here, it should be noted that the ΔS_{int}^{\star} values obtained by the latter are still relatively small. An interesting result is

that for multicharged reactants very large thermodynamic solvation effects translate to much smaller intrinsic entropic barriers. For example, the $\mathrm{Fe(H_20)}_6^{3+/2+}$ self-exchange reaction involves thermodynamic entropy changes amounting to 360 J deg^{-1} mol⁻¹ (180 J deg^{-1} mol⁻¹ for each half reaction) which yields an entropic contribution of just 13 J deg^{-1} mol⁻¹ to the Franck-Condon barrier (Table 5.1). Still, the effects are large enough to warrant consideration. For example, for the $\mathrm{Fe(H_20)}_6^{3+/2+}$ reaction $\Delta \mathrm{S}_{\mathrm{int}}^*$ should contribute a factor of five to the self-exchange rate constant at room temperature. This effect is therefore comparable in magnitude to the nuclear tunneling corrections and nonadiabatic electron tunneling factors which have been emphasized in the recent literature. 23,258

4. Comparisons with Experiment

In addition to the calculated values of ΔS_{int}^{\star} , some "experimental" values for these homogeneous self-exchange reactions, $\Delta S_{int}^{\star}(exp)$, are given in Table 5.1. The latter were extracted from the measured activation enthalpies, ΔH^{\star} , and the rate constants, k, using

$$k = K_{p} \Gamma_{n} \nu_{n} \exp(\Delta S_{int}^{*}/R) \exp(-\Delta H^{*}/RT)$$
 (5.14)

where K_p is the equilibrium constant for forming the precursor complex immediately prior to the electron-transfer step, Γ_n is the nuclear tunneling factor, and ν_n is the nuclear frequency factor. 9,23,258 [Note that the activation entropy in Equation 5.14 can be directly identified with ΔS_{int}^{\star} since $\Delta S^{\circ}=0$ for self-exchange reactions

(Equation 5.1)]. The values of K_p and Γ_n were calculated as described in Chapter VII and reference 10. The values of $\Delta S_{int}^*(exp)$ were corrected for the variation of Γ_n with temperature by calculating this quantity using the relationships given in reference 23.

It is seen in Table 5.1 that the values of $\Delta S_{int}^{*}(exp)$ are uniformly smaller, i.e. more negative, than the estimates of ΔS_{int}^* from both Equation 5.12 and Equation 5.13. Such negative values of ΔS_{int}^{*} (exp) are commonly observed for homogeneous outer-sphere reactions. They have been variously attributed to an unfavorable contribution to the precursor work term arising from reactant-solvent interactions, to the occurrence of nonadiabatic pathways, and to steric factors. 17,207 In any case, in view of the present discussion it appears likely that these negative values of ΔS_{int}^* reflect properties of the bimolecular precursor complex rather than those of the individual redox couples; i.e. reflect the modification of the solvation environment around each redox center brought about by its proximity to the coreactant necessary for electron transfer. In fact, the inclusion of specific reactant-solvent interactions in the calculation of $\Delta S_{ ext{int}}^{\star}$ for the weak interaction limit by employing Equation 5.13 rather than Equation 5.12 leads in most cases to more positive values of ΔS_{int}^{*} (Table 5.1).

Before accepting this conclusion, however, it is worth examining further the various assumptions embedded in Equation 5.13. Given the breakdowns observed thus far in the Born solvation model, it is possible that the assumed quadratic variation of entropy with charge is also incorrect. The magnitude of the intrinsic activation entropy

Table 5.1. Intrinsic Activation Entropies for Selected Homogeneous Self-Exchange Reactions, ΔS_{int}^* (J deg⁻¹ mol⁻¹), calculated without (Equation 5.12) and with (Equation 5.13) Consideration of Specific Reactant-Solvent Interactions, and Comparison with Experiment.

Redox Couple	Solvent '	a r,\$,	b A Sint Equation 5.12	ο Δ S [*] int Equation 5.13	d AS [‡] int (experi me nt)
Fe(OH ₂) ₆ ^{3+/2+}	H ₂ 0	3.3	-1.5	13	-62
V(OH ₂) ^{3+/2+}	u ₂ 0	3.3	-1.5	12.5	-61
Ru (NH ₃) 6	H ₂ 0	3.3	-1.5	2.5	-24 ^e
Co (en)3+/2+5	н ₂ 0	4.2	-1.5	9.5	-45
Ru(bpy) 3+/2+ ^g	H ₂ 0	6.7	-1.0	-4.5	
ferricinium- ferrocene	H ₂ 0	3.8	-1.5	-15	-
ferricinium- ferrocene	methanol	3.8	-6.5	-9.5	-44
ferricinium- ferrocene	nitromethane	3.8	6.0	16	-29

 $a_{\rm Reactant}$ radius, used to calculate $\Delta S_{\rm int}^{*}$ (Equation 5.12). Values taken from references 10 and 255.

Intrinsic activation entropy, calculated from Equation 5.12 using the listed values of r and assuming that R =2r (Reference #182). Literature values of ε , (d ε /dT), ε , (d ε /dT): water - ε =78.3, (d ε /dT)=-0.365, ε =1.78, (d ε /dT)=-0.00024 (values from reference 165, pp. E61, E224); methanol- ε =32.6, (d ε /dT)=-0.20 (references 263); ε =1.76, (d ε /dT)=-0.0011 (reference 264, p. 145); nitromethane= ε =35.5, (d ε /dT)=-0.16 (reference 265); ε op=1.90, (d ε /op/dT)=-0.0010 (reference 264, p. 391).

Intrinsic activation entropy, calculated similarly to footnote b above, using the experimental values of ΔS_{rc}^{0} taken from references 55 and 255.

 $d_{\rm Values}$ extracted from published rate data by using Equation 5.14 and correcting for nuclear tunneling effects. Values of K $_{\rm V}$ are circa. 3 x 10 12 M 1 S $^{-1}$ (see reference 10 and Chapter VII). Literature sources for rate data: Fe(H₂0) $_{\rm 6}^{3+/2+}$ - reference 266, V(H₂0) $_{\rm 3}^{3+/2+}$ - reference 267, Ru(NH₃) $_{\rm 3}^{3+/2+}$ - reference 268, Co(en) $_{\rm 3}^{3+/2+}$ - reference 269, ferricinium/ferrocene-reference 270.

^eBrown and Sutin (reference 28) have questioned the accuracy of this result, based on the more negative ΔS^* value for the Ru(en₃²⁺ - Ru(NH₃)²⁺ cross reaction.

fen = ethylenediammine

gbpy=2,2'-bipyridine

obtained from Equations 5.13 is closely connected to the functional dependence of entropy on charge. For example a linear dependence leads to a value of zero for ΔS_{int}^* . Other functions might lead to large imbalances of forward and reverse entropic barriers and therefore substantial intrinsic activation entropies. Since most couples exhibit positive values of ΔS_{rc}^0 a fractional dependence of entropy on charge would normally be required to deduce negative values of ΔS_{int}^* . The entropy-charge relation was the subject of a number of detailed examinations and some controversy in previous years, and apparently was never unambiguously resolved. 259-261 One reason for this was the difficulty of varying the ionic charge while holding constant the other relevant parameters such as ionic size, ligand composition, coordination number, etc.

In order to determine the relation between entropy and charge for a prototype system we examined the reaction entropies of ruthenium tris bipyridine, for which oxidation states 0, I, II, and III are accessible in acetonitrile. The experimental details are given in reference 253. By employing the same compound in various oxidation states the numerous complications and ambiguities inevitably involved in previous studies are avoided. The reaction entropies thus obtained for the $\operatorname{Ru}(\operatorname{bpy})_3^{3+/2+}$, $\operatorname{Ru}(\operatorname{bpy})_3^{2+/+}$, and $\operatorname{Ru}(\operatorname{bpy})_3^{+/0}$ couples, respectively, in acetonitrile (containing $0.1\ \underline{\mathrm{M}}\ \mathrm{KPF}_6$ supporting electrolyte) are 117, 71 and 23 J deg⁻¹ mol⁻¹. If these data are recast as relative single ion entropies, S⁰ + K, where K is an unknown constant quantity, a straightforward variation of entropy with the square of ionic charge is evident (Figure 5.2), supporting the validity of Equation 5.13.

It is possible of course that the ruthenium trisbipyridine reactions represent an atypical case. (However, additional evidence is assembled in Section V. C). Another way of exploring the possibility that the negative experimental values of ΔS_{int}^* might arise in part from mismatches in the thermodynamic entropic changes occurring in each half reaction is to examine if the magnitude of ΔS_{int}^* depends on the sum of the constituent ΔS_{rc}^{0} values. The larger these entropy changes, the larger should be the mismatch in ΔS_f^* and ΔS_r^* for each half reaction, yielding larger (or more negative) values of ΔS_{int}^* . However, such an examination for about thirty self-exchange and cross reactions shows no signs of such a systematic trend. (Details are given in Chapter VII). In addition, the experimental values of ΔS_{int}^* also show no discernable dependence on the magnitude of the reorganization barrier, comparable negative values of ΔS_{int}^* being obtained even for extremely rapid reactions. 207 This provides evidence that these negative values are associated either with an entropically unfavorable work term and/or nonadiabaticity, rather than residing in the elementary reorganization barrier to electron transfer of which the estimates of ΔS_{int}^* obtained from Equation 5.13 form a part.

Nevertheless, the method of calculating ΔS_{int}^* embodied in Equation 5.13 is considered to be useful since it provides a reliable estimate of ΔS_{int}^* for the limiting "weak interaction" case where the solvating environments of the two reactants do not modify each other, while accounting properly for the influence of the actual reactant-solvent interactions upon the entropic reorganization barrier for these isolated redox environments. It therefore provides a more trustworthy

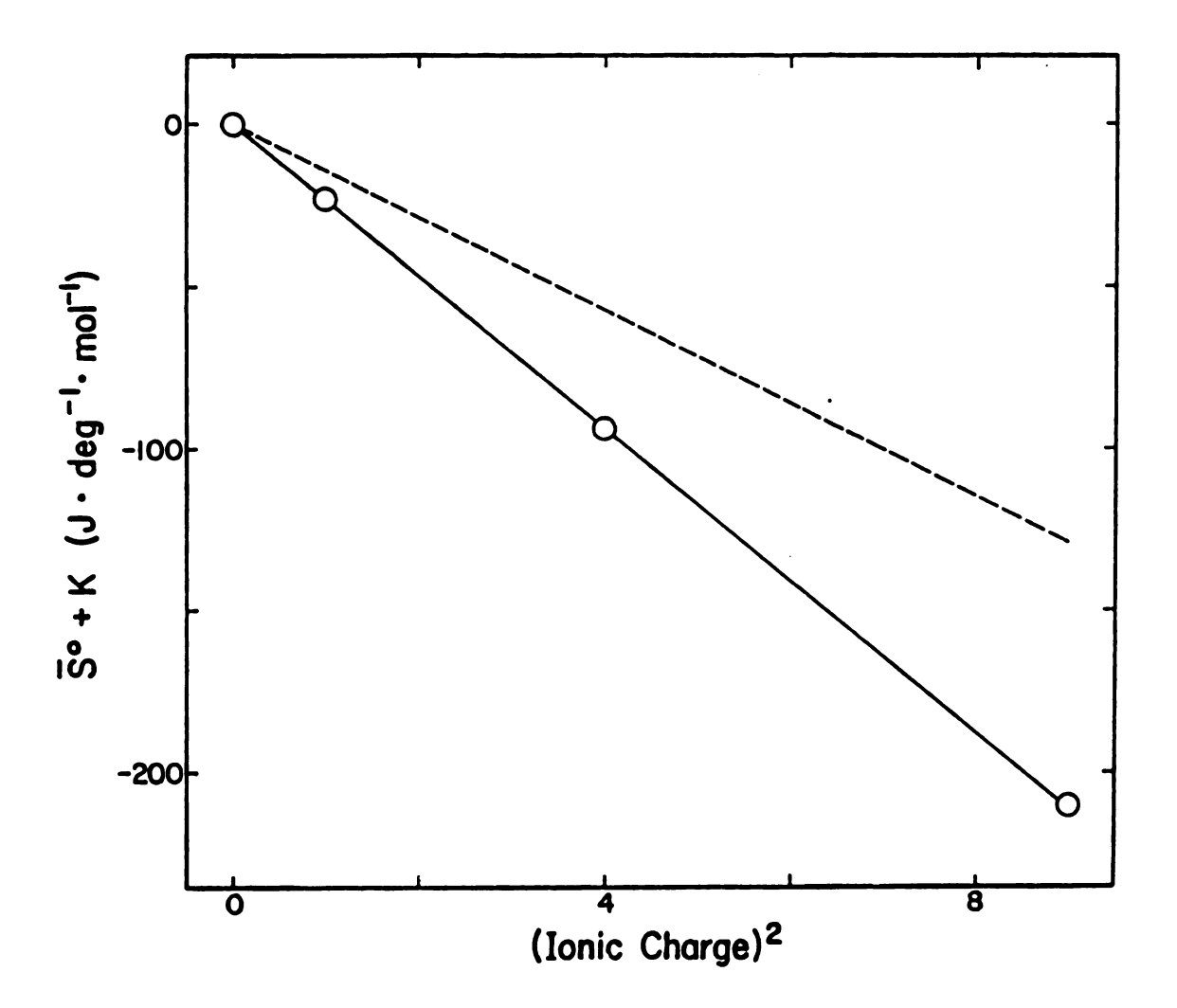


Figure 5.2. Plot of relative ionic entropy of $Ru(bpy)_3^n$ (bpy=2,2'-bipyridine) in acetonitrile as a function of the square of the ionic charge n. The solid line is the best fit line through the experimental points; the dashed line is the slope of this plot predicted by the Born model.

means of gauging the extent of influence of reactant-reactant interactions upon the activation entropy than is obtained by employing the conventional relationship (Equation 5.12), as well as supplying useful insight into the physical and chemical factors that determine this quantity.

A related approach to that described here can also be employed to estimate the effects of isolated reactant-solvent hydrogen bonding on the intrinsic enthalpic component of the Franck-Condon barrier. This involves examining the solvent dependence of the half-cell redox thermodynamics. Preliminary results indicate that such enthalpic effects are markedly larger than the corresponding entropic factors examined here, contributing several kJ mol⁻¹ to the intrinsic free energy barriers for a number of reactions. These findings suggest that such specific reactant-solvent interactions may indeed account in part for the common observation that the experimental rate constants for homogeneous outer-sphere reactions are significantly smaller than the theoretical predictions where the outer-shell reorganization energy is calculated using the conventional dielectric continuum model. 10

B. Utility of Surface Reaction Entropies for Examining

Reactant-Solvent Interactions at Electrochemical Interfaces.

Ferricinium-Ferrocene Attached to Platinum Electrodes

(Accepted for publication in J. Electrochem. Soc.)

1. Introduction

Reactant-solvent interactions are of prime importance to both the kinetics and thermodynamics of electrode processes. Since electro-

chemical reactions inevitably occur within the interfacial region, it is desirable to gain information on the nature of reactant solvation at the electrode surface as well as in bulk solution. Weaver, et al. have demonstrated that useful information on the latter for simple redox couples can be obtained from the so-called "reaction entropy", ΔS_{rc}^{o} , determined from the temperature dependence of the formal potential, E^{f} , using a nonisothermal cell arrangement: 55

$$\Delta S_{rc}^{0} = F(dE^{f}/dT)_{ni}$$
 (1.21)

Since the temperature dependence of the thermal liquid junction potential in such a cell can be arranged to be negligibly small, ΔS_{rc}^{0} essentially equals the difference, $(S_{red}^{0} - S_{ox}^{0})$, between the ionic entropies of the reduced and oxidized forms of the redox couple in the bulk solution. The reaction entropies of simple transition-metal redox couples have been found to be extremely sensitive to the chemical nature of the coordinated ligands and the surrounding solvent, illustrating the importance of specific ligand-solvent interactions to the overall redox thermodynamics. 55,84,253-255

It would clearly be desirable additionally to determine reaction entropies for redox couples residing in the interfacial region. Such "surface reaction entropies", $\Delta S_{rc,s}^{O}$ would yield insight into the solvation changes accompanying the elementary electron-transfer step for the redox couple in a particular interfacial environment. For redox couples present at sufficiently high concentrations at the interface to enable the formal potential for the interfacial (adsorbed)

redox couple, E_a^f , to be measured, values of $\Delta S_{rc,s}^o$ can be obtained directly from (cf. Equation 1.21):

$$\Delta S_{rc,s}^{o} = F(dE_{a}^{f}/dT)_{ni}$$
 (5.15)

Whereas ΔS_{rc}^{o} corresponds to the overall entropy driving force for transforming the <u>bulk-solution</u> reactant to product, $\Delta S_{rc,s}^{o}$ equals the thermodynamic entropy change for the heterogeneous electron-transfer step itself. Thus $\Delta S_{rc,s}^{o}$ and ΔS_{rc}^{o} are related by

$$\Delta S_{rc,s}^{o} = \Delta S_{rc}^{o} + \Delta S_{p}^{o} - \Delta S_{s}^{o}$$
 (5.16)

where ΔS_p^o and ΔS_s^o are the entropic work terms associated with forming the "precursor" state for electron transfer from the bulk reactant, and the "successor" state from the bulk product, respectively. We report here values of $\Delta S_{rc,s}^o$ for a surface-attached ferricinium-ferrocene couple in several solvents in order to illustrate the virtues of such measurements for elucidating the nature of reactant-solvent interactions at electrochemical interfaces.

For surface redox couples where the redox center lies within the inner layer, ΔS_p^0 and ΔS_s^0 are expected to be both nonzero and different, so that $\Delta S_{rc,s}^0 \neq \Delta S_{rc}^0$. Indeed we have recently obtained such a result for a specifically adsorbd Co(III)/(II) sepulchrate couple versus the corresponding bulk solution couple. For electrode reactions where the redox center is present in the diffuse layer or at the outer Helmholtz plane, it is conventional to assume that the work terms are

purely coulombic in nature 272 so that $\Delta S_p^o \Delta S_s^o = 0$ and hence $\Delta S_{rc,s}^o \Delta S_{rc}^o$. This assumption is required in order to extract true frequency factors for electron transfer from the temperature dependence of electrochemical kinetics. 53,54,186 However, in actuality even $\Delta S_{rc,s}^o$ for an outer-sphere reaction might be expected to differ significantly from ΔS_{rc}^o in a given solvent medium, bearing in mind the structure sensitivity of ionic entropies and the possibility that the solvating environment in the vicinity of the surface may differ significantly from that in the bulk solution. Indeed, one reason for pursuing the present study was to discover whether differences which recently have been observed between the energetics of structurally similar electrochemical reactions involving surface-bound and solution-phase redox couples 204 could be rationalized in terms of differences between the bulk and interfacial solvation environments.

2. Measurement of Surface Reaction Entropies

Although it is not feasible to evaluate $\Delta S_{rc,s}^{o}$ for outer-sphere (i.e. unadsorbed) redox couples, a suitably high interfacial concentration of normally unadsorbed, and presumably fully solvated, reactant can be achieved by attaching the redox center to the electrode surface via an inert covalent linkage. As a model system, we studied the ferricinium-ferrocene redox couple attached to a platinum electrode as shown in Figure 5.3. The surface-bound ferrocene was prepared by using the chemical modification procedure described in reference 70. This system was selected since both the bond to the platinum surface and the electroactive center itself are exceptionally stable, placing the redox

center about 6-8 Å from the electrode surface. In addition it was anticipated that the surface-attached couple would exhibit reversible behavior in a variety of solvents.

Efforts to prepare the same ferrocene derivative in solution were unsuccessful. Nevertheless, n-ferrocenemethylene-p-toluidine (Alfred Bader Chemicals), shown in Figure 5.4, was selected as a reasonably close analog of the surface-attached complex since in the vicinity of the redox center the structures of the two substituents are closely similar. Formal potentials for either the surface-attached or bulksolution redox couples were obtained from the average peak potentials of the cyclic voltammograms. (Quasi-reversible, rather than reversible, behavior was typically observed for the surface-attached, as well as bulk-solution, couples, with anodic-cathodic peak separations up to ca 50 mV even in the presence of iR compensation; cf. reference 70). Values of $E_{\mathbf{g}}^{\mathbf{f}}$ for the reduction of the surface-bound ferricinium derivative could be measured with sufficient accuracy to enable $\Delta S_{rc.s}^{O}$ to be determined to within about 6 J. deg 1 mol 1. Representative E data obtained in aqueous solution are plotted against temperature in Figure 5.5. Data also were obtained in methanol, acetonitrile, dimethylsulfoxide and sulfolane. Attempts were made to measure $\Delta S_{rc.s}^{o}$ in formamide, nitromethane and acetone, but were unsuccessful with the first solvent due to instability of the surface complex and with the other two because of irreproducible behavior. Either 0.1 M tetraethylammoium perchlorate or 0.2 $\underline{\text{M}}$ LiClO₄ was used as the supporting electrolyte.

Figure 5.3. Mode of attachment of ferrocene to platinum surface.

$$C = N - CH_3$$

Figure 5.4. Ferrocene derivative (n-ferrocenemethylene-p-toluidine) used as a solution analog of surface-attached ferrocene in Figure 5.3.

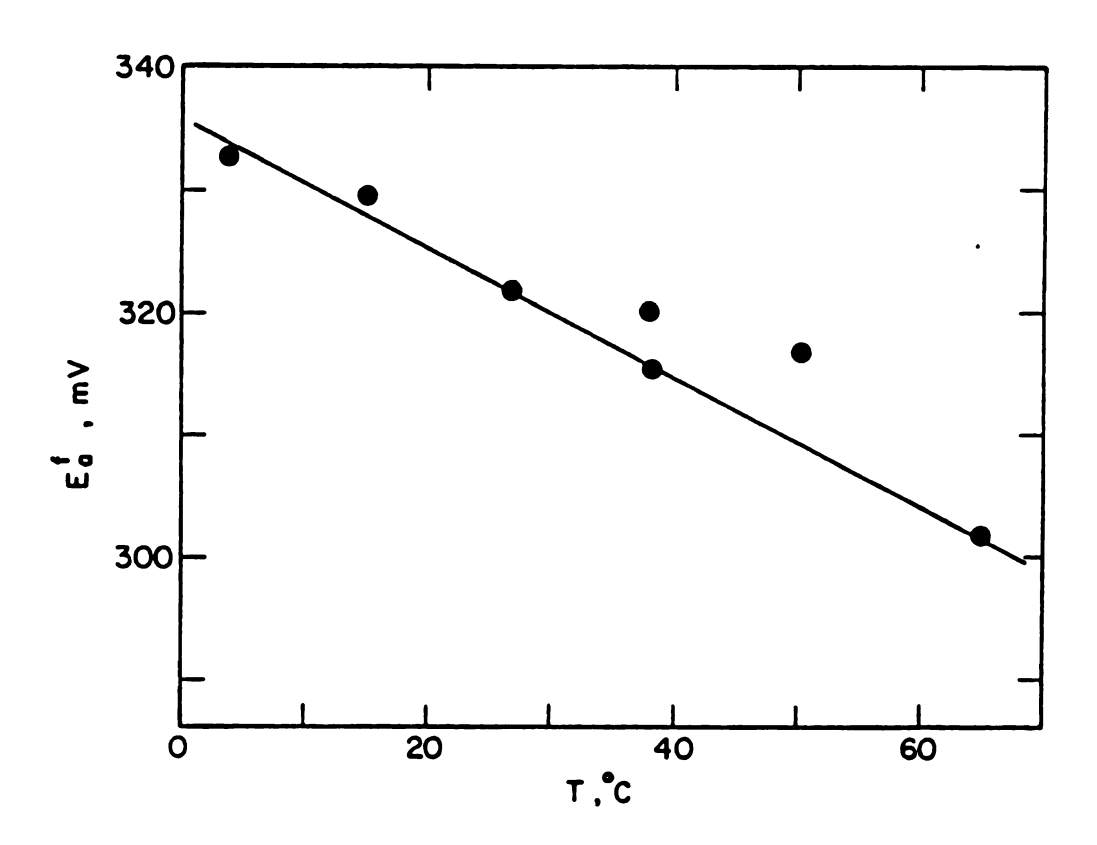


Figure 5.5. Representative plot of formal potential for surface-attached ferricinium-ferrocene couple, E_a^f , versus temperature in aqueous 0.1 M TEAP. Potentials versus saturated calomel electrode at 24 C, using nonisothermal cell arrangement.

The resulting values of $\Delta S_{rc,s}^{O}$ and E_a^f are summarized in Table 5.2. together with ΔS_{rc}^{O} data for the ferrocene and n-ferrocenemethylene-p-toluidine couples in bulk solution. Contrary to our initial expectations, the reaction entropies for the surface couple and its solution analog were found to be in reasonable agreement in each solvent. Evidently the solvent interactions experienced by the surface-attached couple are not noticeably different from the reactant-solvent interactions occurring in bulk solution. At least for this couple, therefore, it appears that differences between solvent structure in bulk solution and in the double layer where the surface redox site is located do not greatly influence the electron-transfer energetics.

3. Interpretation of Surface Reaction Entropy Values

Although the two derivatized ferrocene couples (Figures 5.3 and 5.4) yield similar reaction entropies, these tend to be less positive than the ${}^{AS}_{rc}^{O}$ values for the unsubstituted ferricinium-ferrocene couple (Table 5.2). Furthermore, the formal potentials for the surface-attached couple in various solvents are positive of those for ferrocene itself, while the E^f values for the n-ferrocenemethylene-p-toluidine couple are still more positive (Table 5.2; note that the E^f values quoted are versus that for ferrocene itself in the same solvent). The differences in formal potentials between ferrocene and its derivatives are probably manifestations of the greater electron-withdrawing capabilities of carbon-nitrogen double bonds compared to hydrogen. 273 Thus such an electron-withdrawing substituent would tend to stabilize

Formal Potentials (mV) and Reaction Entropies (J. $\deg^{-1} ext{mol}^{-1}$) for Surface-Attached and Bulk-Solution Ferricinium-Ferrocene Couples Table 5.2.

		surface-attached ferrocene	ached	n-ferrocenemethylene- p-toluidine	lene-	ferrocene	•
Solvent	$^{ m \Delta T}_{ m bp}^{lpha}$	ΔS ^O rc, s	T a	ΔS ^O rc	F F	ΔS ^O rc	(AS' rc, s) Born
Water	174	-50	201	ø	w	-21	10.59
Methanol	117	- 1	48	-12	172	13	27 h
Dimethylsulfoxide 135	le 135	13	122	مه	~180	52	$\frac{i}{14}$
Sulfolane	1	25	74	33	140	31	$\frac{14}{j}$
Acetonitrile	105	25	92	25	146	87	20.5 ¹
Acetone	62	1	1	54	225	29	40 k

at $25^{\rm o}{\rm C}$, except for sulfolane at $30^{\rm o}{\rm C}$. Supporting electrolyte was 0.1 M tetraethylammonium perchlorate; 0.2 M LiClO, used in dimethylsulfoxide. From reference 255. $^{d}\Delta {\rm S}^{\rm o}$ at 25° predicted from the Born model; calculated from Equation 5.17 using dielectric congrant data $^{\rm rc}$,8 from lightanture indicated. b Formal potential versus solution ferrocene/ferricinium couple in the same medium J Irreproducibility of ${f E}^{f I}$ prevented accurate gReference 165, p. E61. Measurements precluded due to insolubility of complex. Jirreproduct determination of ASO. Literature sources for dielectric constants: heference 263. 'Reference 278. JReference 279. Reference 280. a From reference 276.

the relatively electron-rich ferrocene redox center to a greater extent than for ferricinium, leaving the former more difficult to oxidize and thereby yielding a positive shift in the formal potential. The systematic differences in reaction entropies seen between ferrocene and the derivatized couples can also be rationalized on this basis. Whether the differences in formal potentials between the adsorbed couple and its solution analog result from surface attachment or from differences in substitutent properties is not entirely clear.

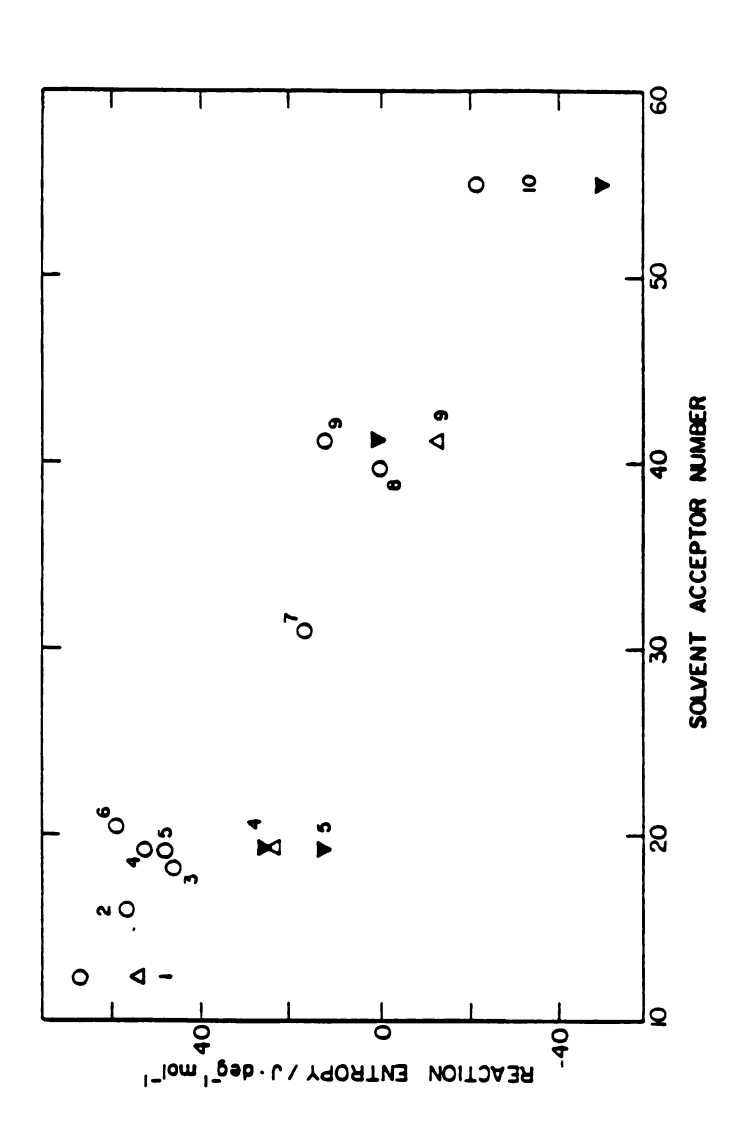
A curious aspect of the results is the marked solvent dependence of both the $\Delta S_{rc,s}^{o}$ and ΔS_{rc}^{o} values. The magnitude of these quantities expected from purely continuum electrostatic considerations is given by Equation 5.17:²⁵⁵

$$\Delta S_{rc.s}^{o}(=\Delta S_{rc}^{o}) = -(e^{2}N/2r \in T)(d \ln \epsilon/d \ln T) \qquad (5.17)$$

where e is the electronic charge, N is Avogadro's number, ε is the dielectric constant of the solvent, and r is the radius of the ferricinium cation. The $\Delta S_{rc,s}^{0}$ values listed in the last column of Table 5.2 are obtained from Equation 5.17, using literature values of ε and assuming that $r = 3.8 \text{Å}.^{274}$ There is clearly no general pattern of agreement between the experimental and these calculated quantities, the Born treatment predicting a much milder solvent dependence of $\Delta S_{rc,s}^{0}$ than is observed. Similar breakdowns of the dielectric continuum model in predicting reaction entropies have been found for several bulk solution couples in a number of solvents. 55,84,253-255

A probable reason for the failure of Equation 5.17 is that the major property determining the entropy of charge-induced solvent reorientation is the degree of "internal order" of the solvent (i.e., self-association and long range structuring induced by hydrogen bonding), rather than the macroscopic dielectric properties. 275,276 Thus, a solvent having a high degree of internal order would be relatively unperturbed by a charged molecule, whereas considerable solvent ordering around the ion would occur in a medium having little intermolecular structure. Since such charge-dipole interactions will be absent for neutral ferrocene, a positive contribution to the reaction entropy (S_{red} - S_{ox}) would be anticipated for the present redox couples, especially in relatively nonassociated solvents. Criss and co-workers have suggested estimating the degree of internal order of a solvent from the difference in boiling point, $\Delta \mathbf{T}_{\mathbf{bp}}$, compared to that for a structurally analogous hydrocarbon. These values of $\Delta T_{\rm bp}$ are also listed in Table 5.2. Indeed, the $\Delta S_{rc.s}^{o}$ values for the surface-attached ferrocene couple do for the most part vary as expected with the corresponding values of ΔT_{bp} .

An unusual result which merits comment is the large negative value of $\Delta S_{rc,s}^0$ (-50 J deg⁻¹ mol⁻¹) found in water (Table 5.2). A small negative value of ΔS_{rc}^0 has previously been oberved for the bulk-solution ferrocene couple, also in water. This indicates that the net solvent ordering in the vicinity of the surface-attached redox center is less extensive in the cationic than in the neutral state, in qualitative disagreement with the expectations from an electrostatic treatment. These negative entropy values possibly result from donor-



tized ferrocene (Figure 5.4); open circles: bulk-solution ferrocene. Key to solvents: 1, acetone; Filled triangles: surface-attached ferrocene (Figure 5.3); open triangles: bulk-solution derivaferrocene couples in various solvents versus solvent Acceptor Number, taken from reference 277. 2, dimethylformamide; 3, propylene carbonate; 4, acetonitrile; 5, dimethylsulfoxide; 6, nitro-Figure 5.6. Plot of reaction entropies for surface-attached and solution-phase ferriciniummethane; 7, N-methylformamide; 8, formamide; 9, methanol; 10, water.

acceptor interactions between the cyclopentadienyl rings and the acidic water hydrogens. 255 (An alternate and additional explanation in terms of an entropy change associated with "solvent disruption" is offered in Section V. C). Since the electron density on the cyclopentadienyl rings will be greater in the reduced state, such specific solvent interactions should be enhanced leading to increased solvent ordering and a decrease in entropy compared with that for the oxidized state. If such an explanation were correct a correlation between $\Delta S_{rc.s}^{0}$ and the acidity of the solvent might be expected. Figure 5.6 shows a plot of the reaction entropies for the adsorbed couple and its solution analog as well as for unsubstituted ferrocene versus the solvent "acceptor number" which is an empirical measure of the electronaccepting capabilities of the solvent. 277 A reasonable correlation is indeed observed. Apparently, both non-Bornian ion-dipole interactions and specific donor-acceptor interactions might be important in determining the redox properties of the surface-attached as well as solution ferrocene couples.

The present work demonstrates the feasibility of determining surface reaction entropies and illustrates the utility of these measurements for elucidating the various elements of interfacial reactant-solvent interactions. Given the sensitivity of $\Delta S_{rc,s}^{0}$ measurements to the solvent structure it is suggested that this approach might also usefully be employed to gain insight into reactant solvation in polymer film electrodes for which the question of solvent penetration within the film is of current interest.

C. Size, Charge, Solvent and Ligand Effects on Reaction Entropies

1. Introduction

Relative entropies of redox reactions were widely measured in the 1950's and 1960's in order to examine basic notions concerning ionic solvation. 281-287 Interest in this topic was revived in 1979 with the report by Weaver and co-workers that absolute measures of the entropy difference ΔS_{rc}^{0} (= S_{red}^{0} - S_{ox}^{0}) between the two ions forming a redox couple could readily be obtained from nonisothermal electrochemical experiments. 55 Numerous papers on reaction entropies have appeared since then. 84,253-255,271.281-304 These have tended to emphasize either the value of such measurements in unraveling the details of solvent reorganization in connection with electron transfer dynamics 55.84,253-255.293,294,297,304 or their usefulness for gaining information concerning the solvation of metalloproteins, 300-302 peptide complexes 298,299 and other biological model compounds. 303 Although many insights have been gained into both problems, a number of puzzles remain.

This section describes some empirical relations which have been uncovered concerning the dependence of ΔS_{rc}^{0} values for simple transition metal couples on reactant size and charge and on the nature of the solvent, and seeks to provide interpretations at the molecular level. Besides offering predictive power, it is suggested that these correlations and interpretations can rationalize some of the more curious findings of earlier studies.

2. Results

The data examined here have been taken largely from previous reports 55,84,89,253-255 although a fair number of new results are included. (The new results are summarized in Appendix I). In each case the redox couple is substitutionally inert in both oxidation states.

Values of ΔS_{rc}^{0} in water, dimethylsulfoxide (DMSO) and acetonitrile for several "3+/2+" couples are plotted against reactant radius in Figure 5.7. For spherically nonsymmetrical complexes (e.g. $Ru(NH_2)_{spy}^{3+/2+}$), the effective radius is taken as equal to half of the cube root of the product of the diameters along the three ligand-metalligand axes. 28 Excluded from the comparisons at this point are redox couples where a difference in spin state occurs between the oxidized and reduced forms. It is evident that there is a good linear fit of the data in water, with the exception of the results for three couples containing aquo ligands. (These three could not be examined in the other solvents). In acetonitrile and DMSO the reaction entropy also varies with -r, but apparently not in a strictly linear fashion. Somewhat better linear correlations, at least in nonaqueous solvents, are found, with 1/r (Figure 5.8). Similar correlations were obtained in solvents other than the three for which data are shown, but these are omitted from the plots for clarity.

The dependence of ΔS_{rc}^{0} on charge was examined by monitoring consecutive reduction reactions of ruthenium— and chromium tris bipyridine complexes. For both of these, at least four redox states are accessible in acetonitrile and acetone. Figure 5.9 shows that the

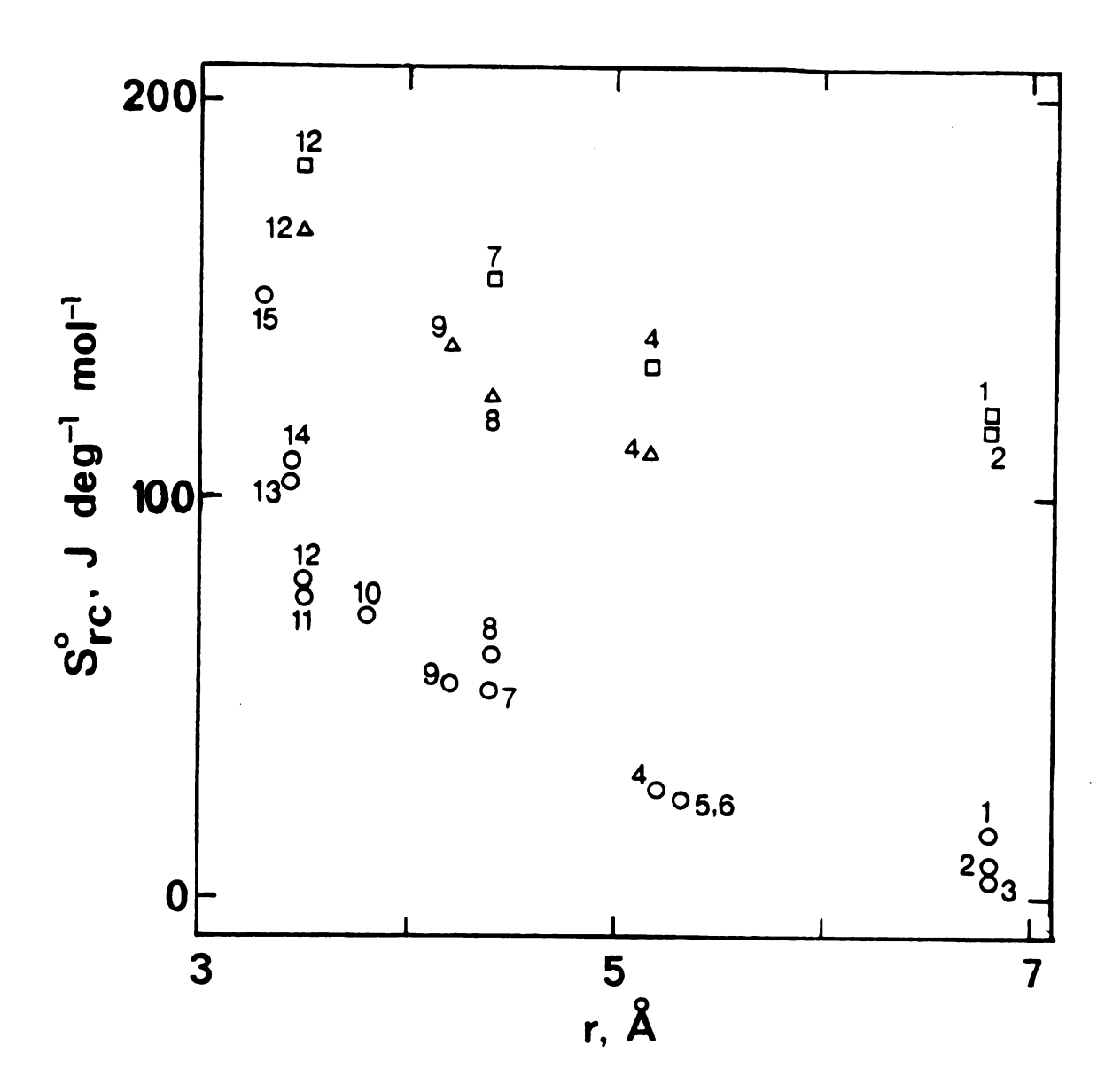


Figure 5.7. Reaction entropy versus effective radius of reactant. Key to solvents: (O) water; (A) dimethylsulfoxide; (□) acetonitrile. Key to reactants: (1) $Cr(bpy)_3^{3+}$; (2) $Fe(bpy)_3^{3+}$; (3) $Ru(bpy)_3^{3+}$; (4) $c-Ru(NH_3)_2(bpy)_2^{3+}$; (5) $c-Ru(H_20)_2(bpy)_2^{3+}$; (6) $t-Ru(H_20)_2(bpy)_2^{3+}$; (7) $Ru(NH_3)_4bpy^{3+}$; (8) $Ru(NH_3)_4phen^{3+}$; (9) $Ru(en)_3^{3+}$; (10) $Ru(NH_3)_5py^{3+}$; (11) $Ru(NH_3)_6^{3+}$; (12) $Os(NH_3)_6^{3+}$; (13) $Ru(NH_3)_5H_2O^{3+}$; (14) $Ru(NH_3)_4(H_20)_2^{3+}$; (15) $Ru(H_20)_6^{3+}$.

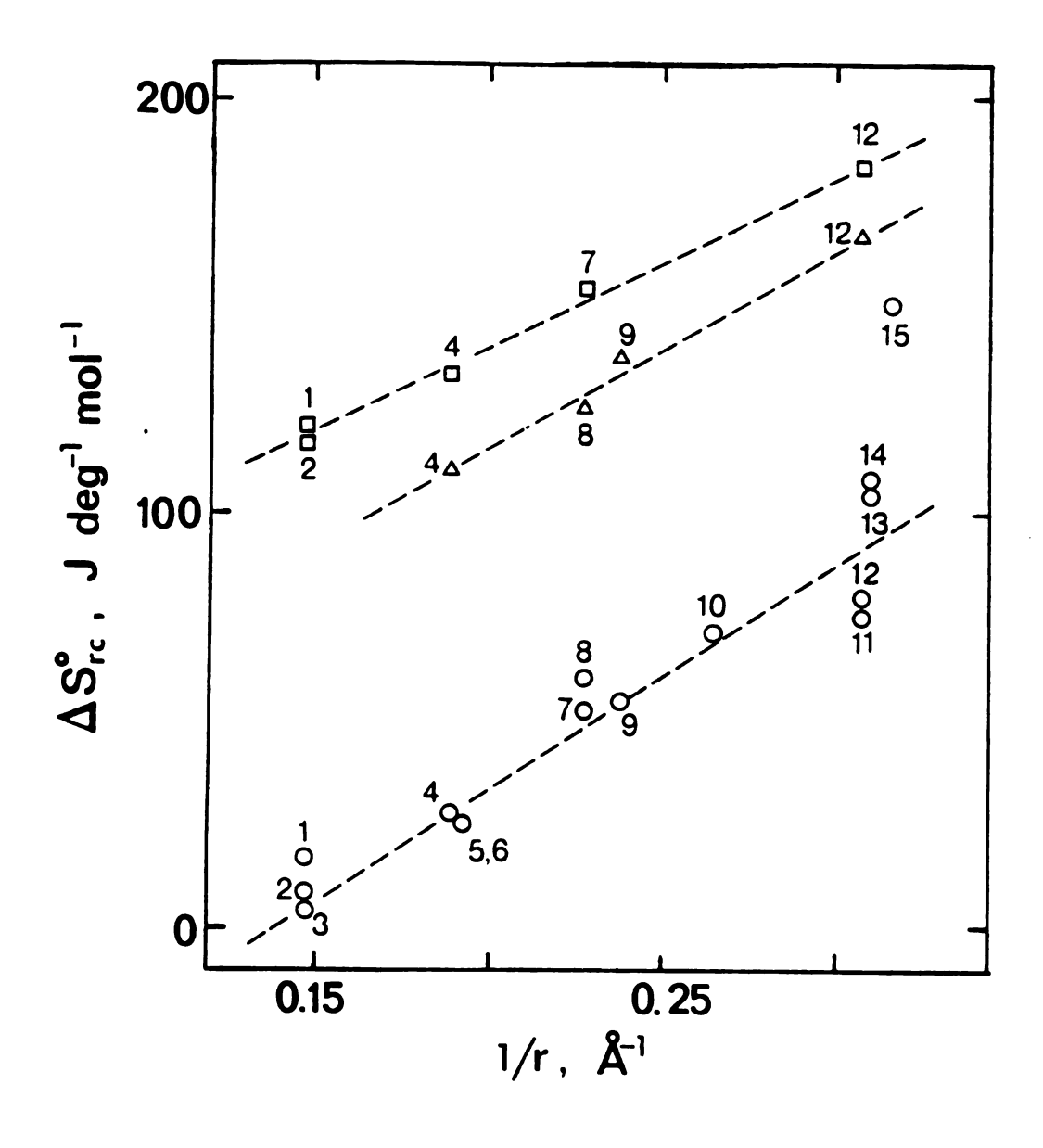


Figure 5.8. Reaction entropy versus 1/r. Keys to solvents and reactants as in Figure 5.7.

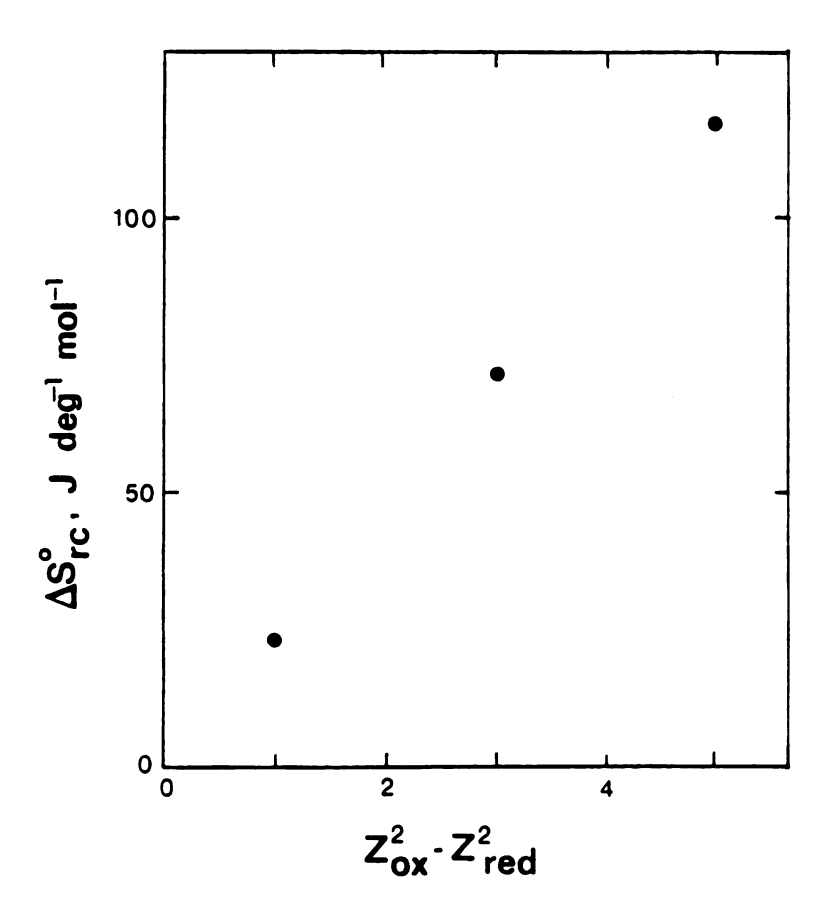


Figure 5.9. Reaction entropy for ruthenium tris bipyridine couples in acetonitrile versus the difference in the squares of the charges on the oxidized and reduced states.

reaction entropy for $Ru(bpy)_3^{n+1/n}$ in acetonitrile varies with $(Z_{red}^2 - Z_{ox}^2)$, where Z_{ox} and Z_{red} are the charges of the oxidized and reduced states of each couple. Unfortunately, there are only a few complexes and solvents for which consecutive electron transfer reactions can be examined.

The connection between reaction entropies and the nature of the solvent is illustrated in Figures 5.10 and 5.11. Linear correlations are found between ΔS_{rc}^{o} and the so-called solvent acceptor number. ²⁷⁷ regardless of the reactant charge, size, electronic state or ligand composition. The ΔS_{rc}^{o} values for $Ru(NH_3)_5NCS^{2+/+}$ are taken from the dissertation of Dr. Saeed Sahami. ⁸⁹ while those for $Co(EFME-oxosar-H)^{2+/+}$ (structure in Figure 5.12) were measured by Dr. Peter Lay and this author.

3. Discussion

The simplest theoretical treatment of reaction entropies is based on the Born electrostatic model in which the solvent is treated as a continuum. According to this model:

$$\Delta S_{rc}^{o} = (e^{2}N/2\varepsilon Tr)(d\ln\varepsilon/dT)(z_{ox}^{2}-z_{red}^{2})$$
 (5.8)

where ϵ is the dielectric constant of the solvent. Although this approach has rightly been criticized for failing to provide accurate overall estimates of ΔS_{rc}^{0} , the empirical analyses confirm the predicted variations with 1/r and $(z_{ox}^{2}-z_{red}^{2})$. The chief problem seems to lie in the representation of the solvent.

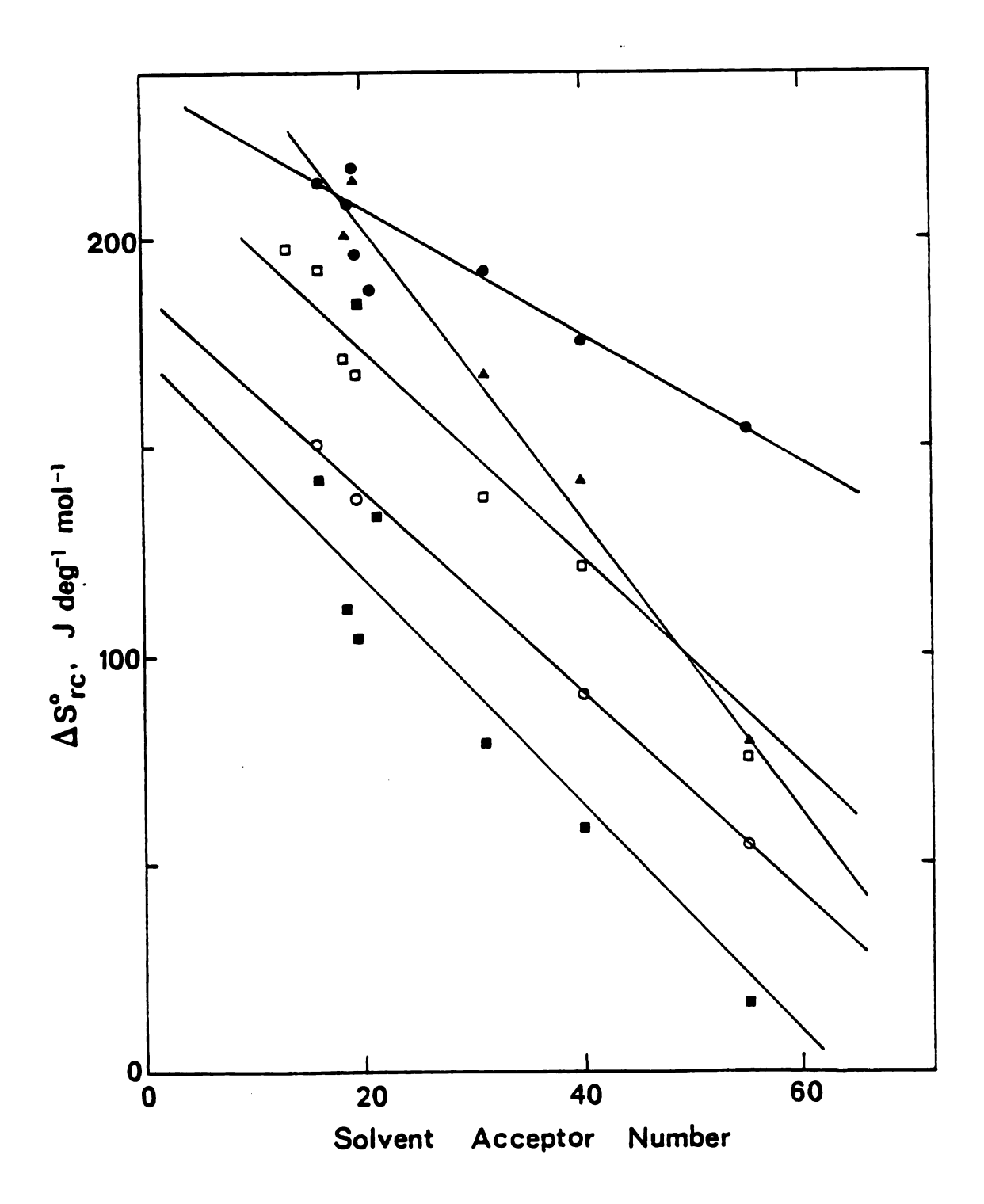


Figure 5.10. Reaction entropy versus solvent acceptor number. Key to reactants: () Cr(bpy) 3 +, (O) Ru(en) 3 +, (D) Ru(NH3) 6 +, (O) Co(en) 3 +, (A) Co(sepulchrate) 3 +. Solvents (and acceptor numbers): water (55), formamide (40), N-methylformamide (31), nitromethane (20.5), acetonitrile (19), dimethylsulfoxide (19), propylenecarbonate (18), dimethylformamide (16), acetone (12.5).

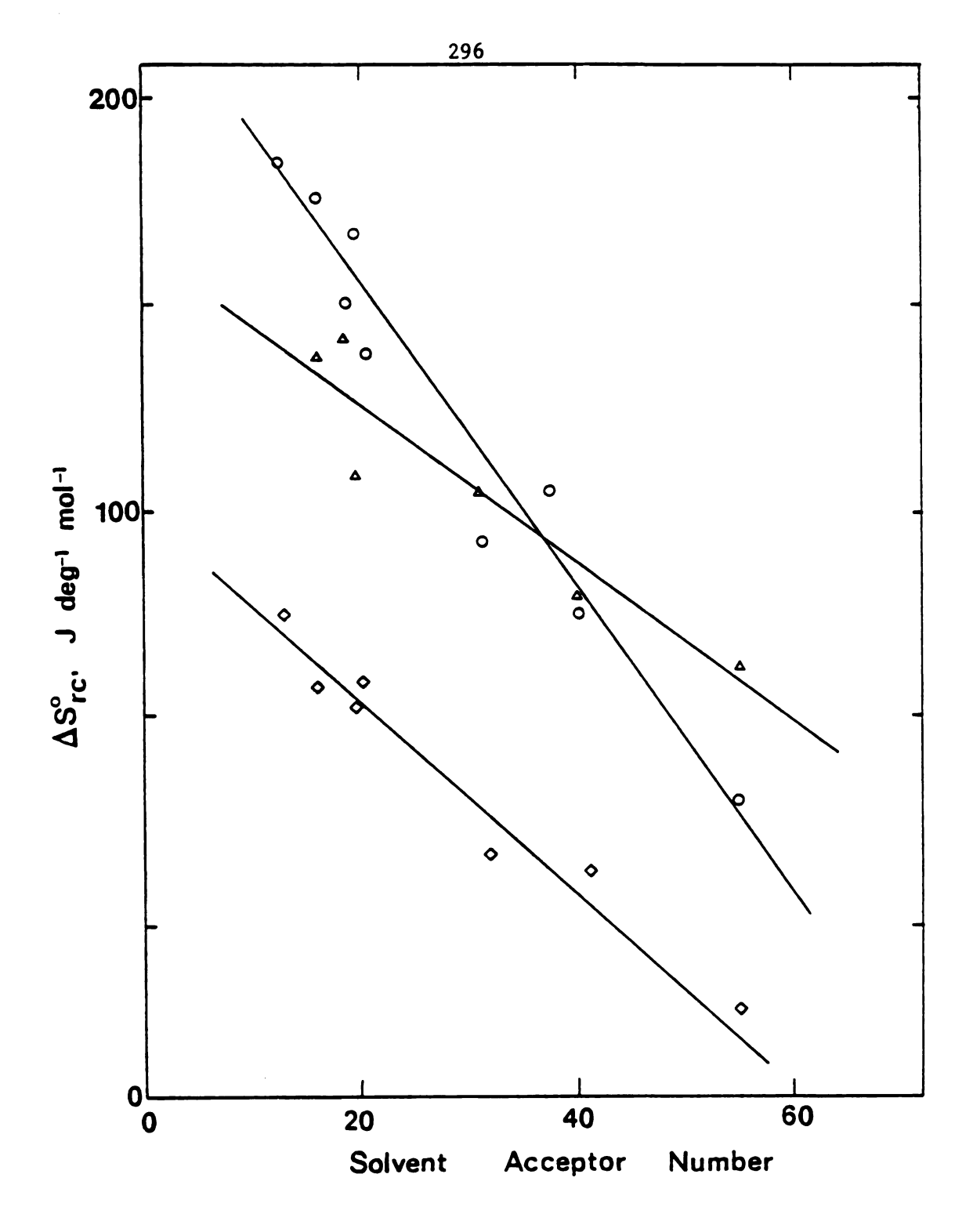


Figure 5.11. Reaction entropy versus solvent acceptor number. Key to reactants: (\diamondsuit) ferricinium, (O) Co(EFME-oxosar-H)²⁺, (\triangle) Ru(NH₃)₅NCS²⁺. Solvents as in Figure 5.10, plus methanol (41).

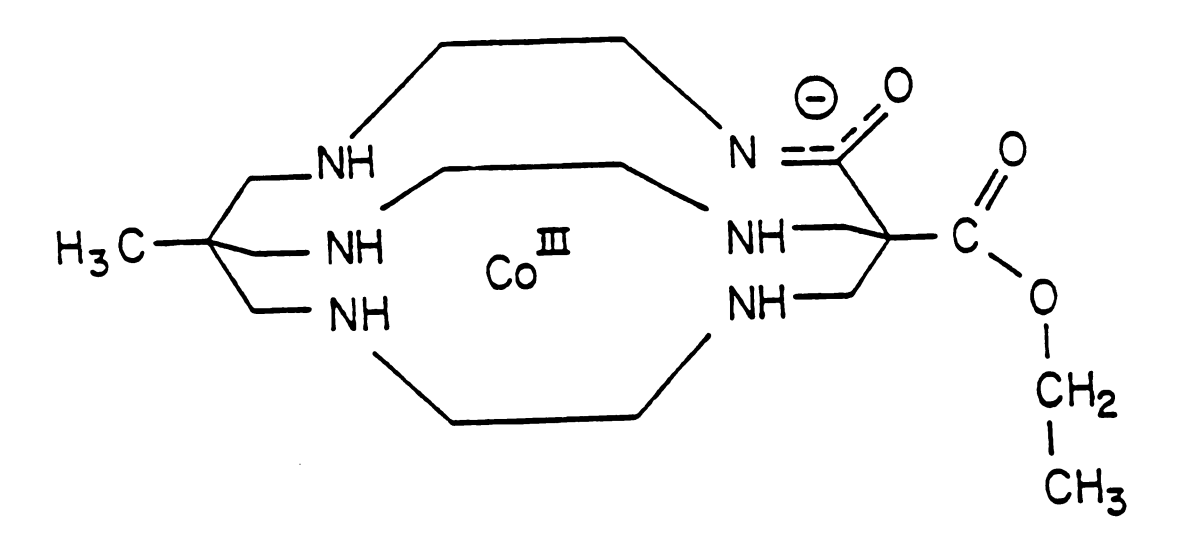


Figure 5.12. Structure of Co(EFME-oxosar-H)²⁺.

Evidently specific donor and acceptor interactions, rather than nonspecific Bornian effects, are primarily responsible for the changes in reaction entropy as the solvent is varied. We have previously suggested that such interactions might involve solvent molecules as acceptors and metal complexes as donors. Although plausible for redox couples containing electron-rich ligands such as bipyridine or cyclopentadiene, such behavior is hardly possible for couples such as $\operatorname{Ru}(\operatorname{NH}_3)_6^{3+/2+}$ which contain acidic ligands and act instead as electron acceptors.*

The alternative to solvent-ligand interactions would be solvent-solvent interactions, which would account for the insensitivity of the reaction entropy-acceptor number correlation to the nature of the redox couple. If strong donor-acceptor interactions induce significant intermolecular solvent structuring, a straightforward explanation of our empirical observations emerges. Highly structured solvents will experience a loss of order, at substantial entropic expense, when disrupted by short-range complex ion-solvent dipole (NOT donor-acceptor) interactions. 276 (Ion-dipole interactions are suggested in order to account for the observed size and charge dependence of $\Delta S_{\rm rc}^{\rm o}$). The "entropy of disruption" will be greater with ions of higher charge, yielding a negative contribution (for cationic couples) to $\Delta S_{\rm rc}^{\rm o}$ (=So red - So). This contribution will be less significant in less structured

^{*}The electron-accepting tendencies of ruthenium(III) ammine complexes are demonstrated quite convincingly by Curtis, Sullivan and Meyer's solvatochromic experiments which show that such complexes are selectively solvated by strongly basic (i.e. electron-donating) solvents when placed in mixed media (reference 305).

solvents. On the other hand, an increase in order and decrease in entropy will result if a complex ion is able to orient disrupted solvent molecules, again via charge-dipole interactions. Ions of higher charge should be more effective and therefore, a positive contribution to ΔS_{rc}^{o} (= S_{red}^{o} - S_{ox}^{o}) can be expected. This contribution should be greatest in unstructured solvents where reorientation of solvent molecules will be relatively unhindered. Note that together the two effects predict that the largest positive ΔS_{rc}^{0} values will be found with highly charged cationic redox couples in unstructured solvents, while smaller or even negative values (e.g. ferrocene/ ferricinium in water)84 would be predicted in more structured solvents. It is suggested that increases in solvent accepting capabilities are parallelled closely by increases in solvent structuring and order, 291 thereby accounting for the decrease of ΔS_{rc}^{o} with acceptor number. One might expect that some combination of donor and acceptor properties would lead to a better description of the degree of solvent ordering and structure, but apparently this is not the case.

In light of these obervations and interpretations it is useful to consider some specific reactions. Several authors have commented on the very small reaction entropies for tris bipyridine couples in water. Explanations are often sought in terms of "hydrophobic" interactions between the aromatic ligands and water molecules. However, the correlations in Figures 5.7 and 5.8 indicate that the small ΔS_{rc}^{o} values reflect simply the large size of such couples in comparison to most others. One suspects that the negative ΔS_{rc}^{o} values commonly observed for metalloproteins ΔS_{rc}^{o} values commonly observed for metalloproteins ΔS_{rc}^{o} might also represent size effects rather than hydrophobic interactions.

(This is not to deny the possible importance of hydrophobic interactions to ionic solvation, but rather to point out that these need not be invoked to account for entropy differences between oxidation states).

On the other hand, the $\operatorname{Ru}(\operatorname{NH}_3)_6^{3+/2+}$ and $\operatorname{Ru}(\operatorname{H}_20)_6^{3+/2+}$ couples are closely similar in size, yet exhibit very different reaction entropies. From the empirical correlations of size with entropy change, it is evident that it is the aquo couple which behaves anomalously. In this case, as well as with other aquo couples, the idea of specific ligand-solvent interactions (most likely, hydrogen-bonding) probably does represent the best explanation of the unusual behavior.

Various authors have noted that ΔS_{rc}^{0} values for "mixed ligand" complexes can be estimated approximately by linearly interpolating from the values for complexes possessing homogeneous ligand compositions. 84,281,282 It has been suggested that each ligand provides an additive contribution to ΔS_{rc}^{0} . It now seems that the influences of individual ligands can best be understood in terms of their effects on the overall charge and size of a redox couple. Such effects may not be strictly additive and the influence of a particular ligand should depend on the size and charge of the complex to which it is being added. A stringent test of these ideas would be to compare reaction entropies for redox couples of diverse charge, size and structure. In Figure 5.13 ΔS_{rc}^{0} values for $Fe(CN)_{6}^{3-/4-}$, $Fe(CN)_{4}^{4}bpy^{-/2-}$, ferricinium/ferrocene, $Ru(NH_{3})_{5}NCS^{2+/+}$, $Ru(NH_{3})_{5}Cl^{2+/+}$, $Ru(en)_{3}^{3+/2+}$, $Ru(NH_{3})_{6}^{3-1}$ and $Cr(bpy)_{3}^{3+/2+}$, all in water, are plotted against $(z_{ox}^{2}-z_{red}^{2})/r$. A fairly reasonable linear correlation is observed, which

merely from the size and charge of a redox couple. Note that a negative, rather than a zero, entropy intercept is found, in disagreement with the expectations from continuum models.

The 1/r dependence of ΔS_{rc}^{O} appears also to account at least partially for the approximate correlation between the reaction entropy and self-exchange reactivity for several redox couples in water. 288 Thus, according to Marcus' theory 13 the outer-shell reorganization energy for electron transfer also depends on 1/r. An increase in r will decrease the outer-shell barrier thereby increasing the exchange rate and yielding an inverse correlation between the log of the exchange rate constant and the reaction entropy, when other factors can be neglected. With regard to electron transfer energetics the findings concerning the solvent dependence of ΔS_{rc}^{O} and the shortcomings of the Born model hint that a molecular approach is needed for understanding not only the thermodynamics of solvent reorganization but also for the static component, at least, of the nonequilibrium kinetic process.

Finally, it is worthwhile to consider the cobalt(III)/(II) couples. Although the number and variety of such redox couples are necessarily limited, the indications are that these also exhibit a charge and size sensitivity. Thus, the ΔS_{rc}^{0} values for $Co(en)_{3}^{3+/2+}$ are greater than those for the larger $Co(phen)_{3}^{3+/2+}$ and $Co(bpy)_{3}^{3+/2+}$ couples. The values for $Co(EFME-oxosar-H)^{2+/+}$ generally are smaller than for the more highly charged parent sepulchrate complex. Reaction entropies for these complexes are essentially always about 80 J deg⁻¹ mole⁻¹ greater than those for similar complexes containing different

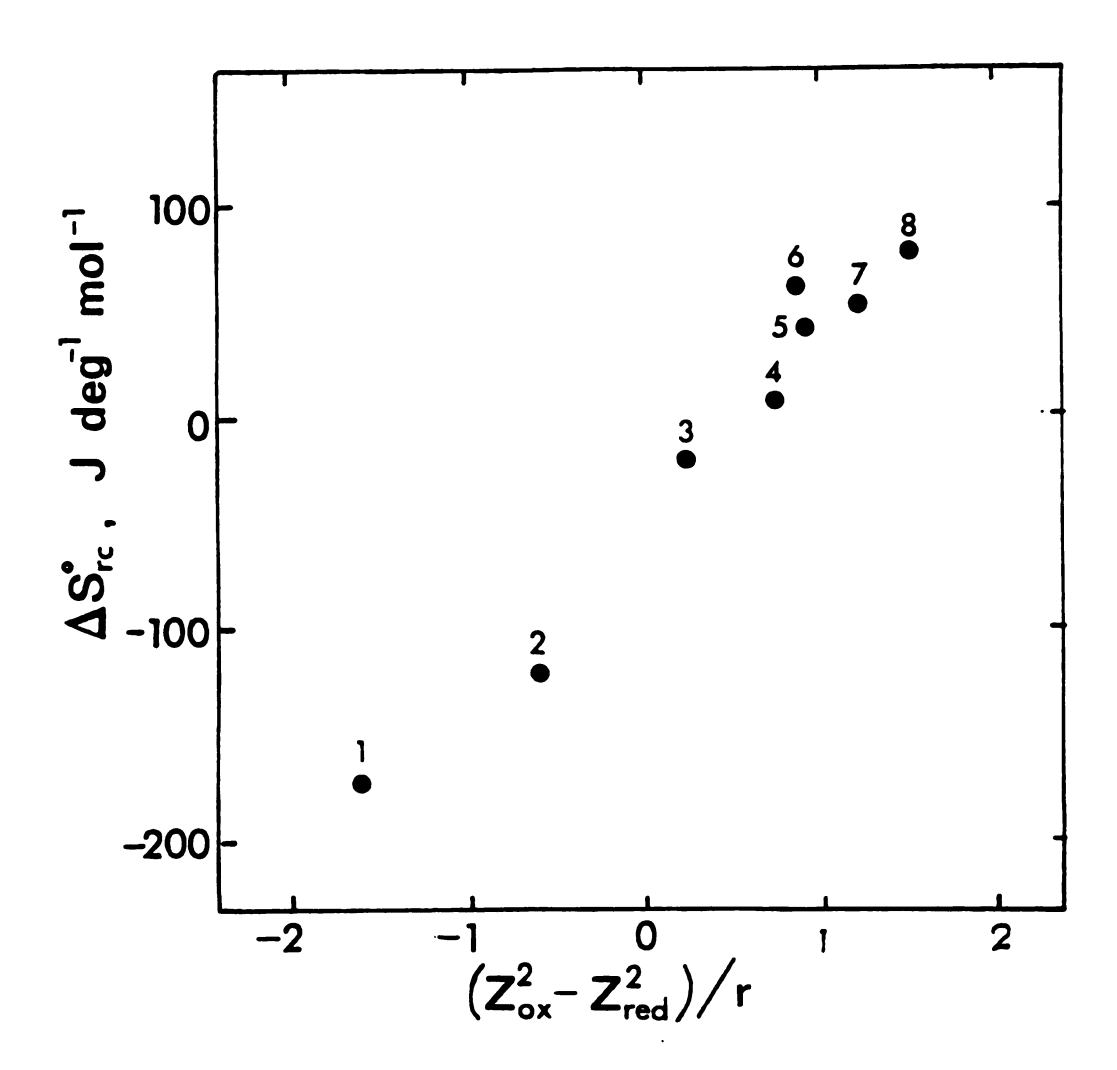


Figure 5.13. Reaction entropy in water versus $(Z_{ox}^2 - Z_{red}^2)$ /radius. Key to reactants: (1) $Fe(CN)_6^{3-}$; (2) $Fe(CN)_4 bpy^{2-}$; (3) ferricinium; (4) $Cr(bpy)_3^{3+}$; (5) $Ru(NH_3)_5C1^{2+}$; (6) $Ru(NH_3)_5NCS^{2+}$; (7) $Ru(en)_3^{3+}$; (8) $Ru(NH_3)_6^{3+}$.

metal centers. The distinguishing feature of the cobalt(III)/(II) reactions is the change of spin multiplicity. One is almost forced to conclude that the extra 80 J \deg^{-1} mol⁻¹ of reaction entropy must be associated directly with the change of electronic spin state. ²⁹⁴ Interestingly, the cobalt(II)/(I) bipyridine couple, which is low-spin in both oxidation states, yields the same reaction entropy in acetonitrile as the $\operatorname{Cr}(\operatorname{bby})_3^{2+/+}$ couple.

4. Conclusions

Empirical correlations of the reaction entropies for transition metal couples are found with the inverse of the effective radius of the redox couple and with the difference of the squares of the charges on the two ions comprising the redox couples. The solvent dependence of ΔS_{rc}^{O} is described by Gutman's acceptor number. The size and charge correlations are expected on the basis of the Born model. However, the solvent dependence requires a molecular rather than a continuum representation of the solvent. Solvent disruption and reorientation effects can adequately account for most of the entropy data. A number of interesting observations can be rationalized. Little evidence is found for specific donor-acceptor (hydrogen bonding) interactions between redox couples and solvent molecules, except in the case of aquo couples in water.

CHAPTER VI

APPLICATIONS OF THE RELATIVE ELECTRON-TRANSFER THEORY

Bennett has emphasized that there are actually two "electrontransfer theories": the absolute theory which enables rate constants to be calculated from structural parameters and the relative theory which emphasizes the predictive power of reactivity patterns. 307 latter approach exploits the conceptual similarities between related homogeneous and electrochemical reactions and between homogeneous selfexchange and cross reactions, and is embodied in the so-called Marcus cross relations. The success of this approach relies on a type of ideal behavior - sometimes termed the "weak overlap limit" - in which isolated reactants retain their same degree of intrinsic reativity when combined together in bimolecular reactions. The weak overlap limit appears to provide a fairly reliable guide to outer-sphere reactivity in various environments, although it sometimes breaks down for homogeneous inner-sphere reactions. On the assumption that outer-sphere electrochemical reactions at mercury approximately achieve this ideal behavior, the relative electron-transfer theory is applied to some problems involving homogeneous redox reactions.

A. <u>Electrochemical and Homogeneous Exchange Kinetics for</u>

<u>Transition-Metal Aquo Couples: Anomalous Behavior</u>

of Hexaaquo Iron(III)/(II)

[Originally published in Inorg. Chem., 22, 2557 (1983)]

1. Introduction

Recent developments in the theory of outer-sphere electron transfer have focused attention on the contribution of inner-shell reorganization, ΔG_{is}^* , to the intrinsic free energy barrier for electron exchange ΔG_{ex}^* . 14,23,56b,250,307,308 Transition-metal redox couples containing only aquo ligands, of the type $M_{aq}^{3+} + e^- + M_{eq}^{2+}$ where M = Ru, Fe, Co, V, and Ru form an especially interesting series in which to compare the theoretical predictions with experiment since they exhibit large differences in redox reactivity which are likely to be due primarily to the influences of the metal electronic structure upon ΔG_{is}^* . Some of these reactions exhibit remarkably small exchange rates. 309

Experimental estimates of $\Delta G_{\rm ex}^{\star}$ can be obtained from the rates of homogeneous self exchange or electrochemical exchange, or, less directly, from the kinetics of suitable homogeneous cross reactions with other redox couples having self-exchange kinetics that are known or can be estimated. 13,180 Relationships between the kinetics of these reactions are given by the well-known equations derived from an adiabatic electron-transfer model: 13,180

$$(k_{ex}^{e}/A_{e}) < (k_{ex}^{h}/A_{h})^{1/2}$$
 (4.15)

and

$$k_{12}^{h} = (k_{11}^{h} k_{22}^{h} K_{12}^{f})^{1/2}$$
 (6.1a)

where

log f =
$$(\log K_{12})^2/[4 \log(k_{11}^h k_{22}^h/A_h^2)]$$
 (6.1b)

In Equation 4.15. k_{ex}^e and k_{ex}^h are the corresponding rate constants for electrochemical exchange and homogeneous self exchange for a given redox couple, and A_e and A_h are the electrochemical and homogeneous frequency factors, respectively. In Equation 6.1, k_{11}^h and k_{22}^h are the rate constants for the parent self-exchange reactions corresponding to a homogeneous cross reaction having a rate constant k_{11}^h and equilibrium constant k_{12}^h . All these rate constants are presumed to be corrected for work terms. A given rate constant for homogeneous self-exchange k_{ex}^h can be related to the corresponding intrinsic barrier ΔG_{ex}^* by k_{13}^h , k_{13}^h

$$k_{ex}^{h} = A_{h} \exp(-\Delta G_{ex}^{*}/RT)$$
 (6.2)

where κ is an electronic transmission coefficient. The rate constant for electrochemical exchange k_{ex}^e can also be related to ΔG_{ex}^* by

$$k_{ex}^{e} = A_{e} \exp(-G_{ex,e}^{*}/RT)$$
 (6.3a)

$$k_{ex}^{e} = A_{e} \exp[-(\Delta G_{ex}^{*} + C)/2RT]$$
 (6.3b)

where $\Delta G_{\mathbf{ex},\mathbf{e}}^{*}$ is the intrinsic electrochemical barrier. The factor 2 arises in Equation 6.3b because only one reactant is required to be activated in the electrochemical reaction, rather than a pair of reactants as in the homogeneous case. The contributions to $\Delta G_{\mathbf{ex}}^{*}$ and $\Delta G_{\mathbf{ex}}^{*}$ arising from inner-shell (i.e. metal-ligand) reorganization, $\Delta G_{\mathbf{is}}^{*}$ and $\Delta G_{\mathbf{is},\mathbf{e}}^{*}$. respectively, are therefore related by $\Delta G_{\mathbf{is}}^{*} = 2\Delta G_{\mathbf{is},\mathbf{e}}^{*}$. The relationship between the components of $\Delta G_{\mathbf{ex}}^{*}$ and $\Delta G_{\mathbf{ex},\mathbf{e}}^{*}$ due to outershell (i.e. solvent) reorganization, $\Delta G_{\mathbf{os}}^{*}$ and $\Delta G_{\mathbf{os},\mathbf{e}}^{*}$, is somewhat less straightforward. According to a dielectric continuum treatment these quantities are given by 13 , 180

$$\Delta G_{os}^{*} = \frac{e^{2}}{4} (\frac{1}{a} - \frac{1}{R_{h}}) (\frac{1}{\varepsilon} - \frac{1}{\varepsilon})$$
 (6.4a)

$$\Delta G_{os,e}^{*} = \frac{e^{2}}{8} (\frac{1}{a} - \frac{1}{R_{e}}) (\frac{1}{\varepsilon_{op}} - \frac{1}{\varepsilon_{s}})$$
 (6.4b)

where e is the electronic charge, a is the (average) reactant radius, $\varepsilon_{\rm op}$ and $\varepsilon_{\rm s}$ are the optical and static dielectric constants, $R_{\rm h}$ is the close contact distance between the homogeneous redox centers, and $R_{\rm e}$ is twice the distance between the reactant and the electrode surface. Since it is generally expected for outer-sphere reactions that $R_{\rm e}$ > $R_{\rm h}$, therefore $\Delta G_{\rm os}^* < 2\Delta G_{\rm os,e}^*$. The quantity C in Equation 6.3b accounts for this inequality which is also the origin of the inequality sign in Equation 4.15; from Equations 6.3 and 6.4

$$c = \frac{e^2}{4} (\frac{1}{R_h} - \frac{1}{R_e}) (\frac{1}{\epsilon_{op}} - \frac{1}{\epsilon})$$
 (6.5)

Equation 4.15 can therefore be written in the more general form

2
$$\log (k_{ex}^e/A_e) = \log (k_{ex}^h/A_h) - C/2.303 \text{ RT}$$
 (6.6)

For a series of reactants having a similar size and structure, as for the present aquo couples, $R_{\hat{h}}$ and $R_{\hat{e}}$ and hence C should remain approximately constant.

It is desirable to obtain a self-consistent set of experimental values of k or k for comparison with theoretical predictions obtained from calculated values of ΔG_{ex}^* using Equations 6.2 and 6.3. This task is less straightforward than is commonly presumed for two reasons. Firstly, the experimental values of k_{ex}^h or k_{ex}^e may not refer to outer-sphere pathways since (except for $Ru_{aq}^{3+/2+}$) at least one of the aquo reaction partners is substitutionally labile so that more facile inner-sphere pathways may provide the dominant mechanism. Secondly, values of kh derived using Equation 6.1 from rate constants for appropriate outer-sphere cross reactions rely not only on the availability of values of k_{ex}^{h} for the coreacting redox couple along with values of K_{12} , but depend also on the applicability of this relation. 310,311 The resulting estimates of k for different redox couples are often difficult to compare since large systematic errors can be introduced by the use of cross-reaction data involving structurally different coreactants, inappropriate electrode potential data, etc.

In spite of their direct relationship to the desired intrinsic barriers, electrochemical exchange rate data have seldom been utilized for this purpose. One reason is that these data have commonly been gathered at ill-defined solid surfaces where the work terms arising from double-layer effects are large and unknown, precluding quantitative intercomparison of the results. However, Weaver and coworkers have determined accurate electrochemical rate data for $v_{aq}^{3+/2+}$, $cr_{aq}^{3+/2+}$, $\operatorname{Eu}_{aq}^{3+/2+}$, $\operatorname{Ru}_{aq}^{3+/2+}$ and $\operatorname{Fe}_{aq}^{3+/2+}$ at the mercury-aqueous interface under conditions where the work terms are small and can be estimated with confidence. 228,312,313 The interactions between the reactant and the metal surface are likely to be weak and nonspecific, so that the electrode can be viewed as an inert electron source or sink that does not influence the electron-transfer barrier. This allows information on the electron-transfer barriers to be gathered for individual redox couples as a function of the thermodynamic driving force. information is largely inaccessible from the kinetics of homogeneous electron transfer.

In the present section, suitable rate data for electrochemical and homogeneous reactions involving aquo redox couples are analyzed and compared using Equations 6.1 and 6.6 in order to ascertain as unambiguously as possible how the kinetics of outer-sphere electron exchange depend on the metal redox center.

2. Rate Constants for Electrochemical Exchange

Table 6.1 contains a summary of rate parameters for the electrochemical exchange of $Ru_{aq}^{3+/2+}$, $V_{aq}^{3+/2+}$, $Fe_{aq}^{3+/2+}$, $Eu_{aq}^{3+/2+}$, and

Kinetics and Related Thermodynamics Parameters for the Electrochemical Exchange of some M(III)/(II) Aquo Redox Couples at the Mercury-Aqueous Interface at $25^{\circ}\mathrm{C}$. Table 6.1.

ке е е сп в -1	$\approx 2 \times 10^{-2}$	1×10^{-3}	$\lesssim 1 \times 10^{-4}$	8 x 10 ⁻⁵	2 x 10 ⁻⁶
р ф Vm	10	- 5		-20	-25
ke(app) kex-1 cm s	5×10^{-3}	1.5×10^{-3}	$2 \times 10^{-5} f$	6×10^{-4}	2×10^{-5} 1.0×10^{-5}
b Ef mV vs. s.c.e.	-20	-472	495	-625	-655 -655
a Electrolyte	0.4 M KPF6	0.4 M KPF6	0.4 M KPF6	0.4 M KPF6	0.4 M KPF ₆ 0.4 M La(C10 ₄) ₃
Redox Couple	Ru 3+/2+ Ru aq	v3+/2+ vaq	Fe 3+/2+ aq	E _u 3+/2+ E _u aq	Cr ^{3+/2+}

at E^{f} in given electrolyte; obtained or estimated from references 181 and 228. e Work-corrected $^{\mathcal{A}}$ Electrolyte contained sufficient (>5-10 m<u>M</u>) acid to suppress significant deprotonation of M(OH $_2$) $_6^3$. Formal potential for redox couple in stated electrolyte at 25° C. Values taken potential; obtained from references 181 and 228. d Approximate potential across diffuse layer rate constant for electrochemical exchange. Obtained from k $^{
m e}$ (app) and $^{
m d}$ using Equation from reference $55\,\mathrm{and}$ supplemented by unpublished data from this laboratory. $^{\mathcal{C}}$ Measured (apparent) value of rate constant at mercury electrode in stated electrolyte at formal $^f{
m Estimated}$ as indicated in the text. ${\rm Cr}_{{\rm aq}}^{3+/2+}$ at the mercury-aqueous interface, using potassium hexafluorophosphate and lanthanum perchlorate supporting electrolytes. These experimental conditions minimized the extent of the electrostatic double-layer effect upon the apparent rate constants for electrochemical exchange $k_{\rm ex}^{\rm e}({\rm app})$ (i.e. the "standard" rate constants measured at the formal potential $E^{\rm f}$ for the redox couple concerned), enabling values of the work-corrected rate constants $k_{\rm ex}^{\rm e}$ to be evaluated with confidence using 314

$$\ln k_{\text{ex}}^{\text{e}} = \ln k_{\text{ex}}^{\text{e}}(\text{app}) + \frac{F}{RT}(Z_{\text{r}} - \alpha_{\text{corr}}) \phi_{\text{d}}$$
 (6.7)

where $\mathbf{Z}_{\mathbf{r}}$ is the reactant charge number, $\mathbf{\alpha}_{\text{corr}}$ is the work-corrected cathodic transfer coefficient, and $\phi_{\mathbf{d}}$ is the potential drop across the diffuse layer. Details of this procedure are given in references 312 and 313. The KPF₆ electrolyte provides an especially suitable medium for this purpose. This is because $\phi_{\mathbf{d}}$ is small over a wide potential range positive of the potential of zero charge (-440 mV vs. s.c.e.) since the positive electronic charge density at the electrode is matched approximately by the charge density due to specifically adsorbed \mathbf{PF}_{6}^{-} anions. 313,314 The rate data in Table 6.1 all refer to acid-independent pathways. In contrast to homogeneous reactions between aquo cations, the rates of most of these reactions are independent of pH at values (<pH 2.5) below which the formation of hydroxo complexes is unimportant. The single exception is $\mathbf{V}_{\mathrm{aq}}^{3+/2+}$, which exhibits a significant inverse acid-dependent pathway at pH>1. 315

The formal potential for $Fe_{aq}^{3+/2+}$ is too positive (495 mV vs. s.c.e. in 0.4 M KPF6) to allow rate measurements in the vicinity of Ef to be made at mercury since anodic dissolution of the electrode occurs beyond about 375 mV. However, the electroreduction of Fe_{aa}^{3+} was found by Tyma 313 to be sufficiently irreversible so that cathodic d.c. and normal pulse polarograms were obtained over the potential range 300 to 0 mV, yielding values of k_{app} in 0.4 \underline{M} KPF₆ to 4 x 10⁻⁴ cm s⁻¹ at 300 mV, and 0.1 cm s⁻¹ at 0 mV vs. s.c.e. Extrapolation of the cathodic Tafel plots, (i.e. $\ln k_{app}^e$ vs. E, where k_{app}^e is the apparent cathodic rate constant), was therefore required in order to extract k_{ex}^{e} (app). However. this procedure can be applied with confidence: the workcorrected cathodic transfer coefficients α_{corr} for several other aquo couples are close to 0.50 ($^{+}$ 0.02) over a wide range of cathodic overpotentials. The observed transfer coefficient α_{app} (0.48) for Fe $_{aq}^{3+}$ reduction in 0.4 \underline{M} KPF, indicates that the potential dependence of the double-layer effects is likely to be small, as expected. Consequently, the resulting value of $k_{ex}^{e}(app)$, $2x10^{-5}$ cm s⁻¹, is likely to be within a factor of 2- to 5-fold of k_{ex}^e ; we have therefore set an upper limit of 1x10⁻⁴ cm s⁻¹ for k_{ex} in Table 6.1.

These values of k_{ex}^e (app) and k_{ex}^e are smaller than those commonly reported for $Fe_{aq}^{3+/2+}$ at platinum and gold electrodes. The allowers cathodic voltammograms that are highly irreversible (half-wave potential $E_{1/2}^{z_0}$ mV vs. s.c.e.), yielding similarly small values of k_{ex}^e (app) ($^{-10^{-5}}$ cm s⁻¹), have recently been obtained at platinum and gold in perchlorate media from which halide impurities had been rigorously excluded. The larger values of k_{ex}^e (app) are therefore

due to the presence of halide-catalyzed, possibly inner-sphere pathways. Rate measurements at dropping mercury electrodes are not susceptible to such difficulties since the surface is continuously renewed and adsorbs most anions much more weakly than do noble metals.

The electrochemical reactivities of $Fe_{aq}^{3+/2+}$ and $Ru_{aq}^{3+/2+}$ provide an interesting comparison. At the formal potential for $Ru_{aq}^{3+/2+}$ in 0.4 M KPF₆. -20 mV vs. s.c.e., the observed rate constant for electro-reduction of Fe_{aq}^{3+} is 0.15 ($^{\pm}0.05$) cm s⁻¹. This value is only moderately (30-fold) larger than that for Ru_{aq}^{3+} reduction at the same potential, $5(^{\pm}2) \times 10^{-3}$ cm s⁻¹, despite the enormous cathodic overpotential (515 mV, corresponding to an equilibrium constant of 5 x 10⁸) for the former reaction. Since these rate constants were obtained under the same conditions and the reactants are of very similar structure, the work terms should be essentially identical. Any reasonable driving force correction for Fe_{aq}^{3+} reduction therefore must yield a value of k_{ex}^{6} ca. 10^{3} -fold smaller than for Ru_{aq}^{3+} reduction, irrespective of the work term corrections upon the individual rate constants. From Equation 6.7, this results in a corresponding estimate of k_{ex}^{h} that is ca. 10^{5} -fold smaller for the former reaction (vide infra).

3. Rate Constants for Electron Exchange from Homogeneous Cross-Reaction Kinetics

Table 6.2 summarizes pertinent rate and equilibrium data for the acid-independent pathways for cross reactions involving $Fe_{aq}^{3+/2+}$, $Ru_{aq}^{3+/2+}$, $V_{aq}^{3+/2+}$, $Eu_{aq}^{3+/2+}$ and $Cr_{aq}^{3+/2+}$, together with the values of k_{ex}^h for these couples resulting from the application of Equation 6.2. The

Estimation of Work-Corrected Rate Constants $k_{\rm ex}^{\rm h}({\rm M}^{-1}~{\rm sec}^{-1})$ at 25°C for ${\rm Fe}_{\rm aq}^{3+/2^+}$, ${\rm R}_{\rm aq}^{3+/2^+}$, ${\rm V}_{\rm aq}^{3+/2^+}$, ${\rm R}_{\rm aq}^{3+/2^+}$ $\mathrm{Eu}_{aq}^{3+/2+}$, and $\mathrm{Cr}_{aq}^{3+/2+}$ Self-Exchange from Selected Cross-Reaction Data. TABLE 6.2.

Cross Reaction "	K ₁₂ ^a	$k_{12}^{h}(app)^{f}$	kh m	kh n k22	f P	kh q
Fe ³⁺ + Fe ²⁺	1.0	4(0.55)	15		1.0	15
Fe 3+ Ru 2+	5 × 10 ⁸	$2.3 \times 10^{3}(1)$	7×10^{3}	~ 20 %	0.18	$\sim 1 \times 10^{-3}$
$Fe_{aq}^{3+} + Ru(NH_3)_{5py}^{2+}$	$1.5 \times 10^7 b$	5.8×10^4 (1)	1.7×10^{5}	1.5 × 10 ⁶	0.23	6×10^{-3}
$\operatorname{Fc}_{aq}^{3+} + \operatorname{Ru}(\operatorname{NII}_3)_4 \operatorname{bpy}^{2+}$	$4.5 \times 10^3 b$	$7.2 \times 10^3 (1)^{9}$	2×10^{4}	$\sim 1 \times 10^7 \text{ K}$	0.73	1.2×10^{-2}
$\operatorname{Fe}_{aq}^{3+} + \operatorname{Co}(\mathrm{phen})_{3}^{2+}$	1.2×10^{6}	$5.3 \times 10^{2}(1)^{h}$	1.6×10^{3}	150	0.40	3.5×10^{-2}
$0s(bpy)_3^{3+} + Fe_{aq}^{2+}$	80 0	$1.4 \times 10^3 (0.5)^{i}$	3×10^{3}	$(\sim 1 \times 10^9)$	0.89	$\sim 2 \times 10^{-4}$
$Fe(bpy)_{3}^{3+} + Fe_{aq}^{2+}$	5.5×10^{5}	$2.7 \times 10^4 (0.5)^{\frac{j}{2}}$	6×10^4	$(\sim 1 \times 10^9)$	0.38	$\sim 3 \times 10^{-5}$
Fe(phen) $\frac{3}{3}$ + Fe $\frac{2}{aq}$	1.2×10^6	$3.7 \times 10^4 (0.5)^3$	1.5×10^{5}	$(\sim 1 \times 10^9)$	0.33	$\sim 5 \times 10^{-5}$
$Ru(bpy)_{3}^{3+} + Fc_{aq}^{2+}$	1.8×10^{9}	$7.2 \times 10^{5}(1)$	2 × 10 ⁶	$\sim 1 \times 10^{9}$	0.068	$\sim 3 \times 10^{-4}$
$R_{aq}^{3+} + V_{aq}^{2+}$	5.8 × 10 ⁷	$2.8 \times 10^2 (1)^d$	9 × 10 ²	3×10^{-2}	0.25	. 2
$Ru_{aq}^{3+} + Ru(NH_3)_6^{2+}$	6×10^2	$1.4 \times 10^4(1)^d$	4 × 10 ⁴	$\sim 5 \times 10^4$	0.78	7.0
$Co(phen)_3^{3+} + Ru_{aq}^{2+}$	4.2×10^2	53(1) ^d	1.5×10^{2}	150	0.78	4.0
$Ru(NH_3)_5py^{3+} + Ru_{aq}^{2+}$	35 b	$1.1 \times 10^4 (1)^d$	3.5×10^4	1.5×10^{6}	0.92	25
$Ru(NH_3)_5 i sn^{3+} + Ru^{2+}_{aq}$	6.5×10^{2}	$5.5 \times 10^4 (1)^a$	1.5 × 10 ⁵	1.5×10^{69}	0.76	30

Table 6.2 continued

$v^{3+} + v^{2+}$	1.0	$1.5 \times 10^2 (2)$	3×10^{-2}		1.0	3×10^{-2}
$v_{aq}^{3+} + Cr(bpy)_3^{2+}$	1.2 @	$4.2 \times 10^2(1)^{K}$	1×10^{3}	$(\sim 1 \times 10^9)$	1.0	1×10^{-3}
$Co(en)^{3+}_3 + v^{2+}_{aq}$	2.5	$7 \times 10^{-4}(1)$	2.5×10^{-3}	2.5×10^{-4}	1.0	6×10^{-2}
$Ru(NH_3)_{6}^{3+} + v_{aq}^{2+}$	1 × 10 ⁵	$1.5 \times 10^{3} (0.5)$	2×10^4	$\sim 5 \times 10^4$	0.49	0.15
$Co(bpy)_3^{3+} + v_{aq}^{2+}$	1.3×10^{9}	$1.1 \times 10^3(2)$	2×10^3	80	0.15	3×10^{-4}
Co (phen) $\frac{3^+}{3} + V^{\frac{2}{4}}$	2.5×10^{10}	$4 \times 10^3(1)$	1.5×10^4	150	80.0	1×10^{-3}
$Ru(NH_3)_{5}py^{3+}+\dot{v}_{aq}^{2+}$	2 × 10 ^{9 b}	3 × 10 ⁵ (1)	1 × 10 6	1.5 × 10 ⁶	80.0	4 × 10 ⁻³
$V_{30}^{3+} + Eu_{30}^{2+}$	3.5×10^{2}	$9 \times 10^{-3}(2)$	2 × 10 ⁻²	3×10^{-2}	88.0	4.5 × 10 -5
$(c)^{3+} + c^{2+}$	7.5×10^2	$\sim 5 \times 10^{-3}(1)$	$\sim 1 \times 10^{-2}$	2.5×10^{-4}	0.86	$\sim 5 \times 10^{-4}$
$Ru(NII_3)_6^3 + Eu_{aq}^2$	3.5×10^{7}	$2.3 \times 10^{3}(1)$	7×10^3	$\sim 5 \times 10^4$	0.25	1×10^{-4}
$Co(phen)\frac{3}{3} + Eu^{\frac{2}{3}}$	1.3×10^{13}	$9 \times 10^2 (1)^{-k}$	2.5×10^{3}	150	0.03	1×10^{-7}
$Ru(NII_3)_{5}py^{3+} + Eu_{aq}^{2+}$	$7 \times 10^{11} ^{b}$	$5.4 \times 10^4(1)$	1.5 × 10 ⁵	1.5 × 10 ⁶	0.03	7×10^{-7}
$\operatorname{Eu}_{aa}^{3+} + \operatorname{Cr}_{aa}^{3+}$	3.5	$\sim 2 \times 10^{-5} (0.5)$	8 × 10 ⁻⁵	2×10^{-4}	1.0	9 × 10 ⁻⁶
$Co(en)^{3+}_3 + Cr^{2+}_{au}$	2.5×10^3	$3 \times 10^{-4}(1)$	1×10^{-3}	2.5×10^{-4}	0.82	2×10^{-6}
$Ru(NII_3) \frac{3+Cr^{2+}}{6}$	1.2×10^{8}	$2 \times 10^2 (0.2)$	2×10^3	$\sim 5 \times 10^4$	0.22	3×10^{-6}
Co (phen) $\frac{3}{3} + Cr \frac{2}{3}$	6×10^{13}	33(1) h	06	150	0.03	3×10^{-11}
$Ru(NII_3)_5py^{3+} + Cr_{aq}^{2+}$	$2.5 \times 10^{12} ^{b}$	$3.4 \times 10^3(1)$	1 × 10 ⁴	1.5 × 10 ⁶	0.10	3×10^{-10}
Notes to Table 6.2 on the following page.	following page.				THE PLANE STREET, STREET, ST. STR. ST. ST. ST. ST. ST. ST. ST. ST. ST. ST	7 # 4 4 7 7 9 8 8 8 7 1 7 1 8 8 8 9 9

Notes to Table 6.2

after correction for work terms as outlined in reference 311. n Work-corrected value of k for coreactant, values of K₁₂, k_{12}^n , k_{22}^n using Equation 6.1 p ps = pyridine, en = ethylenediammine, bpy = 2,2'-bipyridine, and $\mathbf{E}_{ox}^{\mathbf{f}}$ are the formal potentials of the redox couples undergoing reduction and oxidation respectively in s-1) are estimated (see text). ^{o}F rom this work. p Quadratic driving force factor, defined by Equation 6.16. qWork-corrected rate constant for self exchange of aquo redox couple, obtained from corresponding ^bFrom reference 84. c E for Os(bpy) $_{3}^{3+/2+}$ = 619 mV vs. s.c.e., μ = 0.1 (reference 386) d From (reference listed cross reaction at 25°C and ionic strength given in parentheses. Values taken from sources quoted 334. ⁷From reference 335. ^kReference 310. ^lFrom reference 360. ^mRate constant for cross reaction, in reference 311 unless otherwise stated. $^g\mathrm{From}$ reference 321. $^h\mathrm{From}$ reference 337. $^i\mathrm{From}$ reference a Formal equilibrium constant for cross reaction. Calculated from lnK $_{12}$ = (F/RT)($^{\mathrm{f}}_{\mathrm{red}}$ - $^{\mathrm{f}}_{\mathrm{ox}}$), where $^{\mathrm{f}}_{\mathrm{red}}$ taken from reference 311 unless otherwise noted. Values for low-spin M(bpy) $\frac{3+/2+}{3}$ couples (1 x 10 M⁻¹ e E for Cr(bpy) $^{3+/2+}$ = -480 mV vs. s.c.e., μ = 0.1 (reference 253) f Measured rate constant for the range of ionic strengths (μ =0.2-1) employed for the kinetics measurements. Values of ${
m E}^{
m f}$ for aquo couples given in Table 6.1; values for other couples taken from reference 55 unless otherwise noted. phen = 1,10-phenanthroline, isn = isonicotinimide. rate constants for the cross reactions, k_{12}^h , and for self exchange of the various coreactants, k_{22}^{h} , listed in Table II are taken from literature data; they are corrected for Debye-Huckel work terms as described in reference 311 (see the footnotes to Table 6.2 and reference 311 for the data sources). The measured values of k_{12}^h , k_{12}^{h} (app), are also listed, with the ionic strength at which they were determined in parentheses. The equilibrium constants K12 given in Table 6.2 were obtained from measurements of formal potentials for the appropriate redox couples at ionic strengths comparable (0.1 $<\mu<1$) to those at which the kinetic data were gathered. (Most of these formal potentials were obtained in our labotatory using cyclic voltammetry. The uniform use of these data avoids the substantial errors that can arise if literature electrode potential values gathered under disparate conditions are employed to calculate K_{12} , as is commonly done.) Although values of k for some of the polypyridine redox couples utilized in Table 6.2 [Fe(bpy) $_{3}^{3+/2+}$, Fe(phen) $_{3}^{3+/2+}$, Os(bpy) $_{3}^{3+/2+}$, and $Cr(bpy)_3^{3+/2+}$ (bpy = 2,2'bipyridine, phen = 1, 10-phenanthroline)] have not been determined, they are assumed to be comparable to that obtained for Ru(bpy) $_3^{3+/2+}$, ca. 1 x 10⁹ \underline{M}^{-1} . 310,317 The inner-shell reorganization energy for all these couples are likely to be close to zero since they uniformly involve the transfer of a delocalized $t_{2\sigma}$ electron.310

Detailed inspection of Table 6.2 reveals that work-corrected values of $k_{\rm ex}^{\rm h}$ are obtained for each aquo redox couple that are reasonably constant (mostly within ca. tenfold of each other), at least using cross reactions having relatively small driving forces (say K_{12} <1 x

 10^6 , f>0.2). There are good reasons to prefer such weakly excergic cross reactions for extracting values of $k_{\rm ex}^{\rm h}$ using Equation 6.2. The assumptions made in deriving Equation 6.2 that the reactions are adiabatic (κ =1), the work terms are nonspecific and the reactant and product free energy profiles are harmonic are questionable, especially for reactions involving aquo cations. However, these factors have only a minor influence upon its applicability for reactions having small driving forces providing that the work terms and are comparable for the corresponding self-exchange and cross reactions. 310,311 Indeed, progressively smaller estimates of $k_{\rm ex}^{\rm h}$ are generally determined using Equation 6.1 from cross reactions having increasingly large driving forces. These discrepancies have been attributed to the influence of unfavorable specific work terms, 311 anharmonicity. 249 and nonadiabaticity. 310

The extraction of relative values of $k_{\rm ex}^{\rm h}$ for $V_{\rm aq}^{3+/2+}$, $Eu_{\rm aq}^{3+/2+}$, and $Cr_{\rm aq}^{3+/2+}$ is facilitated by the proximity of the formal potentials for these couples (-472 mV, -625 mV, and -655 mV vs. s.c.e., μ = 0.5, Table 6.1). Thus especially reliable values of $k_{\rm ex}^{\rm h}$ can be determined from cross reactions with similarly small driving forces involving common coreactants having known self-exchange kinetics. Suitable oxidants for this purpose are $Co(en)_3^{3+}$, $Ru(NH_3)_6^{3+}$. $V_{\rm aq}^{3+}$. Careful inspection of Table 6.2 yields average values of $k_{\rm ex}^{\rm h}$ for $V_{\rm aq}^{3+/2+}$, $Eu_{\rm aq}^{3+/2+}$, and $Cr_{\rm aq}^{3+/2+}$ of ca. $5(^{+}4) \times 10^{-2}$, $2(^{+}1.5) \times 10^{-4}$, and $2 \times 10^{-6} \, {\rm M}^{-1} \, {\rm s}^{-1}$, respectively.

The estimation of k_{ex}^h for $Ru_{aq}^{3+/2+}$ self exchange in the same manner is slightly less straightforward on account of the more positive

formal potential for this couple (-20 mV vs. s.c.e., μ = 0.4, Table 6.1). Values of $k_{\rm ex}^{\rm h}$ obtained from suitable cross reactions (f>0.2), involving $V_{\rm aq}^{2+}$, ${\rm Ru(NH_3)}_6^{2+}$, ${\rm Co(phen)}_3^{3+}$ ${\rm Ru(NH_3)}_5{\rm py}^{3+}$, and ${\rm Ru(NH_3)}_5{\rm isn}^{3+}$ as coreactants, vary by a factor of almost 200 (Table 6.2). However, the relatively low value $(0.4~{\rm M}^{-1}~{\rm s}^{-1})$ obtained using ${\rm Co(phen)}_3^{3+}$ is also characteristic of cross reactions involving this oxidant with $V_{\rm aq}^{2+}$, ${\rm Eu}_{\rm aq}^{2+}$, and ${\rm Cr}_{\rm aq}^{2+}$ (Table 6.2). Also, the estimate of $k_{\rm ex}^{\rm h}$ obtained from the ${\rm Ru}_{\rm aq}^{3+} - V_{\rm aq}^{2+}$ reaction $(2~{\rm M}^{-1}~{\rm s}^{-1})$ is likely to be too small since the free energy barrier for $V_{\rm aq}^{2+}$ oxidation appears to respond to changes in driving force to a noticeably smaller extent than predicted from Equation 6.2. The remaining cross reactions yield a reasonably consistent estimate of $k_{\rm ex}^{\rm h}$ for ${\rm Ru}_{\rm aq}^{3+/2+}$ of ca. ${\rm 50(\frac{+20}{20})}{\rm M}^{-1}~{\rm s}^{-1}$. (A somewhat larger estimate of $k_{\rm ex}^{\rm h}$, ca. 200 ${\rm M}^{-1}~{\rm s}^{-1}$, was arrived at previously from related arguments, 319 but involving extrapolation of values of $k_{\rm ex}^{\rm h}$ obtained from cross reactions having highly varying driving forces. 304

The "observed" value of $k_{\rm ex}^{\rm h}$ for $V_{\rm aq}^{3+/2+}$, $3 \times 10^{-2} \, {\rm M}^{-1} \, {\rm s}^{-1}$, (i.e. that obtained directly from the observed self-exchange kinetics) is close to the estimates obtained from cross reactions with ${\rm Co(en)}_3^{3+}$ and ${\rm Ru(NH_3)}_6^{3+}$. In contrast, the "observed" value of $k_{\rm ex}^{\rm h}$ for ${\rm Fe}_{\rm aq}^{3+/2+}$, 15 ${\rm M}^{-1} \, {\rm s}^{-1}$. is considerably (10⁴- to 10⁵ fold) larger than those derived from cross reactions having suitably small driving forces (f>0.2) (Table 6.2). Equation 6.1 can be rewritten as

$$\log k_{12}^{h} = 0.5(\log k_{11}^{h} + \log k_{22}^{h}) + 0.5 \log K_{12} + (\log K_{12})^{2}$$

$$4 \log(k_{11}^h k_{22}^h / A_h^2)$$
 (6.8)

Figure 6.1. Plot of (2 log k_{12}^h - log k_{22}^h) vs. $[\log K_{12} + (\log K_{12})^2]$ 4 log $(k_{11}^h k_{22}^h/Z_h^2)$] for homogeneous cross reactions involving $Fe_{aq}^{3+/2+}$, calculated as Fe_{ad}^{2+} oxidations. k_{ex}^{h} for low spin M(III)/(II) polypyridines taken as 1 x 10⁹ \underline{M}^{-1} sec⁻¹ (see text). k_{11}^{h} refers to $Fe_{aq}^{3+/2+}$ self exchange; k_{22}^{h} to self exchange for coreactant couples. Z_{h} assumed to equal 1 x 10^{12} $\underline{\mathbf{M}}^{-1}$ sec⁻¹; value of \mathbf{k}_{11}^{h} required for plot obtained by iteration: \mathbf{k}_{11}^{h} = $10^{-3} \ \underline{\text{M}}^{-1} \ \text{sec}^{-1}$. Data sources given in Table 6.2 or reference 311 unless otherwise stated. Closed points refer to cross reactions; open point to "observed" Fe $_{aq}^{3+/2+}$ self exchange. Key to oxidants: 1. Ru $_{aq}^{3+}$; 2. Eu $_{aq}^{3+}$; 3. $\operatorname{Cr}_{aq}^{3+}$; 4. $\operatorname{U}_{aq}^{4+}$; 5. $\operatorname{V}_{aq}^{3+}$; 6. $\operatorname{Ru}(\operatorname{NH}_3)_6^{3+}$; 7. $\operatorname{Ru}(\operatorname{en})_3^{3+}$; 8. $\operatorname{Ru}(\operatorname{NH}_3)_5\operatorname{py}^{3+}$; 9. $Ru(bpy)_{3}^{3+}$; 10. $Ru(NH_{3})_{5}nic^{3+}$, reference 320; 11. $Ru(NH_{3})_{5}isn^{3+}$; 12. Ru(NH₃)₄bpy³⁺, reference 310; 13. Os(bpy)₃³⁺, reference 334; 14. Fe(bpy) $_{3}^{3+}$, reference 335; 15. Fe(phen) $_{3}^{3+}$, reference 336; 16. Co(phen) $_{3}^{3+}$, reference 337; [17-19 from reference 330]; 17. Ru(terpy) $_{2}^{3+}$; 18. Ru(phen) $_{3}^{3+}$; 19. Ru(bpy) $_{2}^{2}$ (py) $_{2}^{3+}$; [20-23 from reference 338] 20. $Os[5,5'-(CH_3)_2bpy]_3^{3+}$; 21. $Os(phen)_3^{3+}$; 22. $Os(5-C1-phen)_3^{3+}$; 23. Ru[5,5'-(CH₃)₂bpy] $_3^{3+}$; [24-31 from reference 339]; 24. $Ru[3,4,7,8-(CH_3)_{\Delta}phen]_3^{3+}$; 25. $Ru[3,5,6,8-(CH_3)_{\Delta}phen]_3^{3+}$; 26. $Ru[4,7-(CH_3)_2phen]_3^{3+}$; 27. $Ru[4,4'-(CH_3)_2ppy]_3^{3+}$; 28. $Ru[5,6-(CH_3)_2 phen]_3^{3+};$ 29. $Ru(5-CH_3 phen)_3^{3+};$ 30. $Ru(5-C_6 H_5 phen)_3^{3+};$ 31. Ru(5-C1-phen) $_{3}^{3+}$; 32. Fe $_{20}^{2+}$.

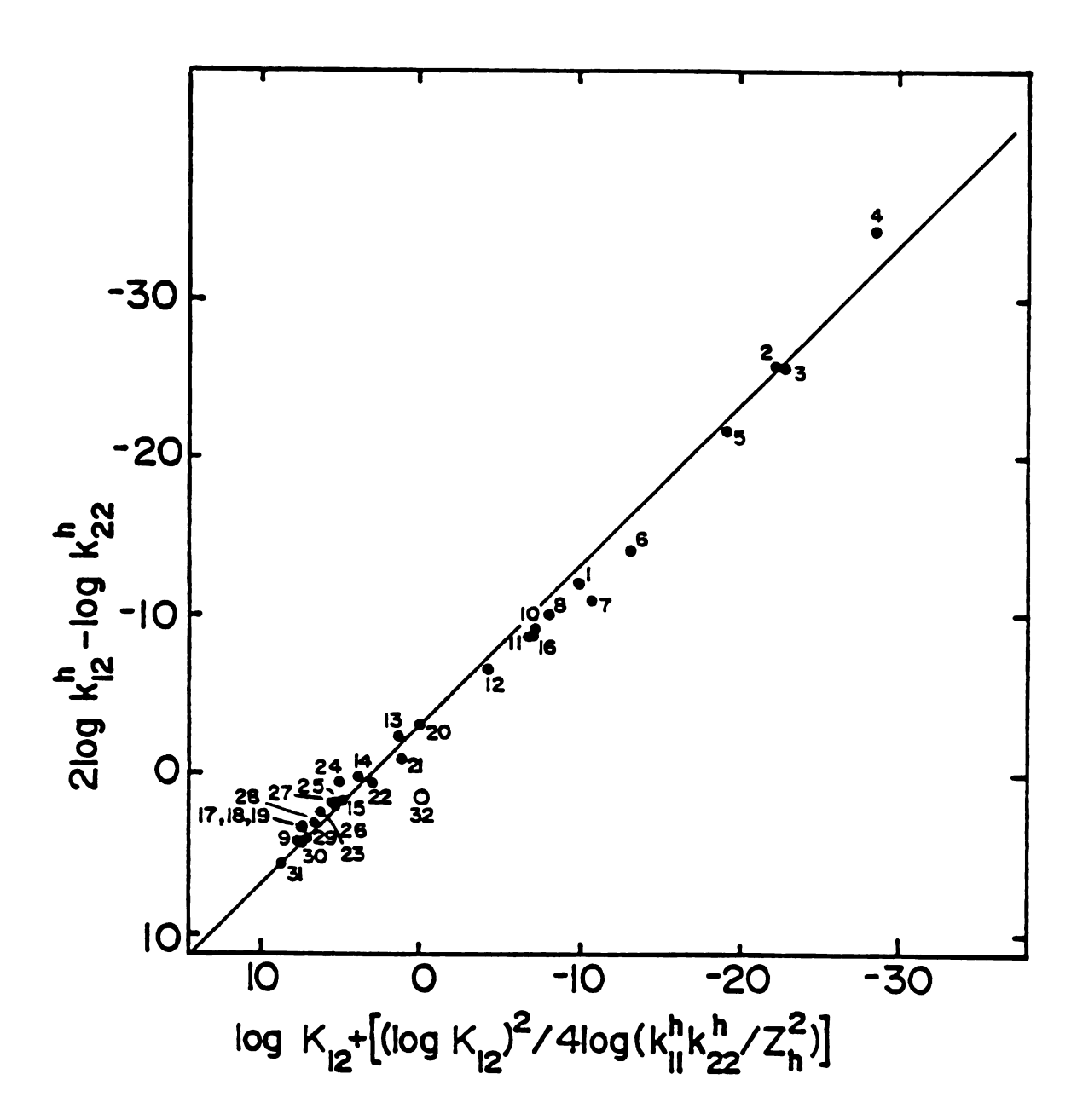


Figure 6.1

Therefore a plot of (2 log k_{12}^h - log k_{22}^h) vs. $[\log K_{12} + (\log K_{12})^2/4]$ $\log(k_{11}^h k_{22}^h/A_h^2)$] should yield a straight line of slope 1.0 with an intercept equal to $log k_{11}^h$. Figure 6.1 shows such a plot for 32 reactions involving $Fe_{aq}^{3+/2+}$, formally expressed as Fe_{aq}^{2+} oxidations. (The data sources are summarized in the footnotes; A, is assumed to equal 1 x 10^{12} M⁻¹ s⁻¹. The value of k_{11}^h in the last term in Equation 6.8 was obtained by iteration; for most reactions choosing any reasonable value of k_{11}^h in the range ca. 10^{-4} to $10 \text{ M}^{-1} \text{ s}^{-1}$ led to essentially identical results.) The straight line of slope 1.0 in Figure 6.1 provides the best fit to the solid points which refer to the cross reactions. The intercept, which equals $\log k_{ex}^{h}$ for $Fe_{aq}^{3+/2+}$, corresponds to $k_{ex}^{h} = 7 \times 10^{-4} \, \underline{\text{M}}^{-1} \, \text{s}^{-1}$. The open point, which refers to the "observed" value of k_{ex}^{h} (15 \underline{M}^{-1} s⁻¹), is clearly at variance with the other points; yielding a discrepancy of over 104 -fold in kh. Figure 6.2 shows a similar plot for cross reactions involving $v_{aq}^{3+/2+}$. Although the data points are less numerous, the open point for $V_{ad}^{3+/2+}$ self exchange ($k_{ex}^{h} = 3 \times 10^{-2} \, \underline{M}^{-1} \, s^{-1}$) is consistent with the remaining entries. Admittedly, the slope (0.9) of the best fit line in Figure 6.2 differs somewhat from unity; possible causes are discussed elsewhere. 249

Such a behavioral difference between $V_{\rm aq}^{3+/2+}$ and $Fe_{\rm aq}^{3+/2+}$ has been noted previously. The striking discrepancies with Equation 6.2 for $Fe_{\rm aq}^{3+/2+}$ were ascribed in part to especially facile reaction pathways for self exchange of the cross-reaction partners that contain pyridinetype ligands arising from interpenetration of the pyridine rings. Since such interactions will be absent for the $Fe_{\rm aq}^{3+/2+}$ cross reactions,

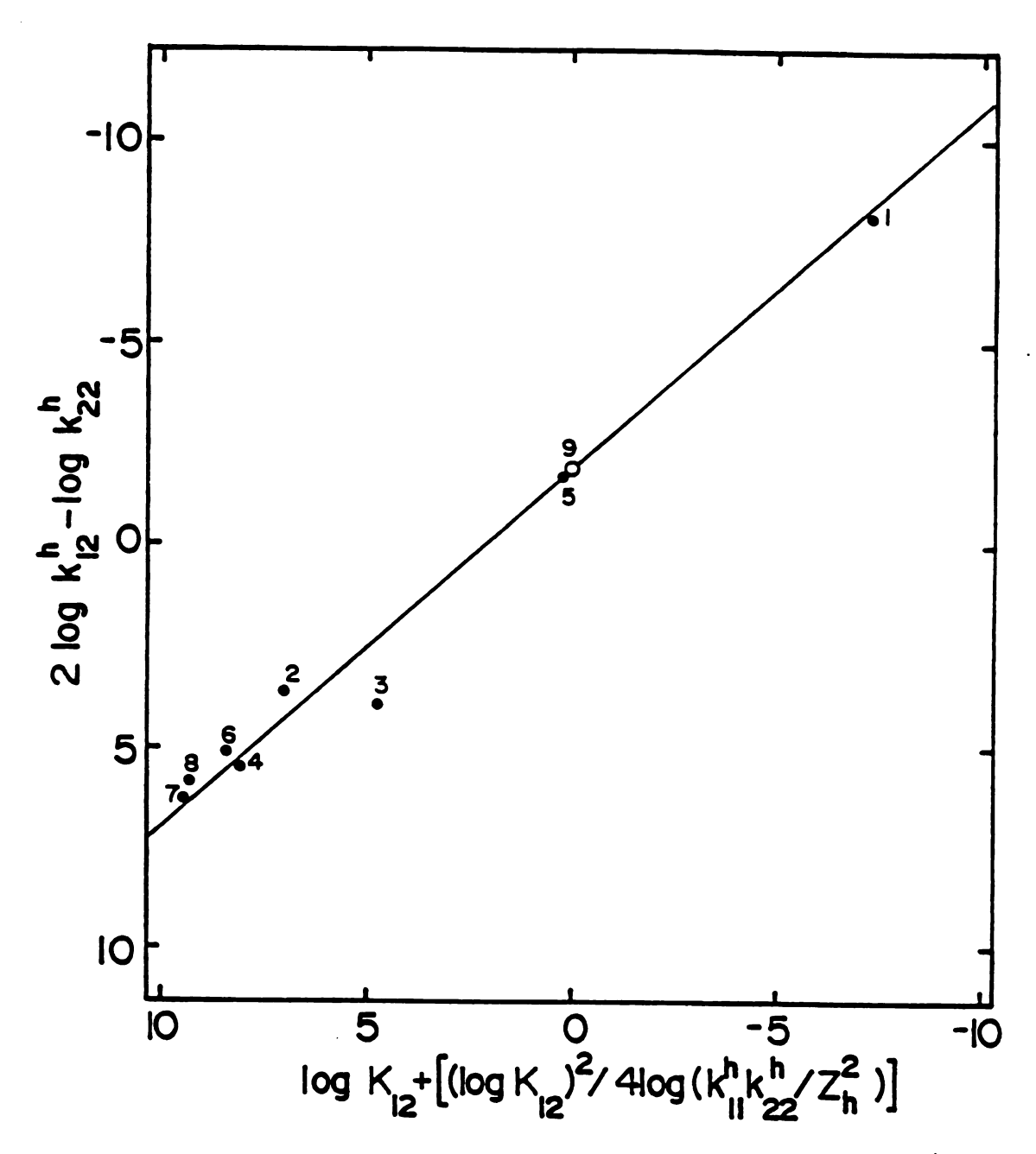


Figure 6.2 As for Figure 6.1 but for cross reactions involving $V_{aq}^{3+/2+}$, expressed as V_{aq}^{2+} oxidations; k_{11}^{h} refers to $V_{aq}^{3+/2+}$ self exchange. Data sources From Table 6.2 or reference 311 unless otherwise stated. Key to oxidants: 1. U_{aq}^{4+} ; 2. Ru_{aq}^{3+} ; $Ru(NH_3)_{6}^{3+}$; 4. $Ru(NH_3)_{5}^{py}$; 5. $Co(en)_{3}^{3+}$; 6. $Co(bpy)_{3}^{3+}$; 7. $Ru(NH_3)_{5}^{1sn}$, reference 321; 8. $Co(phen)_{3}^{3+}$; 9. V_{aq}^{3+} .

the resulting estimates of k_{ex}^h for $Fe_{aq}^{3+/2+}$ (ca. 10^{-4} to 10^{-3} M s⁻¹) were considered to be falsely small, the observed self-exchange rate constant being presumed to reflect a "normal" outer-sphere pathway. 310

A difficulty in comparing data for cross reactions involving $Fe_{ac}^{3+/2+}$ with the other aquo couples is that the formal potential for $Fe_{ac}^{3+/2+}$ is substantially more positive of those for the remaining aquo couples. Therefore cross reactions having suitably small driving forces inevitably involve different coreactants with the likelihood that systematic errors in the applicability of Equations 6.1 could occur. These errors could vitiate its use for obtaining even relative values of the self-exchange kinetics of $Fe_{aq}^{3+/2+}$ with respect to the other couples. However, the comparison of the kinetics of the $0s(bpy)_3^{3+}-Fe_{aq}^{2+}$ and $V_{aq}^{3+}-Cr(bpy)_3^{2+}$ cross reactions provides a way of circumventing this problem. Both these reactions have suitably small driving forces [equilibrium constants of 80 and 1.2, respectively (Table 6.2)] and the coreacting redox couples, $0s(bpy)_3^{3+/2+}$ and $Cr(bpy)_3^{3+/2+}$, have not only the same ligand composition but are also likely to have similarly small barriers to electron exchange since they both involve electron acceptance into a delocalized t_{2g} orbital. 310 Assuming therefore that the rate constants for $0s(bpy)_3^{3+/2+}$ and $Cr(bpy)_3^{3+/2+}$ self exchange, k_{22} and k_{44} , are equal and noting that the f terms are essentially unity, the ratio of the rate constants for $Fe_{aq}^{3+/2+}$ and $V_{aq}^{3+/2+}$ self exchange, $k_{ex,Fe}^h/k_{ex,V}^h$, can be found from the kinetics and thermodynamics data for the corresponding cross reaction using [cf. Equation 6.1]:

Summary of Rate Constants for Electron Exchange at 25°C, and Comparison with Theoretical Predictions. Table 6.3.

${ m \Delta s^{0}_{rc}}$ J deg $^{-1}$ mol $^{-1}$	150		155	180	200	205
$k_{\mathbf{ex}}^{\mathbf{h}}(\mathbf{calc})^d$ $\underline{\underline{\mathbf{M}}}^{-1} = 1$	2.5 x 10 ⁵	(1)		$^{90}_{(3.5 \times 10^{-4})}$		$\begin{array}{ccc} 1 & \times & 10^{-4} \\ (4 & \times & 10^{-10}) \end{array}$
$k_{\mathbf{e}\mathbf{x}}^{\mathbf{h}}(6.7)$ ° $\frac{\sigma}{\mathbf{M}^{-1}}$ \mathbf{a}^{-1}	25	(1)	6×10^{-2} (2.5×10 ⁻³)	$\begin{array}{l} \text{$\leq$ \times 10^{-4}$} \\ \text{$(\sim3\times10^{-5})$} \end{array}$	${4 \times 10^{-4} \atop (1.5 \times 10^{-5})}$	2.5×10^{-7} (1 x 10 ⁻⁸)
$\ker_{\mathbf{ex}} b$ $\underbrace{\mathbb{A}^{-1}}_{\mathbf{g}^{-1}}$	50	(1)	$5 \times 10^{-2} (3 \times 10^{-2})$ $(1 \times 10^{-3}), (6 \times 10^{-4})$	1 x10 $^{-3}$, [15] (2 x10 $^{-5}$), (0 3)	$\begin{array}{ccc} 2 \times 10^{-4} \\ (4 \times 10^{-6}) \end{array}$	$\begin{array}{ccc} 2 \times 10^{-6} \\ (4 \times 10^{-8}) \end{array}$
$k = \alpha$ $k = \alpha$ $cm s = 1$	2×10^{-2}		1×10^{-3}	≤1 x 10 ⁻⁴	8×10^{-5}	2 x 10 ⁻⁶
Redox Couple	3+/2+ Ru aq		v ^{3+/2+} aq	3+/2+ Fe aq	3+/2+ Eu aq	3+/2+ Cr aq

b Average work-corrected rate constant for homogeneous self exchange, determined from cross-reaction data (Table 6.2) using Equation 6.1 (see text). Values for V_{aq}^{4} and $\mathrm{Fead}_{aq}^{4}/2^{4}$ in brackets obtained "directly" from self-exchange kinetics. Values in parentheses underneath are ratios of $k_{\rm Ex}^{\rm h}$ with respect to that for $^{\mathcal{Q}}$ Work-corrected rate constant for electrochemical exchange at mercury-aqueous interface; from Table 6.1.

Ru $^{37/47}$. Estimates of $k_{\rm ex}^{\rm in}$ from corresponding values of $k_{\rm ex}$ using Equation ... Values in parentheses 3.5 x $_{\rm in}$ $_{\rm in}$ sec $_{\rm in}$, $_{\rm in}$ = 1 x $_{\rm in}$ sec $_{\rm in}$ and $_{\rm in}$ $_{\rm in}$ sec $_{\rm in}$, $_{\rm in}$ $_{\rm in}$ sec $_{\rm in}$ $_{\rm$ $^{\mathcal{C}}$ Estimates of k_{ex}^{h} from corresponding values of k_{ex}^{e} using Equation 6.6 assuming that k_{n}^{e} 3+/2+

$$k_{ex,Fe}^{h}/k_{ex,V}^{h}(\equiv k_{11}/k_{33}) = (k_{12})^{2}k_{44}K_{34}/(k_{34})^{2}k_{22}K_{12}$$
 (6.9)

Inserting the experimental values $k_{12} = 3 \times 10^3 \, \underline{\text{M}}^{-1} \, \text{s}^{-1}$, $k_{34} = 1 \times 10^3 \, \underline{\text{M}}^{-1} \, \text{s}^{-1}$, $k_{12} = 80$, $k_{34} = 1.2$ (Table 6.2), into Equation 6.9 yields $k_{\text{ex,Fe}}^{\text{h}}/k_{\text{ex,V}}^{\text{h}} = 0.14$. Taking $k_{\text{ex,V}}^{\text{h}}$ to be $5 \times 10^{-2} \, \underline{\text{M}}^{-1} \, \text{s}^{-1}$ (vide supra) yields the result $k_{\text{ex,Fe}}^{\text{h}} = 7 \times 10^{-3} \, \underline{\text{M}}^{-1} \, \text{s}^{-1}$. This value of k_{ex}^{h} for k_{ex}^{h} is again over k_{ex}^{h} and k_{ex}^{h} is again over k_{ex}^{h} in the k_{ex}^{h} is again.

4. Comparison Between Electrochemical and Homogeneous Exchange Kinetics

Strong evidence supporting the validity of such smaller estimates of $k_{\rm ex,Fe}^{\rm h}$ is obtained from the rate constants for electrochemical exchange, $k_{\rm ex}^{\rm e}$. Table 6.3 contains a summary of the "best fit" values of $k_{\rm ex}^{\rm e}$ and $k_{\rm ex}^{\rm h}$ for each redox couple, along with estimates of $k_{\rm ex}^{\rm h}$, $k_{\rm ex}^{\rm h}$ (Equation 6.6), obtained from the corresponding values of $k_{\rm ex}^{\rm e}$ using Equation 6.6. The values given in parentheses are ratios of $k_{\rm ex}^{\rm h}$ and $k_{\rm ex}^{\rm h}$ (Equation 6.6) with respect to those for $Ru_{\rm aq}^{3+/2+}$, $(k_{\rm ex}^{\rm h}/k_{\rm ex,Ru}^{\rm h})$. The frequency factors $A_{\rm h}$ and $A_{\rm e}$ required in Equation 6.6 were estimated from an "encounter preequilibrium" model 10 , 18 , 186 , 323 using the expressions $A_{\rm h} = 4\pi N r_{\rm h}^2 \delta r_{\rm h} v_{\rm n}/10^3$ and $A_{\rm e} = \delta r_{\rm e} v_{\rm n}$, 186 where N is Avogadro's number, $r_{\rm h}$ is the average distance between the homogeneous redox centers in the transition state, $\delta r_{\rm h}$ is the approximate range of encounter distances ("reaction zone thickness") within which electron transfer occurs, $\delta r_{\rm e}$ is the corresponding reaction zone thickness close to the electrode surface, and $v_{\rm n}$ is the effective nuclear activation

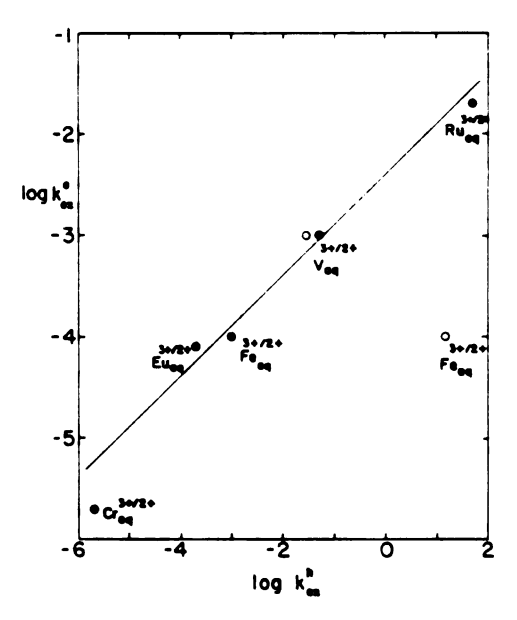


Figure 6.3. Comparison of rate constants for electrochemical exchange at mercury-aqueous interface, k_{ex}^e (cm sec⁻¹), with corresponding rate constants for homogeneous self exchange, k_{ex}^h (\underline{M}^{-1} sec⁻¹), taken from Table 6.3. Closed points refer to values of k_{ex}^h obtained from homogeneous cross reactions; open points to those obtained from measured self-exchange kinetics. The straight line is the relationship between log k_{ex}^e and log k_{ex}^h expected from Equation 6.6.

frequency.²³ Inserting the anticipated values $r_h = 7R$, $\delta r_h = \delta r_e$ 1R, 10 , 186 $v_n = 1 \times 10^{13}$ s⁻¹ for the present aquo couples¹⁰, 23 into these expressions yields $A_h = 3.5 \times 10^{12}$ M^{-1} s⁻¹ and $A_e = 1 \times 10^5$ cm s⁻¹. The value of C in Equation 6.6 was estimated to be 3.0 kcal. mol⁻¹ by inserting the values $R_h = 7R$, $R_e = 13R^{324}$ into Equation 6.5. (Note that although there is some uncertainty in the appropriate absolute values of both R_h and R_e , this partially cancels in Equation 6.5).

The absolute as well as relative values of $k_{\rm ex}^h$ (Equation 6.6) are seen to be uniformly in good agreement with those values of $k_{\rm ex}^h$ (Equation 6.6) obtained from homogeneous cross reactions. This is also illustrated in Figure 6.3 as a plot of log $k_{\rm ex}^e$ against log $k_{\rm ex}^h$. The straight line represents the correlation predicted from Equation 6.6. The solid points refer to values of $k_{\rm ex}^h$ obtained from cross reactions, and the open circles represent the values of $k_{\rm ex}^h$ for $V_{\rm aq}^{3+/2+}$ and $F_{\rm ex}^{3+/2+}$ obtained from the self-exchange kinetics. Although all the other entries are consistent with this correlation, that obtained from the $F_{\rm ex}^{3+/2+}$ self-exchange kinetics is again about 10^4 -fold larger than expected.

5. Correlation of Intrinsic Barriers with Reactant Structure

As noted above, it is instructive to compare the variations in the experimental values of k_{ex}^h and k_{ex}^e with the structural properties of the redox couples. To a certain extent, the observed reactivity sequence $Ru_{aq}^{3+/2+} > V_{aq}^{3+/2+} > Fe_{aq}^{3+/2+} > Eu_{aq}^{3+/2+} > Cr_{aq}^{3+/2+}$ is consistent with structural expectations; the three most reactive couples all

involve the acceptance of the transferring electron into a t_{2g} orbital for which the required distortions of the metal-ligand geometry, and hence ΔG_{is}^{\star} , are anticipated to be relatively small.³⁰⁹

It is stressed that the calculations to follow are only approximate, with more detailed calculations to appear in Chapter VII. The primary purpose here is to discover the relative reactivity sequence that is predicted by electron-transfer theory on the basis of structural information. The absolute values of calculated rate constants may well be in error by one to three orders of magnitude due to uncertainties in the values of critical parameters (e.g. metal-ligand stretching force constants) as well as to simplifications introduced in the calculations. Nevertheless, such calculational errors should be closely similar for each redox couple, so that a useful prediction concerning the sequence of reactivity can still be obtained.

The calculation of ΔG_{1s}^{*} and hence k_{ex}^{h} or k_{ex}^{e} from electron-transfer theory requires quantitative information on the changes in the metal-ligand bond distances, Δa . accompanying electron transfer. 13,23 Although sufficiently reliable determinations of Δa are sparse, recent X-ray diffraction measurements have established values for $Ru(0H_2)_6^{3+/2+}$ and $Fe(0H_2)_6^{3+/2+}$ of 0.09 R^{11} and 0.14 $R^{325,326}$ respectively. An effective value of Δa for $Cr(0H_2)_6^{3+/2+}$ equal to 0.20 R^{11} has also been determined from solution EXAFS measurements. R^{10} The relation R^{23}

$$\Delta G_{is}^* = nf_2 f_3 (\Delta a)^2 / 2(f_2 + f_3)$$
 (6.10)

where n is the number of metal-ligand bonds involved (six) and f₂ and f, are the metal-ligand force constants in the divalent and trivalent oxidation states, assuming that the corresponding metal-oxygen stretching frequencies are 390 cm⁻¹ and 490 cm⁻¹, respectively, yields values of ΔG_{is}^* of 14.6, 35 and 72 kJ mol⁻¹ for $Ru_{aq}^{3+/2+}$ $Fe_{aq}^{3+/2+}$, and $Cr_{aq}^{3+/2+}$, respectively. Errors in these values may arise both from anharmonicity of the potential-energy surfaces as well as from uncertainties in the appropriate force constants. The effective values of $\Delta G_{i,a}^{\star}$ are slightly smaller as a result of nuclear tunneling 23; the nuclear tunneling factors, Γ_n , of 1.5, 2 and 6 for $Ru_{aq}^{3+/2+}$, $Fe_{aq}^{3+/2+}$, and $Cr_{aq}^{3+/2+}$, respectively, 10,23 yield effective values of ΔG_{is}^* equal to 13.6, 33.5 and 67.4 kJ mol⁻¹, respectively. The outer-shell contribution to ΔG_{ex}^{*} , ΔG_{ox}^{*} , can be estimated from Equation 6.4a again using the values a = 3.5 %, $R_h = 7 \text{ Å yields } \Delta G_{08}^{*} = 27 \text{ kJ mol}^{-1}$. Inserting the resulting estimates of ΔG_{ex}^{*} into Equation 6.2 along with the above estimate of A_{h} , 3.5 x $10^{12} \ \underline{\text{M}}^{-1} \ \text{s}^{-1}$, and assuming that $\kappa = 1$ yields the calculated values of k_{ex}^{h} , k_{ex}^{h} (calc), listed in Table 6.3. Ratios of k_{ex}^{h} (calc) with respect to that for $Ru_{aq}^{3+/2+}$ $(k_{ex}^h/k_{ex,Ru}^h)$ (calc), are also listed in parentheses in Table 6.3 alongside the corresponding experimental rate ratios.

For all three couples it is seen that $k_{\rm ex}^{\rm h} < k_{\rm ex}^{\rm h} ({\rm calc})$, the calculated values being about 3-4 orders of magnitude larger than both $k_{\rm ex}^{\rm h}$ and $k_{\rm ex}^{\rm h}$ (Equation 6.6). The "observed" value of $k_{\rm ex}^{\rm h}$ for ${\rm Fe}_{\rm aq}^{3+/2+}$ self exchange, $k_{\rm ex,Fe}^{\rm h}$. is substantially closer to $k_{\rm ex,Fe}^{\rm h}$ (calc), which might be viewed as evidence that this value corresponds more closely to the "true" intrinsic barrier for ${\rm Fe}_{\rm aq}^{3+/2+}$. Nowever, the overriding evidence suggests otherwise. Thus the calculated rate ratio,

 $(k_{\rm ex,Fe}^{\rm h}/k_{\rm ex,Ru}^{\rm h})_{\rm calc}$, for the Fe $_{\rm aq}^{3+/2+}$ versus Ru $_{\rm aq}^{3+/2+}$ couples (3.5 x 10^{-4}) is roughly comparable to the corresponding experimental rate ratio obtained from cross reactions (2 x 10^{-5}) and electrochemical reactivities (3 x 10^{-5}), but substantially smaller than that obtained using the "observed" value of $k_{\rm ex,Fe}^{\rm h}$ (0.3) (Table 6.3).

Recent calculations suggest that the $Fe_{\underline{a}\underline{a}}^{3+/2+}$ self-exchange reaction is significantly nonadiabatic (< 0.01) at the normal ion-ion "contact" distance of 6.9 A. 14.15 although some overlap of the reactant cospheres seems feasible. 15.17 Since the values of κ will depend upon the extent of electronic coupling with the coreactants, and hence upon the electronic and ligand structure, such nonadiabaticy (<<< 1) may account for some disparities in k_{ex}^h obtained using different coreactants; for example, the low values obtained here using $Co(phen)_3^{3+/2+}$ (<u>vide supra</u>). Nevertheless, although nonadiabatic effects could account in part for the discrepancies between k_{ex}^h and k_{ex}^{h} (calc), their inclusion is unlikely to increase the ratio (k ex.Fe/k ex.Ru) calc since the 4d ruthenium orbitals are more likely to couple effectively than the more compact 3d iron orbitals, thereby yielding larger values for the $Ru_{aq}^{3+/2+}$ reactions. Consequently, the rate ratio $k_{ex,Fe}^{h}/k_{ex,Ru}^{h}$ (0.3) obtained from the $Fe_{aq}^{3+/2+}$ self-exchange kinetics is not consistent with these theoretical expectations.

It might be argued that the discrepancies k_{ex}^h (Equation 6.6) < k_{ex}^h (calc) arise at least in part from nonadiabaticity of the electrochemical reactions, especially since current physical models of the double layer suggest that the reactant-electrode distance at the plane of closest approach may be approximately the same as the distance

separating the reacting pair in homogeneous outer-sphere reactions. 178,221,312 Although such reactions may be marginally nonadiabatic, it is unlikely that < <<1. Thus the frequency factors determined from the temperature dependence of rate constants at mercury are not especially anomalous. 18,249 The $Cr_{aq}^{3+/2+}$ electrochemical exchange reaction at mercury has been ascertained to be only marginally nonadiabatic, $\kappa \approx 0.2$ -0.5. from a comparison with the rates of closely related inner-sphere electrode reactions (Section IV. C). Even if the electrochemical as well as the homogeneous reactions are indeed nonadiabatic, the k values would appear to be roughly (to within, say, a factor of ten) independent of a reaction environment for each redox couple in order to account for the consistently good agreement with the predictions of Equations 6.1 and 6.6. Since κ is expected to be sensitive to the nature of the donor and acceptor orbitals in each reactant pair. this implies that k is unlikely to lie below circa 10⁻³, especially in view of the variety of orbital symmetries (t_{2g}, e_{g}, f) involved in the present systems. 180

A major reason for the observed discrepancies between $k_{\rm ex}^{\rm h}$ and $k_{\rm ex}^{\rm h}$ (calc) could arise from a deficiency in the theoretical models used to calculate $\Delta G_{\rm ex}^{\star}$ and/or the work terms. In addition, the outer-shell barrier $\Delta G_{\rm os}^{\star}$ could be larger than calculated from Equation 6.4 in both homogeneous and electrochemical environments as a result of alterations in short-range solvent polarization that are known to accompany electron transfer. 55.222.230 (See also Sections V. A).

Finally, it is instructive to compare the relative values of k_{ex}^h and k_{ex}^e with the reaction entropies ΔS_{rc}^0 for the redox couples (Table

6.3). ²⁸⁸ The latter values provide a monitor of the changes in solvent polarization that accompany formation of M_{aq}^{2+} from M_{aq}^{3+} . The magnitude of ΔS_{rc}^{0} might be expected to parallel ΔG_{is}^{*} and hence ΔG_{ex}^{*} ; larger values of a should yield greater alterations in the electron density of the aquo hydrogens ³²⁷ and hence more extensive changes in the extent of ligand-solvent hydrogen bonding induced by electron transfer. Indeed, the observed sequence of ΔS_{rc}^{0} values $Ru_{aq}^{3+/2+} < V_{aq}^{3+/2+} < Fe_{aq}^{3+/2+} < Eu_{aq}^{3+/2+} < Cr_{aq}^{3+/2+}$ uniformly parallels the observed reactivity sequence, (Table 6.3), although yet again the value of k_{ex}^{h} for $Fe_{aq}^{3+/2+}$ obtained from self-exchange data is not consistent with this trend.

6. Conclusions and Mechanistic Implications

Taken together, the above results provide strong support to the suspicions noted previously 328,329 that the intrinsic barrier to outersphere electron exchange for $\text{Fe}_{aq}^{3+/2+}$ is significantly greater than anticipated from the measured self-exchange kinetics. Persuasive evidence is provided by the observation that the electrochemical reactivity of $\text{Fe}_{aq}^{3+/2+}$ is noticeably smaller than that of $\text{Ru}_{aq}^{3+/2+}$ and even $\text{V}_{aq}^{3+/2+}$ under the same or comparable conditions at the mercury-aqueous interface, and by the uniformly good agreement between k_{ex}^{h} (Equation 6.6) and the values of k_{ex}^{h} extracted from homogeneous cross reactions having suitably small driving forces and structurally similar coresctants. On this basis, the reported self-exchange rate constant for $\text{Fe}_{aq}^{3+/2+}$ may well be ca. 10^4 -fold larger than that corresponding to the "normal" outer-sphere intrinsic barrier for this couple in other homogeneous and also electrochemical environments.

It remains to consider physical reasons for the enhanced reactivity of the $Fe_{aq}^{3+/2+}$ couple when undergoing self exchange. One possibility is that the "observed" value of $k_{\mu x}^h$ refers to a "normal" outer-sphere pathway. the electrochemical and homogeneous crossreaction data corresponding to "abnormal", for example strongly nonadiabatic, pathways that are all less favorable by about 103 to 105 -fold in kh. While not beyond the bound of possibility, the weight of evidence presented above would seem to disfavor strongly this explanation. A more likely possibility is that the self-exchange reaction proceeds via a more facile inner-sphere pathway. Although the presence of an acid-independent pathway for $Fe_{aq}^{3+/2+}$ self exchange has recently been confirmed by using mixed LiClO4-HClO4 electrolytes, 10 this result by no means eliminates the possibility that the observed pathway involves a water-bridged inner-sphere transition state. The observed acid-independent rate constant for $\cos^{3+/2+}$ self exchange has recently been demonstrated to be ca. 10 12 -fold larger than that obtained from cross-reaction data, and attributed to the presence of a water-bridged pathway. It was suggested that the dominant presence of such pathways may be confined to redox couples such as $Co_{aq}^{3+/2+}$ with extremely positive standard potentials on the basis of a model where the innersphere reaction coordinate involves metal-bridging ligand homolysis. 320.330 Such a pathway would, all other factors being equal, be less favorable for $Fe_{aq}^{3+/2+}$ self exchange since Fe_{aq}^{3+} is considerably less strong an oxidant than $Co_{aq}^{3+.320}$ However, this could easily be offset by the manifold other factors that control the relative rates of competing inner- and outer-sphere pathways. 331 In any case, on this

basis water bridging is more likely for Fe^{3+/2+}_{aq} self exchange than for the other aquo complexes considered here; ³³² aside from Ru^{3+/2+}_{aq} which is constrained to follow outer-sphere pathways all the other couples considered here are ca. 1 V less strongly oxidizing than Fe^{3+/2+}_{aq}. Such pathways are clearly unavailable for cross reactions involving substitutionally inert coreactants such as those in Table 6.2, so that the Fe^{3+/2+}_{aq} reactivity within these environments should reflect that for a "normal" outer-sphere pathway. Water- or hydroxo-bridged pathways are also unlikely within electrochemical redox environments, especially at mercury electrodes in view of the weak interaction between water molecules and this surface. ³³³

Regardless of the detailed reasons for the anomalous behavior of Fe^{3+/2+} self exchange it can be concluded that this couple is in some respects a nonideal choice for the detailed comparisons between experimental rate parameters and the predictions of contemporary theory.²³ Nevertheless, the required structural information is becoming available for a number of other redox couples, ¹⁰ enabling such comparisons to be made not only for self-exchange reactions, ¹⁰ but also for a variety of cross reactions and electrochemical processes.

B. Some Comparisons between the Energetics of Electrochemical and Homogeneous Electron-Transfer Reactions

[Excerpted from ACS Symposium Series, 198, 181 (1982)]

1. Introduction

The kinetics of inorganic electrode reactions have long been the subject of experimental study. The advances in methodology, both in the precise treatment of mass transfer effects and the evolution of electrochemical relaxation techniques, have allowed the kinetics of a wide variety of electrode reactions to be studied. In addition, double-layer structural data are becoming available for a wide range of metal-electrolyte interfaces, which is enabling the kinetics of electrode reactions to be explored quantitatively in a variety of interfacial environments. However, the electrode kinetics area is noticeably underdeveloped in comparison with homogeneous redox kinetics, not only in terms of the availability of accurate kinetics data, but also in the degree of molecular interpretation.

Nevertheless, simple electrochemical processes of the type

$$0x + e^{-} (electrode, \phi_m) \rightarrow Red$$
 (1.12)

where both 0x and Red are solution species, form a valuable class of reactions with which to study some fundamental features of electron transfer in condensed media. Thus such processes involve the activation of only a single redox center, and the free energy driving force

can be continuously varied at a given temperature simply by altering the metal-solution potential difference ϕ_m by means of an external potential source. In addition, electrode surfaces may exert only a weak electrostatic influence upon the energy state of the reacting species, so that in some cases they could provide a good approximation to the "outer-sphere, weak overlap" limit described by conventional electron-transfer theory. Electrochemical kinetics measurements therefore provide a unique opportunity to examine separately the reaction energetics of individual redox couples ("half-reactions"), which can only be studied in tandem in homogeneous solution. In this section, some relationships between the kinetics of heterogeneous and homogeneous redox processes are explored in order to illustrate the utility of electrochemical kinetics and thermodynamics for gaining fundamental insights into the energetics of outer-sphere electron transfer.

2. Electrochemical Rate Formulations

Similarly to homogeneous electron-transfer processes, one can consider the observed electrochemical rate constant $k_{\rm ob}$ to be related to the electrochemical free energy of reorganization for the <u>elementary</u> electron-transfer step ΔG^* by

$$k_{ob} = A \exp(-W_p)\exp(-\Delta G^*/RT)$$
 (6.11)

where A is a frequency factor, and W_p is the work required to transport the reactant from the bulk solution to a site sufficiently close to the

electrode surface ("precursor" or "pre-electrode" state) so that thermal reorganization of the appropriate nuclear coordinates can result in electron transfer. Also, for one-electron electroreduction reactions (Equations 1.12) ΔG^* can usefully be separated into "intrinsic" and "thermodynamic" contributions according to 30,245,340

$$\Delta G^* = \Delta G_{\text{int,e}}^* + \alpha [F(E - E^f) + W_s - W_p]$$
 (6.12)

where E is the electrode potential at which k_{ob} is measured, E^f is the formal potential for the redox couple concerned, W_g is the work required to transport the product from the bulk solution to the "successor" state which is formed immediately following electron transfer, α is the (work-corrected) electrochemical transfer coefficient, and $\Delta G_{int,e}^*$ is the "intrinsic" free energy of activation for electrochemical exchange. This last term equals ΔG^* for the particular case when the precursor and successor states have equal energies, i.e. when the free energy driving force for the elementary reaction $[F(E-E^f)+W_g-W_p]$ equals zero. The electrochemical transfer coefficient α reflects the extent to which ΔG^* is altered when this driving force is nonzero; α therefore provides valuable information on the symmetry properties of the elementary electron-transfer barrier. 341

It is conventional (and useful) to define a "work-corrected" rate constant $k_{\scriptsize corr}$ that is related to $k_{\scriptsize ob}$ at a given electrode potential by

$$k_{corr} = k_{ob} \exp\{[W_{p} + (W_{s} - W_{p})]/RT\}$$
 (6.13)

This represents the value of k_{ob} that (hypothetically) would be obtained at the same electrode potential if the work terms W_p and W_s both equalled zero. For outer-sphere reactions, the work terms can be calculated approximately from a knowledge of the average potential on the reaction plane ϕ_{rp} , since $W_p = ZF\phi_{rp}$ and $W_s = (Z-1)F\phi_{rp}$, where Z is the reactant's charge number. Equation 6.13 can then be written as

$$k_{corr} = k_{ob} \exp\{[(Z - \alpha)F\phi_{rp}]/RT\}$$
 (6.14)

Usually $\phi_{\rm rp}$ is identified with the average potential across the diffuse layer ϕ^2 as calculated from Gouy-Chapman theory using the diffuse-layer charge density obtained from thermodynamic data. In view of the use-fulness of $k_{\rm corr}$, it is also convenient to define a "work-corrected" free energy of activation $\Delta G_{\rm e}^{\pm}$ at a given electrode potential, which is related to $k_{\rm corr}$ by [cf. Equation 6.13]:

$$k_{corr} = A \exp(-\Delta G_a^{*}/RT)$$
 (6.15)

so that Equation 6.13 can be written simply as

$$\Delta G_{e}^{*} = \Delta G_{int,e}^{*} + \alpha F(E - E^{f})$$
 (6.16)

Therefore the value of k_{corr} measured at E^f , i.e. the "standard" rate constant k_{corr}^s is directly related to the intrinsic barrier $\Delta G_{int,e}^*$.

Consequently, information on the energetics of electron transfer for individual redox couples ("half-reactions") can be extracted from

measurements of electrochemical rate constant-overpotential relationships. (Similarly, thermodynamics measurements for half-reactions,
e.g. reaction entropies, can also yield information on electrontransfer energetics for individual redox couples as shown in Chapter
V). Such electrochemical measurements can therefore provide information on the contributions of each redox couple to the energetics of the
bimolecular homogeneous reactions which is unobtainable from ordinary
chemical thermodynamics and kinetics measurements.

3. Relation between Electrochemical and Homogeneous Reaction Energetics

Consider the following pair of electrochemical reduction and oxidation reactions

$$0x_1 + e^- (electrode, \phi_m) \rightarrow Red_1$$
 (6.17a)

$$Red_2 + Ox_2 + e^- (electrode, \phi_m)$$
 (6.17b)

and the corresponding homogeneous cross reaction

$$0x_1 + Red_2 + Red_1 + 0x_2$$
 (6.18)

Providing that the interactions between the reactant and the electrode in the electrochemical transition state, and between the two reactants in the homogeneous transition state, are negligible ("weak

overlap" limit), the activation barriers for reactions (6.17) and (6.18) will be closely related.

At a given value of ϕ_m (and hence electrode potential E), the thermodynamics of reactions (6.17) and (6.18) are identical since the energy required to transport the electron across the metal-solution interface in the half reactions (6.17a) and (6.17b) will then cancel. The overall activation free energy $\Delta G_{h,12}^{\star}$ for reaction (6.18) can be considered to consist of separate contributions, $\Delta G_{h,1}^*$ and $\Delta G_{h,2}^*$, arising from the activation of Ox, and Red, respectively. Although a multitude of different transition-state structures may be formed, corresponding to different individual values of $\Delta G_{h,1}^*$ and $\Delta G_{h,2}^*$, the predominant reaction channel will be that corresponding to a minimum in the activation free energy ($\Delta G_{h,1}^* + \Delta G_{h,2}^*)_{min}$. In the "weak overlap" limit, each pair of values of $\Delta G_{h,1}^*$ and $\Delta G_{h,2}^*$ satisfying the thermodynamic constraints of reaction (6.18) will be identical to the corresponding pair of electrochemical free energies of activation, $\Delta G_{e,1}^*$ and $\Delta G_{e,2}^*$, for reactions (6.17a) and (6.17b), respectively, having the same transition-state structures. Therefore the energetics of reactions (6.17) and (6.18) are related in the "weak overlap" limit by

$$(\Delta G_{e,1}^{*} + \Delta G_{e,2}^{*})_{\min}^{E} = (\Delta G_{h,2}^{*})_{\min} = \Delta G_{h,12}^{*}$$
 (6.19)

where $(\triangle G_{e,1}^* + \triangle G_{e,2}^*)_{\min}^E$ refers to the particular electrode potential where the sum of $\triangle G_{e,1}^*$ and $\triangle G_{e,2}^*$ is a minimum. Although only the sum $(\triangle G_{h,1}^* + \triangle G_{h,2}^*)_{\min}$ can be determined experimentally for a given homo-

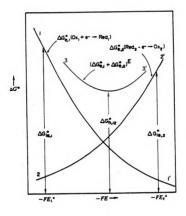


Figure 6.4. Schematic illustration of general relationship between electrochemical and homogeneous reaction energetics. Curves 11' and 22' are plots of activation free energy ΔG_e^* versus thermodynamic driving force -FE for an electroreduction and electrooxidation reaction (reactions 6.17a and 6.17b), respectively. E_1^f and E_2^f are the standard electrode potentials for these two redox couples. Curve 33' is formed by the sum $(\Delta G_{e,1}^* + \Delta G_{e,2}^*)^E$. The corresponding homogeneous activation barrier $\Delta G_{h,12}^*$ is, in the "weak overlap" limit, given by the minimum in this curve.

dually as a function of the free energy driving forces $\triangle G_1^o$ and $\triangle G_2^o$ for these two half reactions (6.17a) and (6.17b), which equal $F(E-E_1^f)$ and $F(E-E_2^f)$, respectively, where E_1^f and E_2^f are the corresponding standard electrode potentials.

This relationship is illustrated schematically in Figure 6.4. Curves 11' and 22' represent plots of ΔG_e^* against the reaction free energy $F(E-E^f)$ for a pair of cathodic and anodic half reactions on a common scale of electrode potential FE; such curves are generally expected to be curved in the manner shown (<u>vide infra</u>) so that a shallow minimum in the plot of $(\Delta G_{e,1}^* + \Delta G_{e,2}^*)$ versus FE will be obtained. In practice, unless ΔG_e^* is small (<3-4 kcal mol⁻¹) the slopes of these plots, i.e., the cathodic and anodic transfer coefficients, are often found to be equal and close to 0.5 so that to a good approximation 182.344,348

$$2\Delta G_{e,12}^* = \Delta G_{h,12}^*$$
 (6.20)

where $\Delta G_{e,12}^{*}$ is the value of ΔG_{e}^{*} at the intersection of the $\Delta G_{e,1}^{*}$ - E and $\Delta G_{e,2}^{*}$ - E plots.

For the special case where the cathodic and anodic half-reactions are identical, since the two ΔG_e^* - E plots must intersect at E^f for the redox couple, then Equation 6.20 can be written in terms of the electrochemical and homogeneous intrinsic barriers:

$$2\Delta G_{\text{int,e}}^{*} = \Delta G_{\text{int,h}}^{*}$$
 (6.21)

Provided that the reactions are adiabatic and the conventional collision model applies, Equation 6.21 can be written in the familiar form relating the rate constants of electrochemical exchange and homogeneous self-exchange reactions: 180

$$(k_{corr}^{g}/A_{e})^{2} = (k_{corr}^{h,ex}/A_{h})$$
 (6.22)

where $k_{corr}^{h,ex}$ is the (work-corrected) rate constant for homogeneous self exchange, and A_e and A_h are the electrochemical and homogeneous frequency factors, respectively. (See Section IV. A).

In the following subsections, we shall explore the applicability of such relationships to experimental data for some simple outer-sphere rections involving transition-metal aquo complexes. In keeping with the distinction between intrinsic and thermodynamic barriers (Equation 6.6), exchange reactions will be reviewed first, followed by a comparison of driving force effects for related electrochemical and homogeneous reactions.

4. Electron Exchange

In the previous section (VI. A) a good correlation was found between homogeneous and electrochemical electron exchange kinetics for reactions of aquo redox couples (e.g. see Figure 6.3). However, the correlation does not strictly follow Equations 6.21 and 6.22. Instead, an equation of the form:

$$(k_{corr}^{s}/A_{e})^{2} = (k_{corr}^{h,ex}/A_{h}) + C$$
 (6.23)

is followed where C is a constant. This constant evidently takes account of the differing imaging conditions in homogeneous versus electrochemical environments (see Sections IV. A and V. A for further discussion). There are few additional reactions which might be used to test Equations 6.21 and 6.22. 345,346 However, we have recently found that the exchange reactions of $\text{Ru}(\text{NH}_3)_6^{3+/2+}$ also obey Equation 6.23, provided that a relatively large reaction zone thickness ($\delta r_e = 2-5 \text{ Å}$) is used in estimating A_e . (In Section IV. C it is shown that δr_e values of this magnitude are appropriate for ammine couples).

5. Influence of Thermodynamic Driving Force

Given that the reorganization parameters for electrochemical exchange of various aquo redox couples are in acceptable agreement with the corresponding homogeneous rate parameters on the basis of the weak overlap model, it is of interest to compare the manner in which the energetics of these two types of redox processes respond to the application of a net thermodynamic driving force.

For one-electron electrochemical reactions, the harmonic oscillator ("Marcus") model 13 yields the following predicted dependence of ΔG_a^{*} upon the electrode potential:

$$\Delta G_{e}^{*} = \Delta G_{ie}^{*} - 0.5 F(E - E^{f}) + F(E - E^{f})^{2}/16\Delta G_{int,e}^{*}$$
 (6.24)

where the plus/minus sign refers to reduction and oxidation reactions, respectively. The transfer coefficient (Equation 6.16) is therefore predicted to decrease linearly from 0.5 with increasing electrochemical

driving force $\stackrel{+}{=}$ F(E - E^f). The derivation of Equation 6.24 involves the assumption that the reactant and product free energy barriers are parabolic and have identical shapes, and that the reactions are adiabatic yet involve only a small "resonance splitting" of the free energy curves in the intersection region. ¹³

A number of experimental tests of Equation 6.24 have been made. 313,347 Generally speaking, it has been found that $\alpha = 0.5$ at small to moderate overpotentials, in agreement with Equation 6.24. Tests of this relation over sufficiently large ranges of overpotential where the quadratic term becomes significant are not numerous. A practical difficulty with multicharged redox couples is that the extent of the work term corrections is frequently sufficiently large to make the extraction of k_{corr} , and hence ΔG_{p}^{*} and α , from the observed ratepotential behavior fraught with uncertainty. However, Weaver and Tyma have recently obtained kinetic data for Cr_{ag}^{2+} , Eu_{ag}^{2+} and V_{ag}^{2+} electrooxidation over wide ranges of anodic overpotential (up to 900 mv) under conditions where the electrostatic work terms are small. 313 The anodic transfer coefficients α_{\bullet} for all those reactions were found to decrease with increasing anodic overpotential, but to a greater extent than predicted by Equation 6.24.313,347 This behavior contrasts that found for cathodic overpotentials, where the cathodic transfer coefficients α remain essentially constant at 0.5, even over regions of overpotential where detectable dcreases in α_c are predicted by Equation 6.24. These aquo redox couples therefore exhibit a markedly different overpotential dependence of the anodic and cathodic rate constants; this contrasts with the symmetrical dependence predicted by Equation 6.24. An example

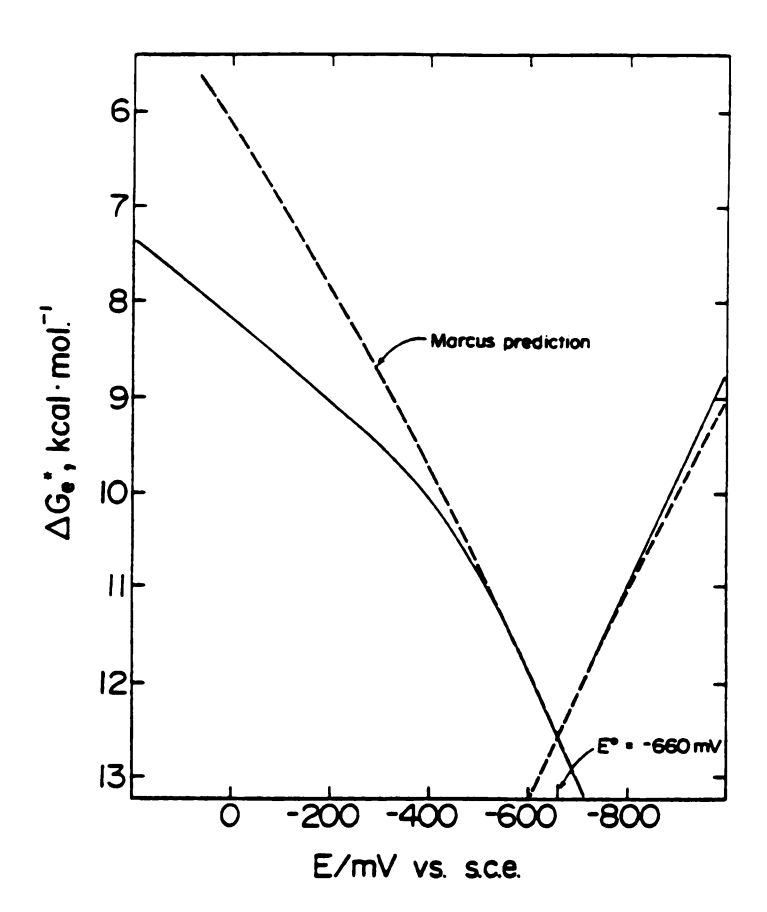


Figure 6.5. The electrochemical free energy of activation, ΔG_{e}^{\star} , for $Cr(H_2O)_6^{3+/2+}$ at the mercury-aqueous interface, plotted against the electrode potential for both anodic and cathodic overpotentials. Solid lines are obtained from the experimental rate constant-overpotential plot in reference 313, by using Equation 6.15. Dashed lines are the predictions from Equation 6.24.

of this behavior is shown in Figure 6.24 which is a plot of $\Delta G_{\mathbf{e}}^{*}$ versus $(\mathbf{E} - \mathbf{E}^{\mathbf{f}})$ for $\mathrm{Cr}_{\mathbf{aq}}^{3+/2+}$ at the mercury-aqueous interface at both anodic and cathodic overpotentials. The solid curves are obtained from the experimental data, and the dashed lines show the overpotential dependence of $\Delta G_{\mathbf{a}}^{*}$ predicted from Equation 6.24.

The prediction corresponding to Equation 6.24 for driving force effects upon homogenous kinetics is 13

$$\Delta G_{h,12}^{*} = \Delta G_{int,h,12}^{*} + 0.5 \Delta G_{12}^{o} + (\Delta G_{12}^{o})^{2}/16 \Delta G_{int,h,12}^{*}$$
 (6.25)

where $\Delta G_{\mathrm{int},h,12}^{\star}$ is the mean of the intrinsic barriers for the parent self-exchange reactions $[0.5(\Delta G_{\mathrm{int},h,1}^{\star} + \Delta G_{\mathrm{int},h,2}^{\star})]$ and ΔG_{12}^{o} is the free energy driving force for the cross reaction. Equation (6.25) has been found to be in satisfactory agreement with experimental data for a number of outer-sphere cross reactions having small or moderate driving forces. However there appear to be significant discrepancies for some reactions having large driving forces (where the last term in Equation 6.25 becomes important) in that the rate constants do not increase with increasing driving force to the extent predicted by Equation 6.25; i.e. the values of $\Delta G_{h,12}^{\star}$ are larger than those calculated from the corresponding values of $\Delta G_{\mathrm{int},h,12}^{\star}$ and ΔG_{12}^{o} using Equation 6.25. ΔG_{12}^{\star} and ΔG_{12}^{o} using Equation 6.25.

It has been suggested that these apparent discrepancies could be due to the values of $\Delta G_{h,12}^{\star}$ and $\Delta G_{int,h,12}^{\star}$ that are obtained from the experimental work-corrected rate constants being incorrectly large due to nonadiabatic pathways, or to the presence of additional unfavorable

work terms arising from solvent orientation required to form the highly charged precursor complex. 207 An alternative, or additional, explanation is that the free energy barriers are anharmonic so that the quadratic driving force dependence of Equation 6.25 is inappropriate. It is interesting to note that the form of the discrepancies between the kinetics data for the electrooxidation of aquo cations and Equation 6.24 is at least qualitatively similar in that both involve unexpectedly small dependencies of the rate constants upon the thermodynamic driving force. Moreover, the large majority of homogeneous reactions for which such discrepancies have been observed involve the oxidation of aquo cations. 207,310 However, nonadiabaticity effects cannot explain the asymmetry between the $\Delta G_{\mathbf{e}}^{*}$ - E plots at anodic and cathodic overpotentials (Figure 6.5). Also, any specific work term effects should be different (and probably smaller) at the mercury-aqueous interface compared with homogeneous reactions between multicharge cations, yet any anharmonicity of the free energy barriers should be similar, at least on the basis of the weak overlap model. A quantitative comparison of the driving force dependence of the kinetics of related electrochemical and homogeneous reactions should therefore shed light on the causes of the observed discrepancies for the latter, more complicated processes.

One can generally express the free energy barriers $\triangle G_e^*$ for the pair of cathodic and anodic electrochemical reactions 6.17a and 6.17b as (cf. Equations 6.16 and 6.24):

$$\Delta G_{e,1}^{*} = \Delta G_{int,e,1}^{*} + \alpha_{1} \Delta G_{1}^{0}$$
 (6.26a)

and

$$\Delta G_{e,2}^* = \Delta G_{int,e,2}^* + \alpha_2 \Delta G_2^0$$
 (6.26b)

where α_1 and α_2 are the transfer coefficients for these two reactions at a given electrode potential. A similar relationship may be written for the free energy barrier $\Delta G_{h,12}^{*}$ of the corresponding homogeneous cross reaction 6.18 (cf. Equation 6.25):

$$\Delta G_{h,12}^{*} = \Delta G_{int,h,12}^{*} + \alpha_{12} \Delta G_{12}^{0}$$
 (6.27)

where α_{12} is a "chemical" transfer coefficient. Although α_1 and α_2 are determined only by the shapes of the free energy barriers for the individual redox couples at a given driving force, α_{12} is a composite quantity which is determined not only by α_1 and α_2 but also by the relative magnitudes of $\Delta G_{\mathrm{int},h,1}^*$, $\Delta G_{\mathrm{int},h,2}^*$ and $\Delta G_{h,12}^*$.

Nevertheless, comparisons of values of $^\Delta G^*_{h,12}$ for a series of related cross reactions having systematically varying driving forces can yield useful information. Figure 6.6 is a plot of $^\Delta G^*_{h,12}$ / $^\Delta G^*_{int,h,12}$ versus $^\Delta G^0_{12}/^\Delta G^*_{int,h,12}$ for a series of cross reactions involving the oxidation of various aquo complexes. (The values of $^\Delta G^*_{12}$ and $^\Delta G^*_{int,h,12}$ were obtained from the measured homogeneous rate constants by using equations exactly analogous to 6.11. Details are given in reference 311). The graphical presentation in Figure 6.6 has the virtue that the values of $^\Delta G^*_{h,12}$ for different cross reactions are normalized for variations in the intrinsic barriers $^\Delta G^*_{int,h,12}$; the

driving force dependence predicted by the Marcus model is such that all $\Delta G_{h,12}^*$ values fall on a common curve (shown as a solid line in Figure 6.6) when presented in this manner. 351 (Omitted from Figure 6.6 are reactions involving $\cos \frac{3+/2+}{aq}$ since there is evidence that the measured self-exchange rate does not correspond to an outer-sphere pathway). 352 It is seen that the experimental points deviate systematically from the Marcus predictions in that the apparent values of α_{12} (Equation 6.27) are significantly smaller than predicted from Equation 6.25 at moderate to high driving forces. Figure 6.7 consists of the same plot as Figure 6.6 but for a number of outer-sphere cross rections involving reductants other than aquo complexes. 351 In contrast to Figure 6.6 reasonable agreement with the Marcus prediction is obtained (cf. reference 351). The data in Figure 6.6 are also shown in Figure 6.8 as a plot of $[\Delta G_{12}^* - \Delta G_{int,12}^*]$ versus $-[0.5\Delta G_{12}^0 + (\Delta G_{12}^0)^2/16\Delta G_{int,12}^*]$. Since this plot is an expression of Equation 6.25, the Marcus model predicts a slope of unity (the solid line in Figure 6.8). However, the points are almost uniformly clustered beneath this predicted line, and increasingly so as $-\Omega_{12}^{0}$ increases, again indicating that α_{12} tends to be smaller than predicted.

It therefore seems feasible that these anomalously small values of α_{12} noted from Figures 6.6 and 6.8 have their primary origin in the oxidation half-reactions which uniformly involve aquo complexes. This possibility was explored by converting the electrooxidation data into a form suitable for direct comparison with the homogeneous data in Figure 6.8 in the following manner. As noted above, the free energy barrier $\Delta G_{h,12}^*$ for each outer-sphere cross section will consist of

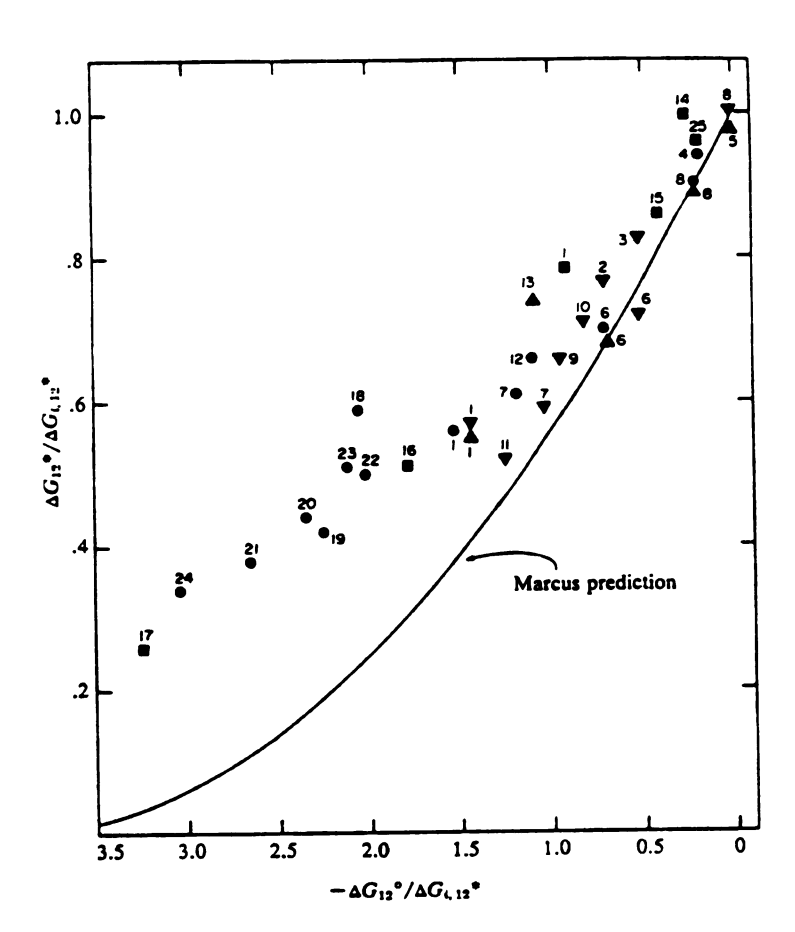


Figure 6.6

Figure 6.6. Plot of $\Delta G_{12}^{*}/\Delta G_{1,12}^{*}$ against $-\Delta G_{12}^{\circ}/\Delta G_{1,12}^{*}$ for homogeneous cross reactions involving oxidation of aquo cations. Reductants: (\bullet) Eu $_{aq}^{2+}$, (\blacktriangle) Cr $_{aq}^{2+}$, (\blacktriangledown) V $_{aq}^{2+}$, and (E) Ru_{ag}²⁺. Key to oxidants and data sources: 1, Fe_{ag}; 2, Ru_{aq}^{3+} ; 3, Np_{aq}^{4+} ; 4, V_{aq}^{3+} ; 5, Eu_{aq}^{3+} ; 6, $Ru(NH_3)_{6}^{3+}$; 7, $Ru(NH_3)_{5}py_{5}^{3+}$; 8, $Co(en)_3^{3+}$; 9, $Co(phen)_3^{3+}$; 10, $Co(bpy)_3^{3+}$ (data sources for 1-10 listed in reference 311); 11, Ru(NH₃)₅isn³⁺ (reference 321); 12, Co(phen) $_{3}^{3+}$ (reference 310); 13, Co(phen) $_{3}^{3+}$ (reference 337); 14 to 17 and 25 are from reference 388; 14, $Co(phen)_3^{3+}$; 15, $Ru(NH_3)_5isn^{3+}$; 16, $Os(bpy)_3^{3+}$; 17, $Ru(bpy)_{3}^{3+}$; 18 to 22 are from reference 304; 18, *Ru[4,4'] $(CH_3)_2 bpy]_3^{2+}$; 19, $Ru(phen)_3^{2+}$; 20, $Ru(bpy)_3^{2+}$; 21, Ru(5-C1 phen) $_{3}^{2+}$; 22, *Ru[4,7-(CH₃)₂phen] $_{3}^{2+}$; 23, *Os(5-C1 phen) $_{3}^{2+}$ (reference 386); 24, $Ru[4,7-(CH_3)_2]$ phen]₃ (reference 387); 25, $Ru(NH_3)_5 py^{3+}$. An asterisk(*) indicates the oxidant is a photoexcited state reactant.

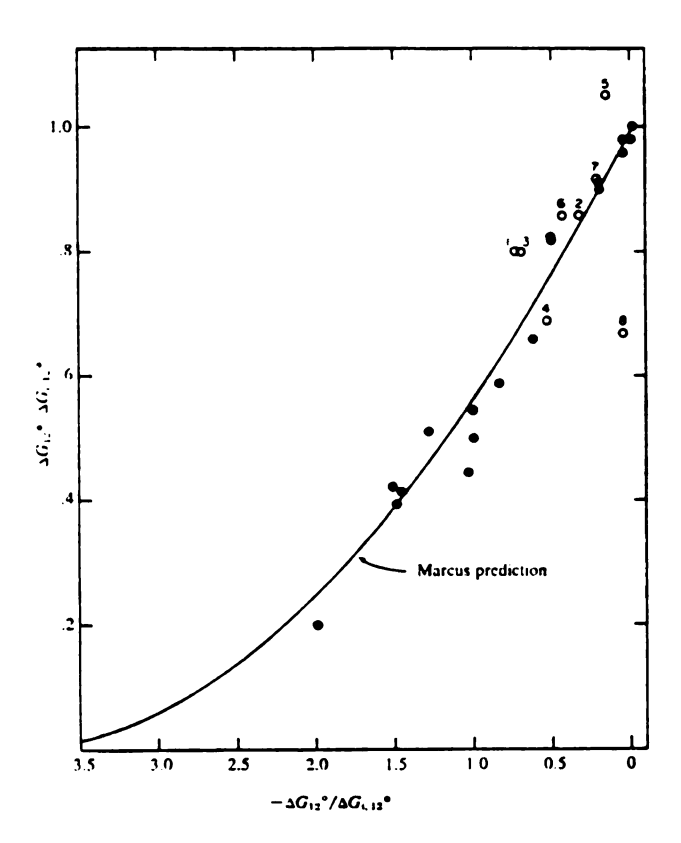


Figure 6.7. Plot as for Figure 6.6, but involving reactants other than aquo complexes. Key to reactants and data sources: (①) Co(III)/(II) macrocycle oxidants (data are given in Figures 2, 5 and 6 of reference 351); (O) other nonaquo oxidants; 1, Ru(NH₃)₅Py³⁺ + Ru(NH₃)₆²⁺; 2, Ru³⁺_{aq} + Ru(NH₃)₆²⁺; 3, Co(phen)₃³⁺ + Ru(NH₃)₆²⁺; 4, Co(bpy)₃³⁺ + Ru(NH₃)₆²⁺; 5, Co(phen)₃³⁺ + Ru(NH₃)₅Py²⁺ (data sources for 1-5 are listed in reference 311); 6, horse heart ferricytochrome c + Ru(NH₃)₆²⁺ (reference 389); 7,Co(phen)₃³⁺ + horse heart ferrocytochrome c (reference 390); 8, Ru(NH₃)₄bpy³⁺ + Ru(NH₃)₅ - py²⁺ (reference 310).

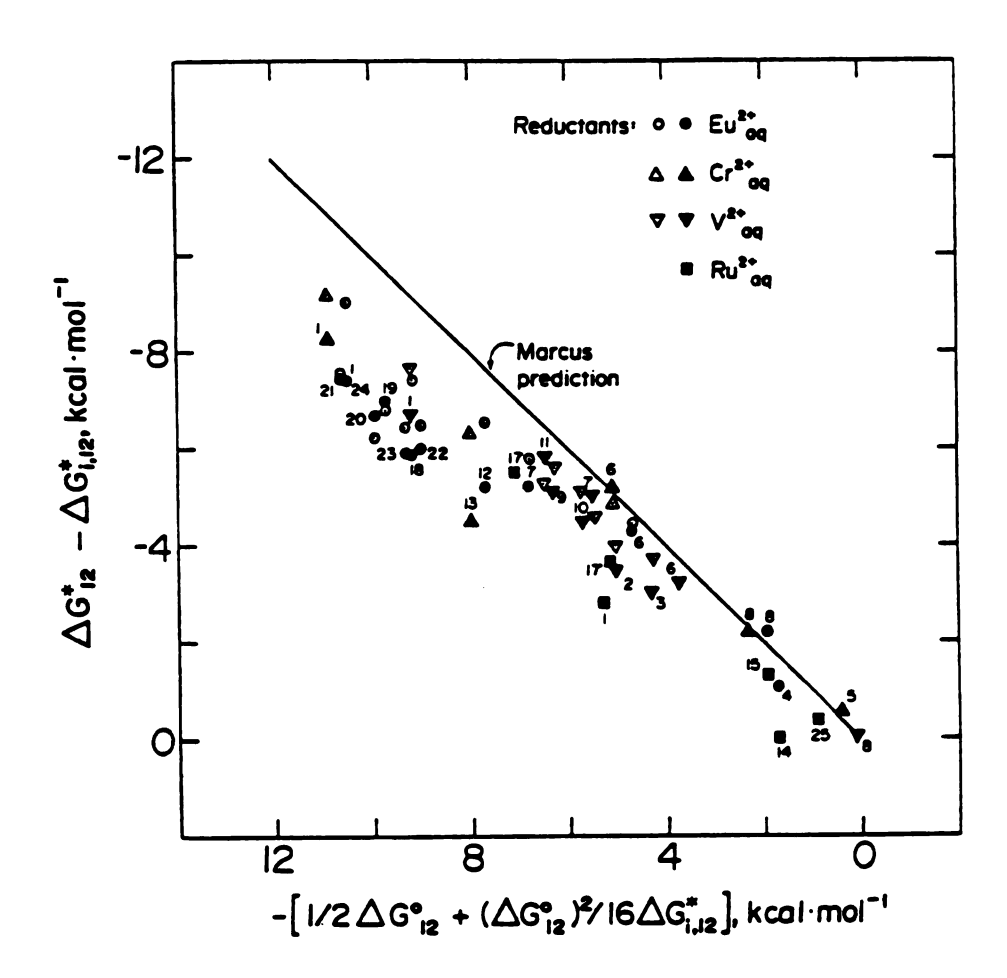


Figure 6.8. Plot of $(\Delta G_{12}^* - \Delta G_{1,12}^*)$ for homogeneous cross reactions involving oxidation of aquo complexes given in Figure 6.5, against the thermodynamic driving force function $-[0.5\Delta G_{12}^{\circ} + (\Delta G_{12}^{\circ})^2/16\Delta G_{1,12}^*]$. Closed symbols are obtained from homogeneous data; key to points as in Figure 6.5. Open symbols are corresponding points obtained from electrochemical kinetic data for oxidation of aquo cations (see text for details).

contributions $\Delta G_{h,1}^{\star}$ and $\Delta G_{h,2}^{\star}$ from the oxidant and reductant, respectively. In the "weak overlap" limit $\Delta G_{h,1}^*$ and $\Delta G_{h,2}^*$ will equal the free energy barriers $\Delta G_{e,1}^*$ and $\Delta G_{e,2}^*$ for the corresponding electrochemical reactions at an electrode potential where the sum $(\Delta G_{e,1}^* + \Delta G_{e,2}^*)$ is a minimum (Equation 6.19 and Figure 6.4). Estimates of $\Delta G_{h,2}^{*}$ for Eu_{aq}, $\operatorname{Cr}_{aq}^{2+}$, and $\operatorname{V}_{aq}^{2+}$ oxidation as a function of the half-reaction driving force G_2^0 = -F(E -E_2^f)] were obtained from the corresponding ΔG_2^* - E plots (see Figure 6.5 and reference 313) by assuming that they have the same shape but replacing the value of ΔG_e^* at $\Delta G_2^0 = 0$ (i.e. $\Delta G_{int.e}^*$) by 0.5 $\Delta G_{int,h}^*$ (this procedure corrects for the differences between $\Delta G_{\text{int.e}}^{*}$ and 0.5 $\Delta G_{\text{int.h}}^{*}$ resulting from the limitations of the weak overlap model (Equation 6.23). The accompanying plots of $\Delta G_{h,1}^{x}$ versus $\Delta G_{f 1}^{f o}$ for the reduction half reactions involved in Figure 6.8 were constructed using the experimental value of $\Delta G_{\text{int.h.}12}^*$ by assuming that the harmonic oscillator model applies, i.e. by utilizing Equation 6.24 written for homogeneous half reactions:

$$\Delta G_{h,1}^{*} = 0.5 \Delta G_{int,h,12}^{*} + 0.5 \Delta G_{1}^{0} + (\Delta G_{1}^{0})^{2} / 8 \Delta G_{int,h,12}^{*}$$
 (6.28)

These pairs of $\triangle G_{h,1}^* - \triangle G_1^o$ and $\triangle G_{h,2}^* - \triangle G_2^o$ curves were plotted on a common driving force (i.e. electrode potential) axis such that $\triangle G_1^o - \triangle G_2^o = \triangle G_{12}^o$, and the required estimates of $\triangle G_{h,12}^*$ for each cross reaction were then obtained from the sum $(\triangle G_{h,1}^o + \triangle G_{h,2}^o)$ at the value of $\triangle G_h^o$ where the quantity has a minimum value (Equation 6.19). These estimates of $\triangle G_{h,12}^*$ are plotted as open symbols in Figure 6.8 for the reactions having moderate to large driving forces $(-\triangle G_{12}^o) > 8$ kcal mol⁻¹),

alongside the corresponding experimental values of $\Delta G_{h,12}^*$. It is seen that the estimated values of $\Delta G_{h,12}^*$ diverge from the straight line predicted from the harmonic oscillator model to a similar, albeit slightly smaller, extent than the experimental values. Admittedly, there is no particular justification for assuming that the reduction half reactions obey the harmonic oscillator model. However, it turns out that the estimates of $\Delta G_{h,12}^*$ are relatively insensitive to alterations in the shapes of the $\Delta G_{h,1}^*$ - ΔG_1^0 plots. It therefore seems reasonable that the deviations of the activation free energies for highly exoergic electrochemical and homogeneous reactions illustrated in Figures 6.5 and 6.8 may arise partly from the same source, i.e. from values of α_2 for the oxidation half reactions that are unexpectedly small. That is not to say that other factors are not responsible, at least in part, for these discrepancies. Nonadiabaticity, work terms, specific solvation, and other environmental effects may all play important roles depending on the reactants. For example, there is evidence to suggest that the true rate constant for outer-sphere $Fe_{ag}^{3+/2+}$ selfexchange is significantly smaller than the directly measured value (see Section VI. A). This can account for a good part of the unexpectedly slow rates of cross reactions involving this couple.

It is remarked here that in the original publication we were unable to uncover the reasons for the peculiar driving-force dependence of the aquo oxidation kinetics, although a number of ideas were advanced. However, absolute calculations reported in Chapter VII indicate that the driving-force anomalies on both the anodic and cathodic sides for electrochemical reactions of $F_{\rm aq}^{3+/2+}$ and $Cr_{\rm aq}^{3+/2+}$ can

be attributed in large measure to differences in inner-shell force constants for the M(III)-L versus the M(II)-L state. Such differences also should account for the homogeneous reactivity patterns. Rather than indicating a failure of electron-transfer theory, these findings point to the unsuitability of the "equal force constant" approximation which is employed in deriving Equation 6.24, as well as 6.25 and 6.28. This discussion therefore illustrates the inadequacy of the relative theory in comparison to the absolute theory for solving one aspect of the problem. However, in another regard the relative theory is the superior approach in that the reaction energetics of redox couples such as $Eu_{-}^{3+/2+}$ can still be examined even though structural data (required in the absolute approach) are lacking. Furthermore the relative electron-transfer theory appears to represent the only method of interpreting kinetics data for chemically irreversible reactions for which thermodynamic data are lacking. Thus, the two approaches are complementary in generating insights and understanding concerning the details of electron-transfer kinetics.

6. Conclusions

It seems clear that kinetics as well as thermodynamics data gathered for simple electrode reactions can contribute significantly towards the development of our fundamental understanding of electron transfer in condensed media. In particular, detailed studies of electrochemical kinetics with due regard for work term corrections can yield information on the shapes of free energy barriers and the isolated "weak overlap" reactivity of metal complexes.

C. Entropic Driving Force Effects Upon Preexponential Factors for Intramolecular Electron Transfer: Implications for the Assessment of Nonadiabaticity

(Accepted for publication in Inorg. Chem.)

Considerable effort has been directed recently towards measuring rate parameters for intramolecular redox reactions, typically involving electron transfer between a pair of transition metals linked by an organic bridge. 353-355 Such reactions offer important advantages over bimolecular processes for investigating detailed aspects of electron transfer, since the uncertainties concerning the energetics of forming the precursor complex are absent and the geometry of the transition state is relatively well defined. 355

The study of intramolecular electron transfer should be particularly useful for examining electronic coupling effects; i.e. the factors influencing the occurrence and degree of nonadiabaticity. Since the rate constant, ket, for such processes should refer to an elementary electron-transfer step, it can be expressed as 342

$$k_{et} = v_{n} \kappa_{el} \exp(\Delta S_{FC}^{*}/R) \exp(-\Delta H_{FC}^{*}/RT)$$
 (6.29a)

$$k_{et} = v_{n} exp(\Delta S_{a}^{*}/R) exp(-\Delta H_{FC}^{*}/RT)$$
 (6.29b)

where ν_n is the effective nuclear frequency factor, κ_{el} is the electronic transmission coefficient, and ΔS_{FC}^{\star} and ΔH_{FC}^{\star} are the entropic

and enthalpic components of the Franck-Condon barrier. Values of $\kappa_{\mbox{el}}$ can therefore be extracted from rate measurements as a function of temperature provided that v_n and ΔS_{FC}^{\pm} are known. For many reactions v_n is numerically very similar to the conventional factor kT/h.9,23 Since work terms are absent for intramolecular reactions, the observation of preexponential factors that are substantially less than v_n , or equivalently, of negative apparent entropies of activation ΔS_a^* is often taken as prima facie evidence of nonadiabaticity (i.e. < a1<1).</pre> Implicit in this interpretation is the assumption that ΔS_{FC}^{\star} is essentially zero. However, contrary to common belief this is probably incorrect for most nonsymmetrical intramolecular reactions, including those featuring charge symmetry. The purpose of this section is to explore the likely magnitudes of AS* for some representative intramolecular reactions and to examine the consequences for the interpretation of unimolecular preexponential factors in terms of nonadiabaticy.

The origin of the Franck-Condon activation entropy can be clarified by considering Marcus' expression 13 for the activation free energy, ΔG_{FC}^{\star} , and its temperature derivative. Thus, 356

$$\Delta G_{FC}^{\star} = \Delta G_{int}^{\star} + 0.5 (1 + \alpha) \Delta G^{o}$$
 (6.30)

where $\Delta G_{\rm int}^{*}$ is the intrinsic barrier, ΔG° is the thermodynamic free energy change, and $\alpha = \Delta G^{\circ}/8\Delta G_{\rm int}^{*}$. The temperature derivative of Equation 6.30 is

$$\Delta S_{FC}^{*} = \Delta S_{int}^{*} (1-4\alpha^{2}) + 0.5 (1 + 2\alpha) \Delta S^{0}$$
 (6.31)

where ΔS_{int}^{\star} is the intrinsic activation entropy and ΔS° is the entropic driving force. For reactions having small or moderate values of G° , = 0 so that Equation 6.31 simplifies to

$$\Delta S_{RC}^{*} \Delta S_{int}^{*} + 0.5 \Delta S^{\circ}$$
 (6.32)

For reactions in aqueous media, $\Delta S_{\rm int}^{\star}$ is usually assumed to be close to zero (within ca. 2 J deg⁻¹ mol⁻¹) as predicted by the conventional dielectric continuum expression, ²⁰³ although as shown in Section V. A there is good reason to suspect that small positive values of $\Delta S_{\rm int}^{\star}$ (ca. 4-12 J deg⁻¹ mole⁻¹) are common. ³⁵⁷ However, $\Delta S_{\rm can}^{0}$ can often be sufficiently large to yield a substantial contribution to $\Delta S_{\rm FC}^{\star}$, even for reactions leading to no net change in ionic charge. For example, the reduction of Fe(phen)³⁺₃ (phen = phenanthroline) by Fe(OH₂)²⁺₆ yields a net entropy change of -167 J deg⁻¹ mole⁻¹, ⁵⁵ corresponding to a value of $S_{\rm FC}^{\star}$ of ca -67 J deg⁻¹ mole⁻¹ from Equation 6.31.

The values of ΔS^{O} can be related to the component entropic changes (the so-called "reaction entropies" ΔS^{O}_{rc})⁵⁵ at the redox centers undergoing reduction and oxidation, $\Delta S^{O}_{rc,red}$ and $\Delta S^{O}_{rc,ox}$, respectively, by

$$\Delta S^{o} = \Delta S^{o}_{rc,red} - \Delta S^{o}_{rc,ox}$$
 (6.33)

Such large entropic driving forces arise because the component reaction entropies are often large and extremely sensitive not only to the charge type of the redox couple, but also the chemical nature of the coordinated ligands, the metal redox center, and the surrounding solvent. 52.82.84 This is due to the large changes in the degree of specific ligand-solvent interactions, and hence the extent of local solvent polarization, brought about by electron transfer. 55,82,222

In order to check the validity of Equation 6.31, values of ΔS_{PC}^{π} were calculated for thirty outer-sphere bimolecular reactions and compared with the experimental activation entropies, ΔS_{exp}^{*} . The choice of reactions was limited to those for which values of ΔS^0 and ΔG^0 are available and sufficient structural information exists to permit the calculation of ΔG_{int}^{\star} . Details will be presented in chapter VII. All these reactions involve reactant pairs having charges of +3 and +2. Figure 6.9 is the resulting plot of ΔS_{FC}^* against ΔS_{exp}^* . This plot demonstrates that the experimental activation entropies do indeed respond to the entropic driving force roughly in the manner predicted by Equation 6.31. although the values of ΔS_{exp}^* are about 60 to 100 J deg^{-1} mole⁻¹ smaller than ΔS_{PC}^* . (Also note that reactions involving high-spin Co(III)/(II) couples do not display noticeably different behavior in spite of the spin state change that occurs for these reactions.) This discrepancy could be taken as an indication of nonadiabaticity (κ_{el} <<1), but more likely it arises chiefly from an additional component of ΔS_{exp}^{*} associated with the unfavorable entropic work of forming the highly charged precursor complex from the separated cationic reactants.

Figure 6.9. Plot of the experimental activation entropy, ΔS_{exp}^{*} , against the activation entropy, ΔS_{FC}^{\star} , calculated from Equation 6.32 for bimolecular reactions involving 3+/2+ redox couples. Data sources quoted reference 311 unless otherwise noted (aq = OH,, en = ethylenediamine, bpy = 2,2'-bipyridine, phen = 1,10'-phenanthroline, terpy = 2,2',2"-terpyridine py = pyridine). Reactions: 1. $\cos_{ag}^{3+} + Fe_{ag}^{2+}$; 2. $\cos_{ag}^{3+} + Cr_{ag}^{2+}$; 3. $Fe_{aq}^{3+} + Ru_{aq}^{2+}$; 4. $Fe_{aq}^{3+} + V_{aq}^{2+}$; 5. $Fe_{aq}^{3+} + Fe_{aq}^{2+}$; 6. $V_{aq}^{3+} + V_{aq}^{2+}$; 7. $Fe_{aq}^{3+} + Ru(NH_3)_6^{2+}$; 8. $Fe_{aq}^{3+} + Ru(NH_3)_5 py_2^{2+}$; 9. $Fe_{aq}^{3+} + Ru(en)_3^{2+}$; 10. $Ru(bpy)_3^{3+} + Fe_{aq}^{2+}$; 11. $Ru(phen)_3^{3+} + Ru_{aq}^{2+}$; 329; 12. $Fe(bpy)_3^{3+}$ + Fe_{aq}^{2+} ; 359 13. $Fe(phen)_3^{3+} + Fe_{aq}^{2+}$; 335 14. $Ru(terpy)_2^{3+} + Fe_{aq}^{2+}$; 329 15. $\operatorname{Ru}(\operatorname{bpy})_{2}(\operatorname{py})_{2}^{3+} + \operatorname{Fe}_{aq}^{2+}; 329$ 16. $\operatorname{Ru}(\operatorname{NH}_{3})_{6}^{3+} + \operatorname{V}_{aq}^{2+}; 17. \operatorname{Ru}(\operatorname{NH}_{3})_{5} \operatorname{py}^{3+} +$ V_{aq}^{2+} ; 18. Co(en) $\frac{3+}{3} + V_{aq}^{2+}$; 19. Co(bpy) $\frac{3+}{3} + V_{aq}^{2+}$; 310 20. Co(phen) $\frac{3+}{3} + V_{aq}^{2+}$ v_{aq}^{2+} ; 310 21. $Ru(NH_3)_{5}py^{3+} + Cr_{aq}^{2+}$; 360 22. $Ru(NH_3)_{4}bpy^{3+} + Ru(NH_3)_{4}phen^{2+}$; 28 23. $Ru(NH_3)_{6}^{3+} + Ru(NH_3)_{6}^{2+}$; 24. $Ru(en)_{3}^{3+} + Ru(NH_3)_{6}^{2+}$: 25. $Co(en)_{3}^{3+} + Ru(NH_3)_{6}^{3+}$ $Co(en)_{3}^{2+}$; 26. $Co(bpy)_{3}^{3+} + Co(bpy)_{3}^{2+}$; 27. $Co(phen)_{3}^{3+} + Co(phen)_{3}^{2+}$; 28. $Co(en)_{3}^{3+} + Cr(bpy)_{3}^{2+}$; 361 29. $Co(phen)_{3}^{3+} + Ru(NH_{3})_{6}^{2+}$; 30. $Co(phen)_{3}^{3+}$ + Ru(NH₂)₅py²⁺.

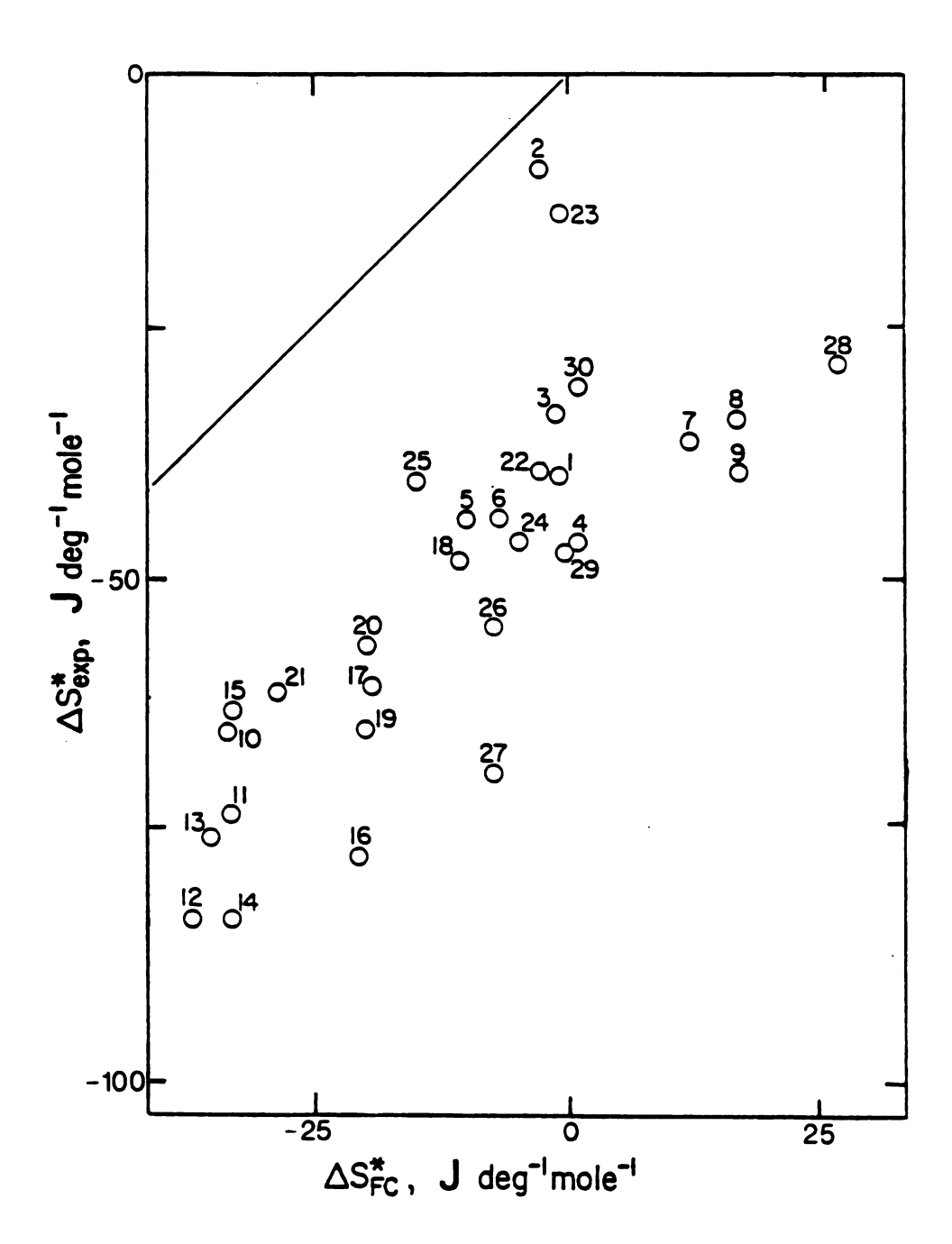


Figure 6.9

Most nonsymmetrical intramolecular reactions will also have nonzero entropic driving forces, thereby yielding nonzero values of ΔS_{PC}^* on the basis of Equation 6.31. This is most obviously the case for systems where electron transfer leads to a net charge decrease at the redox centers, such as the pentaamminecobalt(III) pentacyanoiron(II) reactions examined by Haim and coworkers. 354 the values of $\Delta S_{rc,red}^{O}$ and $\Delta S_{rc,ox}^{O}$ will be positive and negative, respectively (Table 6.4), yielding large positive values of ΔS^{O} (Equation 6.32) and hence ΔS_{PC}^* (Equation 6.31), due to the decrease in solvent polarization attending such charge neutralization. 354c Quantitative values of ΔS^{O} for these systems are difficult to estimate from values of ΔS_{rc}^{0} for the isolated redox centers. This is because ΔS_{rc}^{0} for cyano Fe(III)/(II) couples are known to be extremely sensitive to the cationic environment (Table 6.4) 286 so that the proximity of the cationic Co(III)/(II) redox center is expected to influence the solvation around Fe(III)/(II). Nevertheless, from the ΔS_{rc}^{0} values in Table 6.4, we estimate that ΔS_{rc}^{0} equals roughly 125 J deg⁻¹ mol⁻¹ and -45 J deg^{-1} mol⁻¹ for the Co(NH₂)₅L-^{3+/2+} and -LFe(CN)₅^{2-/3-} fragments, where L is a pyridine-type ligand, yielding $\Delta S^{\circ} \approx 170 \text{ J deg}^{-1} \text{ mol}^{-1}$ (Equation 6.32) and ΔS_{FC}^{*} =80 J deg⁻¹ mo1⁻¹ (Equation 6.31a). Indeed values of ΔS_a^* of this order are obtained for $(CN)_5 Fe^{II} - L - Co^{III} (NH_2)_5^+$ reactions. Similarly, large values of ΔS^{0} are expected for the intramolecular reduction of pentaamminecobalt(III) by the p-nitrobenzoate radical anion since both redox centers will again contribute positive components to ΔS^{0} , thereby explaining the large preexponential factors (i.e. positive values of ΔS_{g}^{*}) observed for these reactions. ³⁶²

Table 6.4

Reaction Entropies, ΔS^{O} (J deg⁻¹ mol⁻¹) for Various Redox Couples in Aqueous Solution.

Redox Couple ^b	1	Metal Center_	
	Co	Ru	Fe
$M(2-bpy)_3^{3+/2+}$	92	4	8
M(phen)3+/2+	92		13
$M(OH_2)_6^{3+/2+}$	250 ^c	150	180
M(en)3+/2+	155	54	
M(NH ₃) ^{3+/2+}	190 ^d	75	
M(NH ₃) ₅ (bpy) ^{3+/2+}		63 ^e	
м(NH ₃) ₅ ру ^{3+/2+}		71	
M(NH ₃) ₅ OH ₂ ^{3+/2+}		105	
m(ne ₃) ₅ ncs ^{2+/+}		63	
M(NH ₃) ₅ C1 ^{2+/+}		42	
$c-M(NH_3)_4C1_2^{2+/+}$		42	
$M(CN)_6^{3-/4-}$		-17	6 ^f , - 96 ^{e,g}
M(CN) ₄ bpy ^{-/-2}			-120 ^f

Notes to Table 6.4

a Ionic strength $\mu=0.1$; data taken from references 55 and 84, except where noted. Uncertainties estimated to equal 2-6 J deg⁻¹ mol⁻¹ for directly measured values. bM denotes metal redox centers. Ligand abbreviations: 2-bpy = 2.2′-bipyridine; bpy = 4.4′-bipyridine; phen = 1. 10-phenanthroline; en = ethylenediamine; py = pyridine. cEstimated from thermodynamic data given in reference 398 by correcting for temperature dependence of reference electrode and likely ionic strength effects. A similar value (ca. $\frac{1}{2}$ 20 J deg⁻¹ mol⁻¹) is obtained from a correlation of S_{rc}^{0} with the self-exchange rate constant k_{ex} , assuming that k_{ex} 10⁻¹⁰ M^{-1} sec⁻¹. dEstimated by comparison with corresponding value for $Co(en)_3^{3+/2+}$. eJ. T. Hupp, unpublished experiments. for Ionic strength $\mu=0$. Spetermined in 0.2 Mac(CLO₆)₃.

Substantial values of ΔS^{O} are expected also for intramolecular reactions between pairs of metal redox centers having the same charge type and similar ligand environments but with different electronic configurations. Important examples of this type are the pentaammine-cobalt(III) - aquotetraamine- ruthenium(II) reactions bridged by nitrogen heterocyclic ligands that have been studied by Taube and coworkers. Since these reactions are charge symmetric, it is usually tacitly assumed that $\Delta S^{O} = 0$ and hence $\Delta S^{*}_{FC} = 0.353b,355b$. However, since reaction entropies for high-spin Co(III)/(II) couples are generally found to be markedly larger than for Ru(III)/(II) and other low-spin couples (Table 6.4),55.84 large positive values of ΔS^{O} and hence ΔS^{*}_{FC} are therefore anticipated for these reactions.

As an illustrative example, we consider the intramolecular reduction of Co(III) by Ru(II) in (H_20) Ru(NH₃)₄(bpy)Co(NH₃)₅⁵⁺ (where bpy = 4,4'-bipyridine). The reaction for the corresponding dipentammine complex Ru(NH₃)₅(bpy)Co(NH₃)₅⁵⁺ is liable to involve a net entropy change of ca 85-105 J deg⁻¹ mol⁻¹ since the reaction entropies of Co(III)/(II) and Ru(III)/(II) couples having similar ligands uniformly differ by this amount (Table 6.4), (references 55 and 82). The effect of replacing one ammonia on ruthenium by an aquo ligand can be gauged from the 30 J deg⁻¹ mol⁻¹ larger reaction entropy for Ru(NH₃)₅OH₂^{3+/2+} than for Ru(NH₃)₆^{3+/2+} (Table 6.4). (To a first approximation, the reaction entropies for mixed-ligand complexes appear to arise from linear additive contributions from each ligand). Thus the entropic driving force for electron tranfer in H_2 ORu^{II}(NH₃)₄(bpy)-Co^{III}(NH₃)₅+ is estimated to be ca. +65 J deg⁻¹

mol⁻¹. Bearing in mind the likely value of ΔS_{int}^* (3-8 J deg⁻¹ mol⁻¹), ³⁵⁷ a value of ΔS_{FC}^* of ca. 35 J deg⁻¹ mol⁻¹ is obtained from Equation 6.31. Therefore the "measured" activation entropy, ΔS_a^* , of 10 J deg⁻¹ mol⁻¹ for this system is suggestive of a significantly nonadiabatic pathway (κ_{el} ~ 0.1; Equation 6.29) rather than the adiabatic pathway that has been inferred without consideration of the entropic driving force. ^{354b},c Since similar values of ΔS_{FC}^* should also be appropriate for other H₂ORu^{II}(NH₃)₄LCo^{III}(NH₃)₅+ reactions with related bridging ligands L, the smaller or negative values of ΔS_a^* seen, for instance, with L = 1,2-bis(4-pyridyl)ethylene (5 J deg⁻¹ mol⁻¹) and 1.2-bis(4-pyridyl)ethane(-40 J deg⁻¹ mol⁻¹) infer the presence of decidely nonadiabatic pathways. Thus from Equation 6.4, if ΔS_{FC}^* = 35 J deg⁻¹ mol⁻¹ then κ_{el} × 10⁻² and 1 × 10⁻⁴ for these two reactions, respectively.

Naturally, these resulting values of $\kappa_{\rm el}$ should be regarded as being only approximate. Since the values of $\Delta S_{\rm rc}^0$ for the intramolecular binuclear reactions are inferred from data for structurally similar mononuclear couples, the reliability of the resulting estimates of $\Delta S_{\rm rc}^0$ and hence $\Delta S_{\rm FC}^*$ may be called into question. Unfortunately, values of $\Delta S_{\rm rc}^0$ cannot be measured directly for these and other thermal intramolecular reactions on account of the rapid aquation that follows the formation of Co(II). However, Steggarda et al. have shown that the values of $\Delta S_{\rm rc}^0$ for mononuclear Ru(III)/(II) couples containing pyrazine ligands are essentially the same as in binuclear complexes where the pyrazine ligand is also bound to another ruthenium redox center. 363 This result therefore provides strong support to the

present method for estimating ΔS^{O} values for binuclear complexes. Providing that the present estimates of ΔS^{O} are accurate to within ca. 20 J deg⁻¹ mol⁻¹, which seem reasonable, then the corresponding estimates of κ_{ol} are reliable to within ca. 4 fold.

Such entropic driving force effects also provide a rationalization of the substantially more positive value of ΔS_a^* , 44 J deg⁻¹ mol⁻¹ for electron transfer in $(SO_3)Ru^{II}(NH_3)_4(pyrazine)$ Co^{III} $(NH_3)_5^{3+}$, 353d especially in comparison with that for $H_2ORu^{II}(NH_3)$ 4(bpy)Co^{III} $(NH_3)_5^{5+}$, 11 J deg⁻¹ mol⁻¹. This increase is difficult to explain on the basis of electronic coupling effects, 353d but can easily be understood in terms of the influence of nonbridging ligand composition on ΔS_a^0 and hence ΔS_{FC}^* . The presence of anionic ligands generally yields substantially smaller values of ΔS_{FC}^0 . The influence of substituting an aquo by a sulfite ligand on the reaction entropy of Ru(III)/(II) can be gauged roughly from the decrease in ΔS_{FC}^0 , 65 J deg⁻¹ mol⁻¹ between Ru(NH₃)₅OH₂^{3+/2+} and c-Ru(NH₃)₄Cl₂^{+/0}, (Table 6.1), 55 corresponding to an increase in ΔS_{FC}^* of ca. 35 J deg⁻¹ mol⁻¹ (Equation 6.31) since the ruthenium undergoes oxidation.

Similar considerations can also be applied to a number of other intramolecular reactions, such as those involving nonsymmetrical bridging ligands. 353,365 Weaver and co-workers have also recently analyzed activation parameter data for a number of intramolecular redox reactions at metal surfaces (i.e. electrochemical processes involving adsorbed reactants) in a similar manner. Entropic driving force effects are generally important for these processes since only one redox center is involved, so that ΔS_{rc}^{O} . Although the

estimation of ΔS_{FC}^{\star} for intramolecular systems should be approached with caution since the factors influencing the thermodynamic entropy changes are incompletely understood, it is clear that careful consideration of the ligand composition and the chemical as well as electrostatic nature of the redox centers is required in order to evaluate the contribution of the Franck-Condon entropy to be measured preexponential factors.

CHAPTER VII

COMPARISONS BETWEEN EXPERIMENTAL KINETICS PARAMETERS AND THE ABSOLUTE PREDICTIONS OF ELECTRON-TRANSFER THEORY

A. <u>Introduction</u>

The kinetics of inorganic electron transfer reactions have been widely investigated over the past thirty years. 366 Experimental work in this area has been spurred by the ongoing development of detailed and sophisticated theoretical treatments of these reactions. The theoretical descriptions of homogeneous outer-sphere reactions of transition-metal complexes in particular have reached a high level of refinement. 56.57 It is probably fair to say that theory has remained one step ahead of experiment since the original work of Marcus. 367 Thus, in the absence of crucial structural and spectroscopic information the predictions of electron transfer theories in an absolute sense have in large measure remained untested. Researchers have had to be content with relative evaluations of theory, such as tests of the so-called cross relations, relative rate comparisons, etc.

Very recently this state of affairs has changed. Sutin and coworkers have determined from EXAFS measurements the magnitude of metal-ligand bond distance alterations accompanying changes of oxidation state for several transition metal complexes. 10 These data together with previous structural measurements 11.12,325,326,368-371 have been

used by Sutin to estimate inner-shell Franck-Condon barriers and absolute electron-transfer rate constants for a number of homogeneous self-exchange reactions. ¹⁰ Broad agreement is found between theory and experiment.

It would be interesting and useful to extend this study to electrochemical reactions. Indeed this is possible by using the newly published EXAFS data. Also it may be enlightening to examine homogeneous cross reactions. In comparison to directly measured self-exchange rate constants, the number of cross-reaction rate data available for comparison with theoretical predictions is quite large. Thus a comprehensive evaluation of contemporary theories should be possible. Besides enabling a considerable expansion of the data set, a virtue of cross reactions is that they enable important supplemental features of the theoretical treatments to be tested, most notably the predictions concerning the response of rate constants to changes in thermodynamic driving force. Comparisons between experimental and theoretical activation parameters provide further tests of theories.

In this chapter, kinetics parameters for approximately ten electrochemical and fifty homogeneous electron-transfer reactions are calculated using current theories and are compared with the corresponding experimental parameters. It is hoped that such comparisons, by uncovering the areas of agreement as well as disagreement, will indicate which aspects of electron-transfer processes are well understood while identifying problems which merit further investigation.

B. Calculation of Kinetics Parameters

In so far as this work overlaps with that of Brunschwig and Sutin, 10 their semi-classical approach is largely retained. (Nevertheless, in instances where commonly employed approximations produce significant errors, more rigorous calculations are made). More sophisticated (and difficult) quantum mechanical analyses are certainly possible, as shown for example by Marcus and Siders. However, it has been demonstrated convincingly that the semi-classical and quantum approaches yield virtually identical results when the same assumptions are used in each calculation. 23

The basic elements of electron-transfer theory have been outlined in Chapter II. According to the semi-classical treatment the overall rate constant can be written as: 23

$$k = K_{A}^{O} v_{n} \Gamma_{K} \epsilon_{1} \exp(-\Delta G^{*}/RT)$$
 (1.24)

or

$$k = K_{A}^{O_{v_{n}} \kappa} \underset{e}{\text{lexp}} \left[-\Delta G(T)^{*} / RT \right]$$
 (7.1)

where K_A^O is the precursor formation constant, ν_n is the nuclear activation frequency κ_{el} is the transmission coefficient for electron tunneling, $_n$ is the nuclear tunneling correction, ΔG^* is the activation free energy representing the height of the classical Franck-Condon barrier, and $\Delta G^*(T)$ is the quantum mechanical equivalent of this barrier. An additional factor which should appear in the rate formula-

tions is the electrostatic work of assembling charged reactants.

However, work terms in both the electrochemical and homogeneous reactions are taken into account instead by correcting the experimental rate parameters for such work. This enables experimental results obtained under dissimilar conditions to be intercompared in a straightforward manner.

1. Pre-exponential Terms

The precursor formation constant for electrochemical reactions is equivalent to the effective thickness of a heterogeneous reaction zone (Section IV. A). A value of $6 \times 10^{-9} \text{cm}$ is deduced from considerations relating to the probable distance dependence of the tunneling coefficient κ_{el} . (This is discussed further in Sections IV A and C). Values of K_A^0 for homogeneous reactions were estimated from: 9

$$K_A^0 = 4\pi N(a_1 + a_2)^2 \delta r$$
 (7.2)

where N is Avogadro's number, a_1 and a_2 are the radii of the reactants (Table 7.1), and δr is the homogeneous reaction zone thickness, again taken as $6 \times 10^{-9} \text{cm.}^{372}$

The activation frequency v_n was calculated from Equation 7.3:

$$v_{n} = (v_{\text{out}}^{2} \triangle G_{\text{out}}^{*} + v_{\text{in}, 1}^{2} \triangle G_{\text{in}, 1}^{*} + v_{\text{in}, 2}^{2} \triangle G_{\text{in}, 2}^{*}) / (\triangle G_{\text{out}}^{*} + \triangle G_{\text{in}, 1}^{*} + \triangle G_{\text{in}, 2}^{*})$$
 (7.3)

where v_{out} and ΔG_{out}^* are the frequency and activation free energy associated with solvent (outer-shell) repolarization, $v_{in,1}$ and $v_{in,2}$

are the inner-shell bond vibration frequencies for each of two reactants, and $\Delta G_{\text{in},1}^{\star}$ and $\Delta G_{\text{in},2}^{\star}$ are the corresponding contributions to the overall activation free energy. (Only one inner-shell term appears in the calculation of v_n for electrochemical reactions). A value of 9 x 10^{11} s⁻¹ was used for v_{out} . The values of v_{in} for the most part are not known with certainty, since the necessary spectroscopic data concerning symmetrical metal-ligand bond vibrations are lacking. The estimates listed in Table 7.1 were obtained by extrapolation from measurements on closely related systems as summarized in the footnotes. The uncertainties in v_{in} values lead directly to only minor uncertainties in calculated rate constants. For almost all of the reactions v_n values in the range from 9 x 10^{12} s⁻¹ to 1.3 x 10^{13} s⁻¹ were calculated. (See Table 7.2). Although some controversy exists concerning the correctness of Equation 7.3, alternative formulations 17 were found to yield similar values of the frequency factor.

Since values of the transmission coefficient can be calculated satisfactorily only by means of <u>ab initio</u> techniques, ^{14,15} this parameter was simply assumed to be unity at the closest separation distance of the reactants. While this assumption represents a possible source of significant error, some justification is provided by Newton's calculations ^{14,15} for the $Fe(H_20)_6^{3+/2+}$ and $Ru(NH_3)_6^{3+/2+}$ self-exchanges as well as our own experimental work (Sections IV. C and V. C, and reference 373). These studies indicate that k_{el} values for homogeneous as well as electrochemical electron-transfer reactions probably lie between 0.2 and 1.

Table 7.1. Thermodynamic and Structural Parameters for Redox Couples.

yreduced (cm-1)		425	411	425	442	977	hh 409			1	i	1				1	Ha H	
f ₂ x10 ⁻⁵ h (dyne cm ⁻¹	1.62	1.47	1.87	1.44	1.58	1.65	1.65hh										1.58 ^{hh}	1.58 ^{hh}
$f_3 x 10^{-5} g$ $(dyne)$ cm^{-1}	2.79	2.76	3.38	2.87	3.01	2.50	2.50 ^{hh}	2.44hh								ļ	2.44 hh	2.44 ^{hh}
°2 (cm ⁻¹)	2 ¹⁶⁶	372 ⁸⁸		368ee		2905	406 hh	35 7 ^{hh}			1	1	ŀ	1		!		
v ₃ (cm ⁻¹)	513 ²	510 ⁸⁸	265 ^{bb}	520cc, dd	533 ^{ff}	500 ⁸⁸	900 hh	494 hh	i	1	ļ		İ	1		-		į
P P Q	0.09±0.02 ^q	0.15±0.02°	0.13±0.01	0.20+0.038,	0.21± ^u	0.04+0.01	0.02+0.02	0.21+0.0018	×o	×0	×o	×o	0.0±0.01	×o		× ₀	0.19±0.02 ^y	0.19±0.028
<u></u>	3.25	3.25	3.25	3.25	3.25	3.5	4.2	4.2	7.8	7.8	7.8	7.8	7.8	7.8		7.8	7.8	7.8
ΔS° b rc -1 J. deg mol-1	151	155	180	205	-250	75	54	155	4	4 b-	-4P	&	12	-4P		16 ⁿ	92	92
E E (m/ vs. E.S.e.)		-475	200	099-	1680 ^j	-180	09-	-460	1040 ^k	1041 ¹	+ 10101	720	870	595 (µ=0.5)™	583 (μ=1.0)™		0/	145
Redox Couple	$Ru(H_2^{0})^{3+/2+}_{6}$	$V(H_2^{0})^{3+/2+}_{6}$	$Fe(H_2^{0})^{3+/2+}_{6}$	$Cr(H_2^{(1)})^{3+/2+}$	$C_0(H_2^{0})_6^{3+/2+}$	Ru(NH ₃)3+/2+	$Ru(en) \frac{3+/2+}{3}$	Co(en) 3+/2+	Ru(bpy) 3+/2+	3+/2+ Ru(phen) 3	Ru(terpy) 3+/2.	$Fe(bpy)\frac{3+/2+}{3}$	Fe(phen) 3+/2+	0s(bpy) 3+/2+		Cr(pby) 3+/2+	Co(bpy) 3+/2+	Co(phen) 3+/2+

state. Calculated by using Equation 7.13 except as noted. i. Estimated value of reduced frequency for symmetrical metal-ligand stretch. Calculated according to: $v^2 = v_3^2 v_2^2 / (v_3^2 + v_2^2)$. j. Reference 392. k. Reference 311. 1. In $1 \underline{M}$ H₂SO₂ E^f values for Ru(bpy) $\frac{3+/2+}{3}$ and Ru(phen) $\frac{3+/2+}{3}$ are identical, while E values for Ru(terpy) $\frac{3+/2+}{2}$ and Ru(bpy) $\frac{3+}{3}$ differ by ~0.03V. References 393 and 394. m. Reference 391. n. Reference v^2 α z/d^3 for aquo and ammine complexes having same metal center. See reference . aa. Taken to be 10 cm smaller than $\text{Cr}(\text{H}_20)^{3+/2+}_{6}$ values by analogy with periodicity trends in $\text{M}(\text{NH}_3)^{4+/2+}_{6-1}$ data. 8B bb. Estimated from $v^2\alpha z/d^3$. cc. Estimated by assuming $v(\text{symmetrical}) \approx v(\text{asymmetrical}) + 30$ cm by analogy with trends in $\text{M}(\text{NH}_3)^{4+/2+}_{6}$ data 8B and related aquo data. dd. Reference 396. ee. Estimated from v_2 by assuming $v^2\alpha z/d^3$. ff. Estimated from corresponding hexaamine data 8B by assuming $v^2\alpha z/d^3$. gg. Reference 397. hh. Assumed to $\frac{3+/2+}{3}$, z. Estimated from symmetrical metal-ligand stretching frequency for Ru(NH $_3$) $_6$ by noting that 253. o. Estimated from thermodynamic data given in reference 395, by correcting for temperature dependence a. Formal potential of redox couple vs. saturated calomel electrode(add 245 mV to convert to electrode potentials vs. NHE). Data are from reference 55 unless otherwise noted. Uncertainties are 2-4 J deg $^{-1}$ mol $^{-1}$. value of symmetrical metal-ligand stretching force constant in M(III) state. Calculated by using Equation q. Reference 11. r. Estimated as outlined in text. s. Reference 10. t. Value represents an average of the 7.13, except as noted. h. Estimated value of symmetrical metal-ligand stretching force constant in M(II) change of oxidation state. e. Estimated value of symmetrical metal-ligand stretching frequency in M(III) c. Reactant radius. Estimates are from reference 10. d. Change in metal-ligand bond length accompanying state. f. Estimated value of symmetrical metal-ligand stretching frequency in M(II) state. g. Estimated axial and equatorial bond length changes (reference 10). u. References 326 and 376. v. Reference 368. of reference electrode and likely ionic strength effects. p. Assumed to equal $\Delta S_{
m rc}^0$ for Ru(bpy) $_3^3$ w. Reference 395. x. Assumed to equal Δd value for Fe(phen) $\frac{3+/2+}{3}$. y. Assumed to equal Δd value for equal values for corresponding hexaammine couples.

2. Franck-Condon Barriers

Three factors contribute to the classical Franck-Condon barrier, namely, the solvent reorganization energy $v_{\rm out}$, the metal-ligand bond (inner-shell) reorganization energy $v_{\rm in}$, and the free energy driving force ΔG^0 . The reorganization energies correspond to the energy required to displace the nuclear (solvent and bond) coordinates of the reactants so that they match those of the products (Figure 7.1) under conditions where $\Delta G^0 = 0$. For a cross reaction such as

$$A^{3+} + B^{2+} \rightarrow A^{2+} + B^{3+} \tag{7.4}$$

the total intrinsic reorganization energies f and r for forward and reverse reactions are given by Marcus additivity rules as 13

$$\lambda_{f} = (\lambda_{in}^{A,3+} + \lambda_{in}^{B,2+} + \lambda_{out})$$
 (7.5)

and

$$\lambda_{r} = (\lambda_{in}^{A,2+} + \lambda_{in}^{B,3+} + \lambda_{out})$$
 (7.6)

where the superscripts on λ_{in} designate the particular reactant being reorganized. Equations 7.5 and 7.6 are sometimes reformulated using a pair of λ_{in} values derived from reduced force constants for metal-ligand vibrations rather than the four λ_{in} values obtained using the individual force constants for inner-shell modes. This approximation was avoided since it yields substantial errors in ΔG^* for certain reactions, e.g.

Table 7.2. Experimental and Theoretical Rate Constants $(M^{-1}s^{-1})$ for Homogeneous Electron-Transfer Reactions.

	oxidant	reductant	<u>k</u>	μ	kcorr	<u>k (T)</u> <u>R</u>	eference
1	V(H ₂ O) ³⁺	V(H ₂ 0) ²⁺ 6	1.5x10 ⁻²	(2)	8x10 ⁻²	1.7	267
2	$\operatorname{Fe}(\mathtt{H}_2\mathtt{0})_6^{3+}$	$Fe(H_2^0)_6^{2+}$	4	(0.55)	52	9.7	266
3	$Co(H_2O)_6^{3+}$	$Co(H_2O)_6^{2+}$	8	(3)	33.	2.2x10 ⁻⁸	399
4	Co(H ₂ 0) ³⁺	$Fe(H_2^0)_6^{2+}$	50	(1)	4.2x10 ²	2x10 ⁵	400
5	Co(H ₂ 0) ₆ ³⁺	$Cr(H_2O)_6^{2+}$	1.3x10 ⁴	(3)	5.3x10 ⁴	5.2x10 ⁷	401
6	Co(H ₂ 0) ³⁺	V(H ₂ O) ₆ ²⁺	9x10 ⁵	(3)	3.7x10 ⁶	3.3x10 ⁹	401
7	$Fe(H_2^{0})_6^{3+}$	$Ru(H_2^0)_6^{2+}$	2.3x10 ³	(1)	1.9x10 ⁴	1.1x10 ⁶	304
8	Fe(H ₂ 0) ³⁺ 6	Cr(H ₂ O) ₆ ²⁺	2.3x10 ³	(1)	1.9x10 ⁴	4.4x10 ⁵	402
9	Fe(H ₂ O) ³⁺ 6	V(H ₂ O) ₆ ²⁺	1.8x10 ⁴	(1)	1.5x10 ⁵	5.6x10 ⁷	379
10	$Ru(H_2O)_6^{3+}$	V(H ₂ O) ₆ ²⁺	2.8x10 ²	(1)	2.3x10 ³	3.2x10 ⁵	304
11	$\operatorname{Fe}(\mathrm{H}_2\mathrm{O})_6^{3+}$	$Ru(NH_3)_6^{2+}$	3.5x10 ⁵	(0.1)	1.5x10 ⁷	8.2x10 ⁸	268
12	$Fe(H_2O)_6^{3+}$	$Ru(en)_{3}^{2+}$	1.4x10 ⁵	(0.1)	3.6x10 ⁶	1.1x10 ⁹	268
13	$Ru(H_2O)_6^{3+}$	$Ru(NH_3)_6^{2+}$	1.4x10 ⁴	(1)	1.1x10 ⁵	5.5x10 ⁶	304
14	$Ru(NH_3)_6^{3+}$	Cr(H ₂ O) ₆ ²⁺	2x10 ²	(0.2)	5.6x10 ³	2.1x10 ⁴	403,404
15	Co(en) 3+	$Cr(H_2O)_6^{2+}$	3x10 ⁻⁴	(1.0)	1.6x10 ⁻³	1.4x10 ⁻³	337
16	$Ru(NH_3)_6^{3+}$	V(H ₂ O) ₆ ²⁺	1.5x10 ³	(0.1)	6.5x10 ⁴	4.8x10 ⁵	405
17	$Co(en)_3^{3+}$	V(H ₂ O) ₆ ²⁺	4.6x10 ⁻⁴	(0.1)	1.2x10 ⁻²	5.2x10 ⁻²	337
18	$Co(H_2O)_6^{3+}$	Fe(phen) $\frac{2+}{3}$	1.4x10 ⁴	(3)	3.8x10 ⁴	3.3x10 ⁹	406
19	$Ru(bpy)\frac{3+}{3}$	$Fe(H_2^0)_6^{2+}$	6.4x10 ⁵	(1)	1.7x10 ⁶	1.3x10 ¹⁰	329
20	Ru(phen) $\frac{3+}{3}$	$Fe(H_2^0)_6^{2+}$	8x10 ⁵	(1)	2.2x10 ⁶	1.3x10 ¹⁰	3 29
21	Ru(terpy) $\frac{3+}{3}$	$Fe(H_2^0)_6^{2+}$	7.2x10 ⁵	(1)	2x10 ⁶	1.3x10 ¹⁰	329
22	Fe(phen) $_6^{2+}$	$Fe(H_2^{0)}_{6}^{2+}$	3.7x10 ⁴	(0.5)	7.4x10 ⁴	4x10 ⁸	335

Table 7.2 (continued)

	<u>oxidant</u>	reductant	<u>k</u>	_μ_	kcorr	<u>k (T)</u> <u>Re</u>	eference
23	Fe(bpy) $\frac{3+}{3}$	$Fe(H_2^{0)}_6^{2+}$	2.7x10 ⁴	(0.5)	9.6x10 ⁴	1.3x10 ⁹	335
24	Os (bpy) $\frac{3+}{3}$	$Fe(H_2^0)_6^{2+}$	1.4x10 ³	(0.5)	5x10 ³	3.2x10 ⁷	334
25	$Fe(H_2^0)_6^{3+}$	$Co(phen)_3^{2+}$	5.3x10 ³	(1)	1.4x10 ⁴	1.9x10 ⁴	337
26	•	$Cr(H_2O)_6^{2+}$			81	4x10 ³	337
27	•	$Ru(H_2O)_6^{2+}$				3x10 ¹²	317
28	Os (bpy) $\frac{3+}{3}$			(1)	7.8x10 ⁸	9.8x10 ¹¹	304
29		$Ru(H_2^0)_6^{2+}$			1.4x10 ²		304
30	$Cr(bpy)_3^{3+}$	V(H ₂ 0) ²⁺ 6	4.2x10 ²	(1)	1.1x10 ³	2.6x10 ⁶	310
31	$Co(phen)_3^{3+}$	$V(H_2^0)_6^{2+}$	4x10 ³	(1)	1.1x10 ⁴	7.3x10 ⁵	310
32	-	$V(H_2^0)_6^{2+}$					
33		$Ru(NH_3)_6^{2+}$					
34	-	$Ru(NH_3)_6^{2+}$					
35		$Ru(en)_3^{2+}$					
36	Co(en) 3+	-				1.1x10 ⁻⁴	
37		$Ru(phen)_{3}^{2+}$				7.2x10 ⁸	
38	•	Fe(phen) $\frac{2+}{3}$					
39	_	Co(bpy) ₃ ²⁺					
40	_	$Co(phen)_3^{2+}$					
	$Co(phen)_3^{3+}$	•					409
	$Co(bpy)_3^{3+}$						409
	$Co(bpy)_3^{3+}$	• -					
	$Co(phen)_3^{3+}$	3 0					
45	Co(en) 3+	$Cr(bpy)_3^{2+}$	35	(0.1)	2.2x10 ²	4.9x10 ³	361

those involving considerable inner-shell reorganization around one metal center and none around the other.

The free energy driving force can be represented as a displacement of the wells of the free energy curves which are generated in calculating $\lambda_{\mathbf{f}}$ and $\lambda_{\mathbf{r}}$. If both outer- and inner-shell reorganization energies are taken to be quadratic functions of the nuclear coordinates, the energy at the intersection point of the free energy curves, i.e. ΔG^* , can be calculated from

$$\Delta G^* = x^2 \lambda_f \tag{7.7}$$

where the value of the nuclear coordinate X is found by solving Equation 7.8:

$$\lambda_{f} x^{2} = \lambda_{r} (1-x)^{2} + \Delta G^{0}$$
 (7.8)

Values of ΔG^0 were determined from the formal potentials listed in Table 7.1. Activation free energies for electrochemical reactions were calculated in a similar manner.

Solvent reorganization energies for homogeneous reactions were calculated by using the ellipsoidal cavity model described by Cannon. 374,375 The ellipsoidal cavity model allows for interpenetration of reactant coordination spheres, whereas as the conventional two-sphere model of Marcus in principle does not. In light of recent theoretical work 14,15 suggesting that reactant interpenetration is generally required in order to achieve significant coupling of donor and acceptor

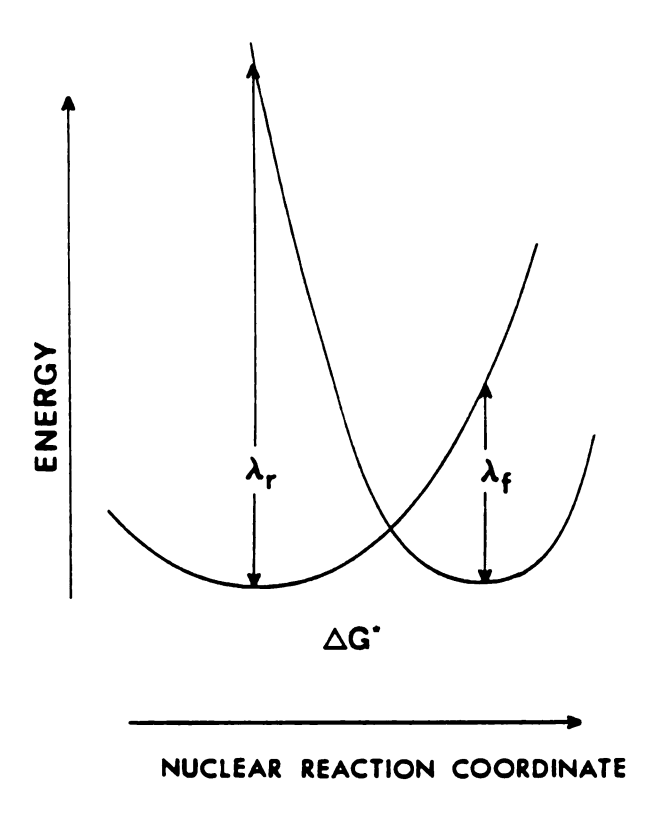


Figure 7.1 Schematic representation of the relationships between the nuclear reaction coordinate, forward and reverse reorganization energies, and the classical free energy barrier to electron transfer.

electronic orbitals, the Cannon model was considered to be more appropriate than the two-sphere model. Reorganization energies were calculated according to Equation 7.9:

$$\lambda_{\text{out}} = (\text{Ne}^2 \text{r}^2 / 21_a^2 1_b^2) (1/\epsilon_{\text{op}} - 1/\epsilon_{\text{s}}) \text{ S } (\lambda_{\text{o}})$$
 (7.9)

where e is the electronic charge, r is the distance between the redox centers, l_a and l_b are the semi-major and semi-minor axes of an ellipsoid encompassing the reactants, ε_{op} and ε_{s} are the optical and static dielectric constant of the solvent and $S(\lambda)$ is the "shape factor." This last term depends in a complicated manner on the eccentricity of the ellipsoid, but can be reasonably approximated as

$$S(\lambda_0) \approx 1.19 - 0.54 e$$
 (7.10)

for $0.8 \le e \le 1$.

The major semiaxis l_a equals $(a_1 + a_2 + r)/2$ with radii a_1 and a_2 listed in Table 7.1. In the absence of additional information, coordination spheres were assumed to interpenetrate such that redox centers were 1.25 Å closer than expected from close contact of reactants. Such an estimate is appropriate at least for reactions between aquo complexes. $^{14.15.17}$ The minor semiaxis l_b were calculated by taking the volume of the ellipsoid to be equal to that of the two isolated reactant spheres. The values of $\epsilon_{\rm op}$ and $\epsilon_{\rm s}$ respectively, at $25^{\rm o}$ C are 1.78 and 78.3.

Solvent reorganization energies for electrode reactions were calculated from 13

$$\lambda_{\text{out}} = (\text{Ne}^2/\text{r})(1/\text{a}-1/\text{R}_{\text{e}})(1/\epsilon_{\text{op}}-1/\epsilon_{\text{g}})$$
 (7.11)

where R_e is twice the distance from the redox center to the electrode (i.e. the distance from the charged reactant to its image in the electrode). A value of $R_e = 7 \text{Å}$ is obtained if the reaction site is assumed to correspond to the outer Helmholtz plane.

Inner-shell reorganization energies were calculated from

$$\lambda \stackrel{\text{M,n+}}{\text{in}} = 3f^{\text{M,n+}} \Delta d \qquad (7.12)$$

where $f^{M,n+}$ is the force constant for the symmetrical breathing motions of six identical metal-ligand bonds and Δd is the difference between the equilibrium bond distances for the two oxidation states. Intraligand bond vibrations and contortions were ignored since these are anticipated to provide only minor contributions to λ_{in} . Values of Δd are listed in Table 7.1. Since structural data are lacking for hexasquo vanadium(II), the change in the metal-oxygen bond length for the $V(H_20)_6^{3+/2+}$ couple was estimated from the vanadium-oxygen bond lengths in related oxide compounds. Beattie, et al. have shown that there is a close correspondence (within circa 0.02 $\frac{\alpha}{\alpha}$) between the metal-oxygen Δd values found in oxides and those found in hexa-aquo metal complexes. $\frac{326}{\alpha}$

Given the structural similarities, the low spin $Fe(bpy)_3^{3+/2+}$, $Ru(bpy)_3^{3+/2+}$, $Ru(phen)_3^{3+/2+}$ and $Ru(terpy)_3^{3+/2+}$ couples were each assumed

to require negligible inner-shell reorganization, as for the low spin $Fe(phen)_3^{3+/2+}$ couple ($\Delta d = 0.0\%$).

Force constants were calculated from

$$f = A \pi v_{in}^2 c^2 \mu \tag{7.13}$$

where c is the velocity of light and μ is the reduced mass of the 11-gand. For cobalt complexes containing large bidentate ligands, force constants for the cobalt-nitrogen stretch were taken to equal those for hexaammine cobalt (III) and (II). Although values of ν_{in} are available for the bidentate ligand complexes suggesting that Equation 7.13 could be employed to calculate force constants, it is not clear what values of the reduced mass should be used since the metal-nitrogen vibration may be partially decoupled from the motion of the ligand as a whole. Nuclear tunneling factors (Γ_{in}) can be expressed as $\Delta G^*(Q)$ values, thus emphasizing that these represent the difference between the average quantum barrier $\Delta G^*(T)$ and the classical Franck-Condon barrier ΔG^* . From Holstein's work on small polaron motion, $^{19},^{20},^{377},^{378},^{378}$, Sutin, et al. have derived expressions for $\Delta G^*(T)$ for reactions without (Equation 7.14) and with (Equation 7.15) a free energy driving force. $^{9},^{23}$ The expressions for $\Delta G^*(T)$ are:

$$\Delta G^{*}(T) = \lambda (kT/h\nu) \tanh(h\nu/\lambda kT) \qquad (7.14)$$

and

$$\Delta G^{*}(T) = 0.5\Delta G^{0} + (kT/hv) \{coth(hv/2kT) -$$

$$[(\Delta G^{\circ})^2/\lambda^2 + csch^2(hv/2kT)]^{1/2} +$$

$$(G^{\circ}/\lambda)\sinh^{-1}[(\Delta G^{\circ}/\lambda)\sinh(\hbar\nu/2kT)]\}$$
 (7.15)

Equations 7.14 and 7.15 were derived for tunneling processes involving a single vibrational mode characterizd by equal force constants and vibrational frequencies in the two oxidation states. Accordingly AG*(T) refer to only one mode in each calculation. Although $\Delta G^*(T)$ values which are calculated assuming equal force constants will certainly differ from those obtained using unequal force constants and frequencies, the difference, $\Delta G^*(Q)$, between quantum and classical barriers under simplified conditions should be similar to that obtained when quantum and classical barriers are both calculated more rigorously. Thus, simple single-frequency modes were assumed in calculating $\Delta G^*(T)$ and $\Delta G^*(Q)$, with the tunneling corrections then being applied to ΔG^* values which had been calculated in a more complicated manner (vide Tunneling corrections for solvent repolarization were considered to be negligible since v_{out} is probably significantly less than kT/h. Tunneling corrections for each inner-shell mode were calculated separately. Thus the driving force AGO, appearing in Equation 7.15 was taken in each calculation to be an appropriate fraction $(\lambda^{M,n+}/\lambda_f)$ of the total driving force ΔG^0 . This insures that $\Delta G^*(Q)$ reaches zero at the same ΔG^O value at which ΔG^* is zero. A point of confusion concerns the use of ΔG^{0} , given that Equation 7.15 is

derived using a temperature independent driving force ΔE° . Although the substantial ΔS° values found for many reactions reflect chiefly the solvation changes accompanying the overall electron transfer process, this entropy change nonetheless would seem to provide a driving force for reorganization of both inner- and outer-shell modes. At least for the present then, ΔG° is used in place of ΔE° .

The methods outlined thus far enable rate constants to be calculated using Equation 7.2. However, it is also of interest to compare the theoretical predictions concerning activation enthalpies and entropies with the corresponding experimental quantities.

Activation entropies (classical limit) were calculated for homogeneous reactions according to:

$$\Delta S_{calc}^{*} = 0.5 \Delta S^{o} + \Delta G^{o} \Delta S^{o} / \lambda_{f}$$
 (7.16)

Contributions to ΔS^* arising from the temperature dependence of λ out were neglected since these amount to 2 J deg⁻¹ mol⁻¹ at most when calculated by Marcus' theory. ¹³ (However, see Section VI. A). Equation 7.16 was derived by assuming equal force constants for inner-shell reorganization in different oxidation states. Nevertheless, this approximation yields little error since the purely thermodynamic term $(0.5 \ \Delta S^0)$ usually provides the dominant contribution to ΔS^*_{calc} . Also, the use of λ_f rather than a "reduced" reorganization energy nullifies to some extent the errors resulting from the force constant approximation. The required values of ΔS^0 were obtained from the thermodynamic reaction

entropies $^{\Delta}S^{o}_{rc}$ for the individual half-reactions (Table 7.1). For electrochemical reactions $^{\Delta}S^{\star}_{calc}$ is given by:

$$\Delta S_{calc}^{*} = \alpha \Delta S_{rc}^{0}$$
 (7.17)

where α is the electrochemical transfer coefficient and the contribution from $-d\lambda_f/dT$ again has been ignored.

Classical activation enthalpies were determined from the relation:

$$\Delta H_{calc}^{*} = \Delta G_{calc}^{*} + T\Delta S_{calc}^{*}$$
 (7.18)

where ΔH^* is defined as $-R(d\ln k/d(1/T))$.

Nuclear tunneling corrections, $\Delta H^*(Q)$ and $\Delta S^*(Q)$, to activation parameters were obtained by calculating $\Delta G^*(Q)$ at various temperatures (Equations 7.14 and 7.15) and noting that $-\Delta G^*(Q)/T = \Delta S^*(Q)$, while $\Delta G^*(Q) + T\Delta S^*(Q) = \Delta H^*(Q)$. The resulting tunneling-corrected parameters are designated as $\Delta S^*(T)$ and $\Delta H^*(T)$.

3. <u>Kinetics Formulations and Work Corrections for Experimental</u> Parameters

Activation parameters are usually extracted from experimental rate data by assuming a pre-exponential factor of kT/h rather than $K_{A}^{O}v_{n}$. These "Eyring" (kT/h) activation parameters (designated using superscript daggers) can be converted to "pre-equilibrium" ($K_{A}^{O}v_{n}$) prefactor) activation parameters using:

$$\Delta S^* = \Delta S \neq -R + R \ln(R_A^0 v_n h/kT) \qquad (7.19)$$

and

$$\Delta \mathbf{H}^{\pm} = \Delta \mathbf{H} \neq + \mathbf{R} \mathbf{T} \tag{7.20}$$

thereby enabling straightforward comparisons to be made between theory and experiment.

Experimental rate constants for homogeneous electron transfer were corrected for the electrostatic work of precursor formation by way of the Debye-Huckel treatment. This approach is embodied in Equation 7.21:

$$\log k_{corr} = \log k + Z_A Z_B e^2 N/2.303RT \epsilon_{s} r(1+\beta r \mu^{1/2}) \qquad (7.21)$$

where $\mathbf{Z}_{\mathbf{A}}$ and $\mathbf{Z}_{\mathbf{B}}$ are the reactant charge numbers, β is the Debye-Hückel parameter, μ is the ionic strength and \mathbf{k}_{corr} is the rate constant which is expected in the absence of electrostatic interactions. Since several kinetics studies have indicated that activation enthalpies decrease systematically with increasing ionic strength while activation entropies remain essentially unchanged, 28,379-381 it was deemed appropriate to incorporate work corrections wholly in $\Delta \mathbf{H}^*$.

Electrochemical rates were corrected for electrostatic diffuse double-layer effects by using the Gouy-Chapman-Stern-Frumkin theory as described in Sections 1.C and 4.D.

C. Results

Calculated rate constants are compared in Figures 7.2 and 7.3 with work-corrected experimental rate constants. The reactions are separated into two groups: those involving a pair of reactants possessing identical ligand compositions (Figure 7.2) and those involving reactants possessing dissimilar ligand compositions (Figure 7.3). In order to compare electrochemical and homogeneous reactions on a common basis, rate constants for the former (k_{calc}^{E}) were converted to second-order rate constants by multiplying $k_{calc}^{\underline{R}}$ values by the ratio of statistical factors for the two types of reactions, i.e. $K_A^O/\delta r$. Values of k_{calc} and k are listed in Tables 7.2 and 7.3 together with observed experimental rate constants. Values of $\Delta G^*(T)$, $\Delta G^*(Q)$, ΔG^0 , λ_f , K_A^0 and v_n are given in Table 7.4. The calculated rate constants plotted in Figures 7.2 and 7.3 were obtained using individual force constants and tunneling corrections for the inner-shell, with the Cannon model being used to calculate the outer-shell barrier for the homogeneous reactions. The use of individual force constants yielded rates that were typically three-fold, but in a few cases as much as twenty-fold, smaller than calculated using reduced force constants. Allowing for reactant interpenetration usually decreased $\Delta G^*(T)$. Nuclear tunneling corrections increased the calculated rate constants. Values of $\Gamma_{\mathbf{n}}$ range from 1 to 17, the largest values being found for low driving force reactions requiring substantial inner-shell reorganization. Values of ${\tt K_A^o}$ range from 0.13 ${\tt M}^{-1}$ for reactions between aquo complexes to 0.9 ${\tt M}^{-1}$ for reactions between polypyridine complexes.

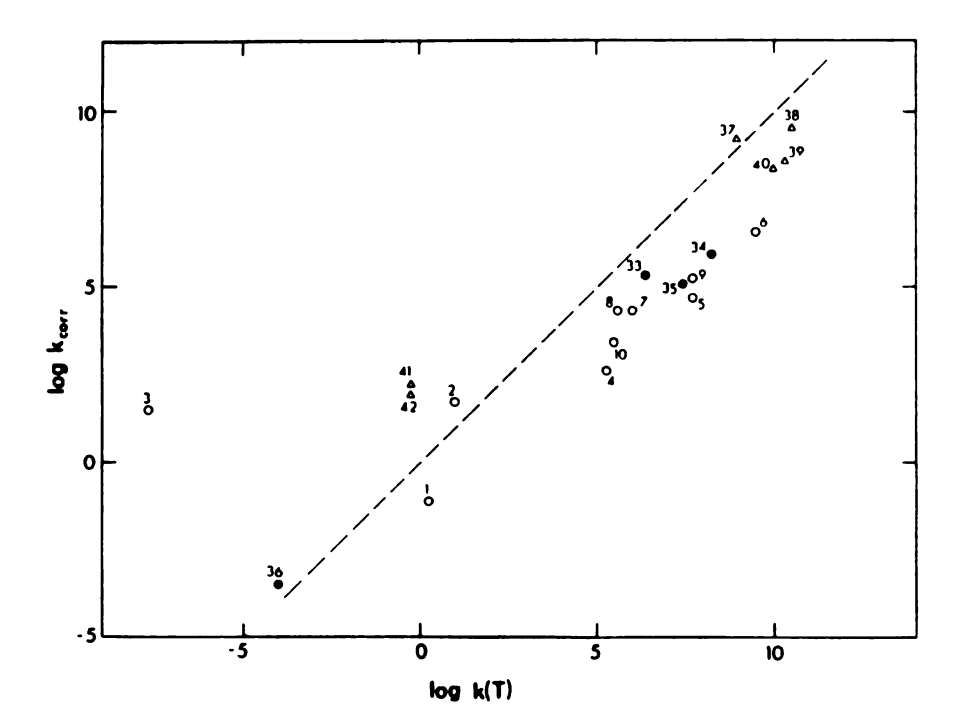


Figure 7.2 The log of the work-corrected experimental rate parameter k_{corr} plotted against the log of the corresponding theoretical parameter k(T) for electron transfer between reactants possessing identical ligand compositions. Key: (O) aquo complexes: (Δ) polypyridine complexes: (Φ) ammine complexes. Reactions and rate constants listed in Table 7.2.

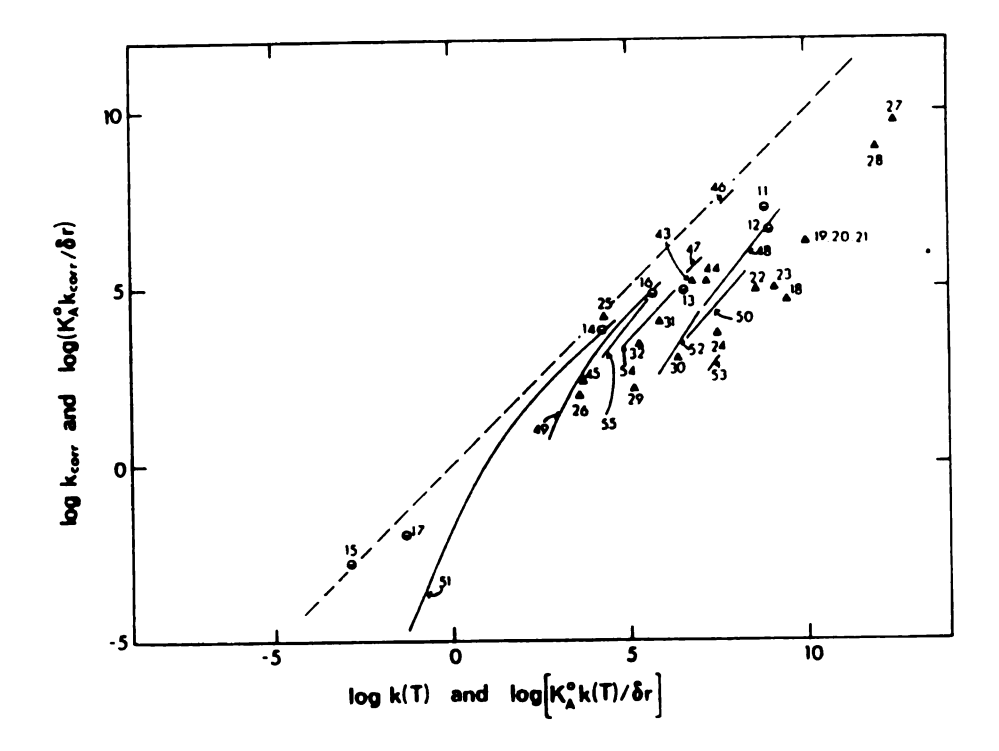


Figure 7.3 The log of the work-corrected experimental rate parameters k_{corr} and $K_A^O k_{corr}/\delta r$ plotted against the log of the corresponding theoretical parameters k(T) and $K_A^O k(T)/\delta r$ for electron-transfer between reactants possessing dissimilar ligand compositions. Key to cross-reactions:

(a) aquo-ammine; (b) aquo-polypyridine: (a) ammine-polypyridine; (---) electrochemical. Reactions and rate constants are listed in Tables 7.2 and 7.3.

Table 7.3. Experimental and Theoretical Rate

Constants for Electrochemical Electron-Transfer Reactions

	Reactant	Δ (kJ·m	.G° (o1 ⁻¹)	k (cm s ⁻¹)	k corr	$(K_p/\delta r)_x$ k_{corr} $(M^{-1}s^{-1})$	$\frac{(K_{p}/\delta r)_{x}}{k(T)}$ $\frac{(M^{-1}s^{-1})}{(M^{-1}s^{-1})}$
46	Ru(NH ₃) ₆ ³⁺ at mercury	410	0	0.3	1.5	3.4x10 ⁷	5.8x10 ⁷
47	Ru(H ₂ O) ³⁺ at mercury	313	0	5x10 ⁻³	2x10 ⁻²	4x10 ⁵	7.2x10 ⁶
48	Fe(H ₂ 0) ³⁺ at mercury		-20	3.0x10 ⁻⁴	~1.2x10 ⁻³	2.5x10 ⁴	1.3x10 ⁷
	at mercury	313	-30	2.3x10 ⁻³	~9x10 ⁻³	2x10 ⁵	8x10 ⁷
			-40	1.7x10 ⁻²	~7x10 ⁻²	1.5x10 ⁶	4x10 ⁸
			-50	1.3x10 ⁻¹	~5x10 ⁻¹	1x10 ⁷	1.7x10 ⁹
49	V(H ₂ O) ₆ ³⁺	313	+30	2.1x10 ⁻⁷	2.6x10 ⁻⁷	5.4	4.9x10 ²
	at mercury	313	+20	4.7x10 ⁻⁶	6×10^{-6}	1.3x10 ²	2.6x10 ³
			+10	1x10 ⁻⁴	8.7×10^{-5}		1.4x10 ⁴
			0	1.6×10^{-3}			8.3x10 ⁴
			-10	2.3×10^{-2}	4.7×10^{-3}		6.8x10 ⁵
50	$V(H_2O)_6^{3+}$ at lead 136			7.5×10^{-4}	-1.8×10^{-4}	~3.8x10 ³	
	at lead			4.7×10^{-3}		$\sim 2.7 \text{x} 10^4$	
			-40	2.8×10^{-2}		~2x10 ⁵	
51	$Cr(H_2O)_6^{3+}$	313	80			3.3x10 ⁻⁹	
	at mercury	313	70			9.5x10 ⁻⁸	7.4×10^{-3}
			60			2.7×10^{-6}	
			50			6.6x10 ⁻⁵	
			40		8.1×10^{-11}	1.7×10^{-3}	3.8×10^{-1}

Table 7.3. (continued)

		g° mo1 ⁻¹)	k (cm s ⁻¹)	kcorr (cm s ⁻¹)	$(K_p/\delta r)x$ k_{corr} $(M^{-1}s^{-1})$	k (T)
		30		1.9x10 ⁻⁹	4.1x10 ⁻²	1.7
		20		3.5×10^{-8}	7.2x10 ⁻¹	8.0
		10		3.7×10^{-7}	7.7	4.2x10 ¹
		0	1x10 ⁻⁵	3.2×10^{-6}	6.6x10 ¹	2.4x10 ²
		-10	1.1x10 ⁻⁴		5.6x10 ²	2.2x10 ³
		-20	1.2×10^{-3}	2.0×10^{-4}		1.8x10 ⁴
		-30	1.2x10 ⁻²	1.6×10^{-3}		1.3x10 ⁵
52	$\operatorname{Cr}(H_2O)_{6_{136}}^{3+}$		1.8x10 ⁻⁴	1.9×10^{-5}	4xk9 ²	8.5x10 ⁵
	at lead 136		$2x10^{-3}$	1.7×10^{-4}	3.6x10 ³	5.1x10 ⁶
			2.6x10 ⁻²	1.6×10^{-3}		2.7x10 ⁷
53	$Cr(H_2O)_6^{3+}$ at gallium 136	-60	1.5x10 ⁻³	3x10 ⁻⁵	6x10 ²	2.7x10 ⁷
54	Cr(H ₂ O) ³⁺	-20	1.7x10 ⁻⁴	5x10 ⁻⁵	1.1x10 ³	1.8x10 ⁴
	at UPD lead/ silver	-30	1.6x10 ⁻³	5x10 ⁻⁴	1x10 ⁴	1.3x10 ⁵
			1.5x10 ⁻²	4.5×10^{-3}	9x10 ⁴	8.5x10 ⁵
55	$Cr(H_2O)_6^{3+}$	-30	1.7x10 ⁻⁴	1.7x10 ⁻⁴	3.5x10 ³	1.3x10 ⁵
	at UPD thallium/silver	-40	1.3×10^{-3}	1.3x10 ⁻³	2.7x10 ⁴	8.5×10^{5}
		- 50	1x10 ⁻²	1x10 ⁻²	2x10 ⁵	5.1x10 ⁶

Table 7.4. Experimental and Theoretical Electron Transfer Parameters.

2ª	(s ⁻¹)	9.5×10^{12}	1×10^{13}	1.1×10^{13}	$9.7x10^{12}$	1.1×10^{13}	1×10^{13}	9.6×10 ¹²	1.1×10^{13}	i_{x10}^{13}	9×10 ¹²	9×10^{12}	9×10^{12}	6.6×10^{12}
K. A	$(M^{-1}g^{-1})$	0.125	0.125		0.125	0.125	0.125	0.125	0.125	0.125	0.125	0.165	0.20	0.165
∇G*(T)	(kJ mol ⁻¹)	67.5	79	113	38.5	25	14.5	35	37	43	37.5	18.5	18.5	30
-√G*(Q)	(kJ mol ⁻¹)	4.0	3.5	7.0	7.0	2.8	2.0	2.3	4.8	2.4	2.0	1.5	1.4	9.0
, r	$(kJ mol^{-1})$	287	270	480	341	448	353	214	377	266	252	177	156	147
γĘ	(kJ mol ⁻¹)	287	270	480	402	458	414	240	319	258	218	219	200	163
-7G°	(kJ mol ⁻¹)	0	0	0	113.8	225.8	207.9	49.7	111.9	94.1	44.4	9.59	54.0	15.9
Reaction	No.	H	7	3	4	5	9	7	∞	6	10	11	12	13

Table 7.4 (continued)

Reaction	, -∇G°	γĘ	۲ ۲	-∆G*(Q)	∇G*(T)	K. A	> ^c
No.	(kJ mol ⁻¹)	$(kJ \text{ mol}^{-1})$	$(k_{\rm J} \text{ mol}^{-1})$	$(kJ mol^{-1})$	$(kJ mol^{-1})$	$(M^{-1}s^{-1})$ (s^{-1})	(s ⁻¹)
14	46.3	226	326	3.1	45	0.165	1x10 ¹³
15	19.2	401	412	5.2	87.5	0.20	1×10^{13}
16	28.5	181	231	1.6	37	0.165	8×10^{12}
17	1.5	352	312	4.5	82	0.20	1×10^{13}
18	78.2	304	191	4.0	18.5	07.0	1.1210^{13}
19	52.1	120	165	1.4	14	07.0	$9.3x10^{12}$
20	52.1	120	165	1.4	14	07.0	$9.3x10^{12}$
21	51.9	120	165	1.4	14	0.40	$9.3x10^{12}$
22	26.9	120	165	1.6	22.5	0.40	9.3×10^{12}
23	33.3	120	165	1.5	20	07.0	$9.3x10^{12}$
24	8.6	120	165	1.7	29	07.0	$9.3x10^{12}$
25	34.3	248	279	2.8	47.5	0.40	$9.3x10^{12}$
26	0.89	328	355	4.0	51	0.40	9.3×10^{12}

Table 7.4 (continued)

action	-∆G°	γ	, r	-∆G*(Q)	\dag{T}	KA A	> ^c
No.	$(kJ mol^{-1})$	(kJ mol ⁻¹)	(kJ mol ⁻¹)	$(kJ mol^{-1})$	$(kJ mol^{-1})$	$(M^{-1}s^{-1})$	(s^{-1})
27	102.8	06	109	0	0	07.0	7.6x10 ¹²
28	57.8	109	06	0	3	0.40	7.6×10 ¹²
29	15.4	249	190	3.9	42	0.40	8x10 ¹²
	7.0	125	177	2.0	35	07.0	8×10 ¹²
	59.8	283	260	2.4	38	07.0	$9x10^{12}$
32	52.6	283	260	2.5	41	0.40	9×10^{12}
	0	124	124	0.3	30.5	0.135	4×10 ¹²
34	11.6	107	109	0.1	21	0.22	3.6×10 ¹²
35	0	100	100	0	25	0.23	3×10 ¹²
36	0	424	424	5.0	93	0.23	1x10 ¹³
37	0	70	70	0	16.5	69.0	9×10 ¹¹
38		70	70	0	7	69.0	9×10 ¹¹
39	93.6	150	226	9.0	13.5	69.0	7.3×10 ¹²

Table 7.4 (continued)

action	-∆G°	γ) r	-∆G*(Q)	∇G*(T)	ж А	> c
No.	$(kJ mol^{-1})$	$(kJ mol^{-1})$	$(k_{\rm J} \text{mol}^{-1})$	$(kJ mol^{-1})$	$(kJ mol^{-1})$	$(M^{-1}s^{-1})$	
40	86.4	150	226	9.0	15.5	0.69	
11	0	322	322	2.4	75	0.69	9×10^{12}
÷2	0	322	322	2.4	75	69.0	9×10^{12}
÷3	24.3	228	156	1.3	33	0.41	7×10 ¹²
7	31.4	228	156	1.2	30	0.41	7×10 ¹²
45	1.5	269	177	2.5	51	77.0	1.x10 ¹³
9,	0	91	88	.1	22.5	0.135	3.6×10^{12}
	0	130	112	1.3	29	0.125	7×10^{12}
8 +	-20	187	142	1.8	28.5	0.125	1.1×10^{13}
	-30	187	142	1.7	24	0.125	1.1×10^{13}
	07-	187	142	1.6	20	0.125	1.1×10^{13}
	-50	187	142	1.3	16.5	0.125	1.1×10^{13}

Table 7.4 (continued)

2 "	(s^{-1})	9×10^{12}		$9x10^{12}$		$9{\times}10^{12}$	9×10^{12}	9×10^{12}	9×10^{12}		1×10^{13}	1×10^{13}	1×10^{13}
K. A	$(M^{-1}s^{-1})$	0.125	0.125	0.125	0.125	0.125	0.125	0.125	0.125	0.125	0.125	0.125	0.125
\(\rangle G*(T)\)	$(kJ mol^{-1})$	53	67	45	40.5	35.5	30.5	26	22	84	81.5	78	75
-∆G*(Q)	$(kJ mol^{-1})$	-1.6	-1.6	-1.7	-1.7	-1.7	-1.6	-1.6	-1.5	-2.3	-2.5	-2.6	-2.8
۲ ^۱	$(kJ mol^{-1})$	146	146	146	146	146	146	146	146	191	191	191	191
γ ^t	$(kJ mol^{-1})$	199	199	199	199	199	199	199	199	294	294	294	294
-∆G°	$(kJ mol^{-1})$	+30	+20	+10	0	-10	-20	-30	07-	80	70	09	90
Reaction	No.	49,50								51-55			

Table 7.4 (continued)

> ^C	(s^{-1})	1×10^{13}	1×10 ¹³	1×10^{13}	1×10^{13}							
K. A	$(M^{-1}s^{-1})$	0.125	0.125	0.125	0.125			0.125	0.125			0.125
∇G*(T)	$(kJ mol^{-1})$	71.5	89	79	09	55.5	20	45	07	35	31	26.5
(ð) ∗ 5∇−	(kJ mol ⁻¹)	-2.9	-3.0	-3.0	-3.1	-3.1	-3.1	-3.0	-3.0	-2.9	-2.8	-2.6
γr	$(kJ mol^{-1})$	191	191	191	191	191	191	191	191	191	191	191
$\lambda_{\mathbf{f}}$	$(k \int mol^{-1})$	294	294	294	294	294	294	294	294	294	294	294
•9∇-	$(kJ \text{ mol}^{-1})$	07	30	20	10	0	-10	-20	-30	-40	-50	09-
Reaction	No.										٠	

The use of individual rather than reduced force constants for electrochemical rate calculations lead to a significant asymmetry between the calculated oxidation and reduction rate-potential plots. Thus Tafel plots of $\log k_{\rm calc}$ versus E exhibit a marked curvature on the anodic side while cathodic plots are nearly linear over several hundred millivolts. For the ${\rm Cr}({\rm H_20})_6^{3+/2+}$ couple for example, the inner-shell asymmetry yields a calculated reduction transfer coefficient of 0.48 at an overpotential of -300 mV, while the oxidation transfer coefficient equals 0.38 when E-E^f = +300 mV. Despite assertions to the contrary, 382,383 neglect of solvent contributions to the reorganization energy results in rather poor agreeement between experiment and theory.

Work-corrected experimental activation entropies are compared with calculated values in Figure 7.4 for the available electrochemical and homogeneous reactions. A similar comparison of activation enthalpies is made in Figure 7.5. Listings of $\Delta H^*(T)$, $\Delta H^*(Q)$, ΔH^*_{corr} , ΔH , $\Delta H^*(Q)$, ΔH^*_{corr} ,

^{*}It is stated in reference 17, that $\triangle H^*(Q)$ represents the amount by which the classical Franck-Condon barrier is lowered by nuclear tunneling, while $\triangle S^*(Q)$ represents a dynamical correction to the rate process. In fact both $\triangle H^*(Q)$ and $\triangle S^*(Q)$ describe the direct influence of tunneling on the Franck-Condon barrier. A "dynamical correction" {2kT sinh $(h_{V_{in}}/2kT)/h_{V_{in}}$ } appears as a pre-exponential factor in some formulations of v_{in} , (reference 377), but is essentially negligible, varying between 1 in the low temperature limit and 1.05 at 298K.

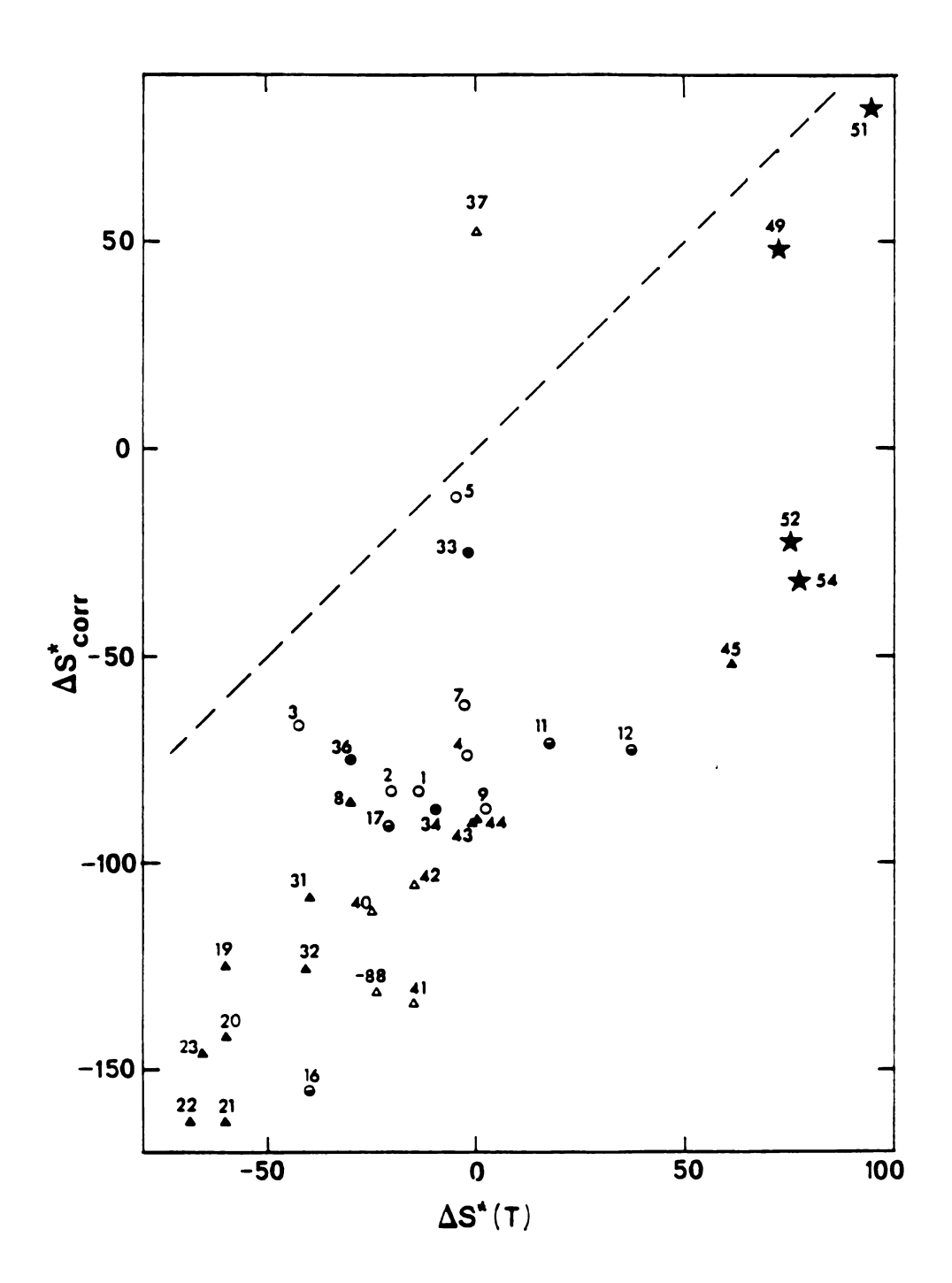


Figure 7.4. Experimental activation entropies versus theoretical activation entropies. Key to reaction type: () electrochemical; others as in Figures 7.2 and 7.3. Results listed in Table 7.4.

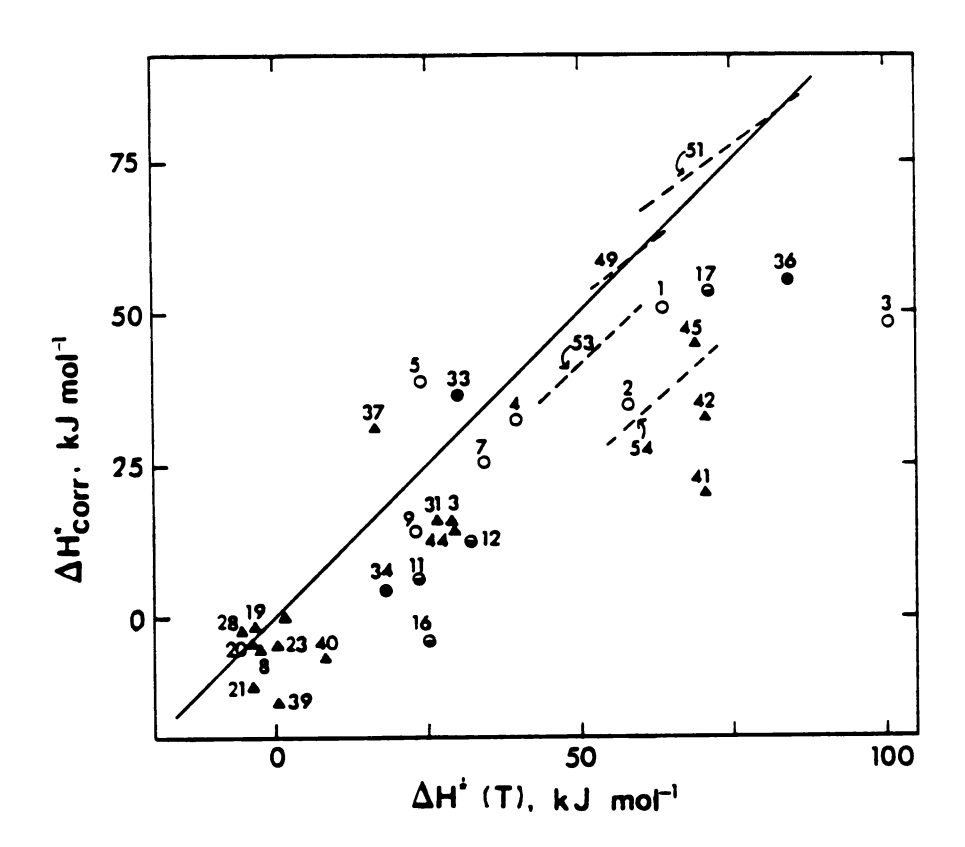


Figure 7.5. Work-corrected experimental activation enthalpies versus theoretical activation enthalpies. Key to reaction type as in Figures 7.2 and 7.3. Results listed in Table 7.5.

Table 7.5. Experimental and Theoretical Activation Entropies and Entropy Driving Forces (J $\deg^{-1} \mod^{-1}$) for Homogeneous Electron Transfer.

Reaction	ι No. ΔS°	ΔS [‡]	ΔS *	ΔS*(Q)	ΔS*(T)
1	0	-105	-83	-14	-14
2	0	-105	-83	-20.5	-20.5
3	0	-88	-67	-42.5	-42.5
4	71	-96	-74	-25	-2.5
5	46	-33	-12	-14	- 5
7	29	-84	-62	-14	-3
9	25	-109	-87	-6.5	2
11	105	-92	-71	-9.5	17
12	126	-92	- 73	-9.5	37
16	- 79	-176	-155	-8.5	-40
17	0	-109	- 91	-22	-22
19	-176	-138	-125	-8.5	-60
20	-176	-155	-142	-8.5	-60
21	-176	-176	-163	-8.5	-60
22	-167	-176	-163	-6.5	-69
23	-172	-159	-146	-6.5	-66
28	-146	-92	-85	0	-30
31	-63	-121	-108	-15	-40
32	-6 3	-138	-125	-15.5	-41
33	0	-54	-25	-1.5	-2
34	-21	-113	-87	-1	-10
36	0	- 92	- 75	-30	-30

Table 7.5 (continued)

Reaction	No. ΔS°	ΔS [‡]	ΔS*	Δ S*(Q)	ΔS*(T)
37	0	29	53	0	0
41	0	-142	-134	-15	-15
42	0	-113	-105	- 15	-15
43	17	-105	-90	-8	-1
45	138	-63	-52	-15	61
44	17	-105	-90	-8	0
39	-88	-124	-131	-4	-24
40	-88	-104	-111	-4	-25

Table 7.6. Experimental and Theoretical Activation Entropies and

Thermodynamic Driving Forces for Electrochemical Electron-Transfer Reactions.

ΔS*(T) J·deg-1 mol-1)	77	72	94	75	62
ΔS*(Q) (J·deg ⁻¹ mol ⁻¹) (.	-0.5	-11	-20	-18	-19
ΔS* corr (J·deg ⁻¹ mol ⁻¹)		50	81	-21	-32
$\Delta S^{\bullet} \qquad \Delta S^{\star} \qquad \Delta S^{\star} \qquad \Delta S^{\star} (Q) \qquad \Delta S^{\star} (T)$ $(J \cdot \deg^{-1} mol^{-1}) \qquad (J \cdot \deg^{-1} mol^{-1}) \qquad (J \cdot \deg^{-1} mol^{-1}) \qquad (J \cdot \deg^{-1} mol^{-1}) \qquad (mol^{-1}) \qquad mol^{-1}$	-29	7.1	102	-2	-23
ΔS° (J·deg ⁻¹ mol ⁻¹)	75	155	205	205	205
ΔG° (kJ·mol ⁻¹)	0	0	0	-40	-30
Reactants	46 Ru(NH ₃) ₆ at mercury	49 V(H ₂ O) ₆ at mercury	Cr(H ₂ 0) ₆ at mercury	52 Cr(H ₂ O) ³⁺ at lead	54 $\operatorname{Cr}(\mathrm{H}_2\mathrm{O})_6^{3+}$ at UPD lead
ež (97	67	51	52	54

Thermodynamic Enthalpy (kJ mol^{-1}) Driving Forces for Homogeneous Electron-Transfer Reactions. Table 7.7. Experimental and Theoretical Activation Enthalpies and

∆H*(T)	63.5	58	100.5	39.5	24	34.5	23	23.5	32	25	71	-3.5
-∆H*(0)	8.2	9.6	19.7	11.5	7.1	6.3	6.9	4.3	1.3	4.1	11	3.8
ΔΗ*	51	35	48.5	32.5	39	25.5	14	6.5	12.5	7-	53.5	-1.5
ΔH	52.5	39	49.5	35.5	39.5	28.5	16.5	13.5	18	2.5	59	-1.5
٥Н٧	0	0	Ö	-93	-212	-41	-87	-34	-17	-52	1.5	-104
reductant	$V(H_2^0)_6^{2+}$	$Fe(H_2^{0})_{6}^{2+}$	$C_0(H_2^0)_{6}^{2+}$	$Fe(H_2^{0})_{6}^{2+}$	$Cr(H_2^0)_6^{2+}$	$Ru(H_2^{0})_{6}^{2+}$	$V(H_2^0)_6^{2+}$	$Ru(NH_3)^{2+}_6$				$Fe(H_2^0)_{6}^{2+}$
oxidant	$V(H_2^0)_6^{3+}$	$Fe(H_2^0)_6^{3+}$	$C_0(H_2^0)_{6}^{3+}$	$c_0(H_2^0)_6^{3+}$	$c_0({\rm H_20})_6^{3+}$	$Fe(H_2^{0})_{6}^{3+}$	$Fe(H_2^{0})_{6}^{3+}$		$Fe(H_2^0)_{6}^{3+}$	$Ru(NH_3)^{3+}_6$	$c_0(e_0)^{3+}_3$	$Ru(bpy)^{3+}_3$
	7	7	3	4	2	7	6	11	12	16	17	19

Table 7.7 (continued)

	oxidant	reductant	οH ^ο	фH∇	∨H∨	-AH(O)	Δ H *(T)
20	Ru(phen) 3+	$Fe(H_2^0)_{6}^{2+}$	-104	-5	-4.5	3.8	-3.5
21	$Ru(terpy)^{3+}_3$		-104	-11.5	-11.5	3.8	-3.5
22		$Fe(H_2^{0})^{2+}_{6}$	-76	8.0	0	4.0	1.5
23	$Fe(bpy)_3^{3+}$	$Fe(H_2^0)^{2+}_{6}$	-85	-3.5	-4.5	3.4	+0.3
28	$0s(bpy)\frac{3+}{3}$	$Ru(H_2^{0})^{2+}_{6}$		-2.5	-2.5	0	-5.5
31	$(co(phen)^{3+}$	$V(H_2^0)_6^{2+}$	-78	16	16	6.9	26.5
32	$(6(bpy)^{3+}_3)$	$V(H_2^0)^{2+}_6$	-71	15	16	7.0	29
33	$Ru(NH_3)^{3+}_6$	$Ru(NH_3)_6^{2+}$	0	43	36.5	0.7	30
34	$Ru(en)\frac{3+}{3}$	$Ru(NH_3)_6^{2+}$	-18	10	4.5	0.4	18
36	$\cos(\mathrm{en})\frac{3+}{3}$	Co(en) ²⁺ 3		56.5	55.5	14	84
37	$Ru(bpy)^{3+}_3$	$Ru(phen)\frac{2+}{3}$	0	32	31.5	0	16.5
41	$(0)^{3+}$	$Co(phen)\frac{2+}{3}$	0	21.5	20.5	8.9	70.5
42	$co(bpy)^{3+}_3$	$c_0(bpy)^{2+}_3$	0	32	33	8.9	70.5
45	45 Co(en) ³⁺	$\operatorname{Cr}(\mathrm{bpy})_3^{2+}$	07	46.5	45	7.0	69

Table 7.7 (continued)

	oxidant	reductant	νην	ΨH∇	∨H∇	-0(0)	ΔH*(T)
77	44 $Co(phen)^{3+}$ $Ru(NH_3)^{2+}_{6}$	$Ru(NH_3)^{2+}_6$	-26	17	14.5	3.6	29.5
39	39 Ru(bpy) 3+	$c_0(bpy)^{2+}_3$	-67	-12	-14	1.7	0.5
40	40 Ru(bpy) 3+	Co(phen) 2+	09-	-4.5	-6.5	1.7	œ

Thermodynamic Enthalpy Driving Forces $(kJ mol^{-1})$ for Electrochemical Electron-Transfer Reactions. Table 7.8. Experimental and Theoretical Activation Enthalpies and

			2	2	5		5	2	5	
VH*(T)		62	55.5	83.5	76.5	70	63.5	57.5	51.5	97
(Ò) * H∇		-5	6.4-	-8.9	-8.9	-8.8	-8.7	-8.4	-8.1	7.7-
ΔH* Corr		61.5	56.5	84	62	74	69	87	43	37.5
νHν		79	59	98	81	92	71	48	43	37.5
• Н∇	22.5	97	36	61	51	41	31	21	11	1
ν QG.	0	0	-10	0	-10	-20	-30	07-	-50	09-
Reactants	46 Ru(NH ₃) ³⁺ at mercury	49 $V(H_2^0)_6^{3+}$	at mercury	51 $Cr(H_2^{0})_6^{2+}$	at mercury			$52 \text{ Cr}(\text{H}_2^{0})_6^{3+}$	at lead	
	46	67		51				52		

Table 7.8 (continued)

		10	, _
(T)*H∇	70	63.5	57.5
νη*(φ)	8.8	-8.7	-8.4
ΔH* Corr	42	36.5	31
*H∇	42	36.5	31
νНΩ	41	31	21
DQ.	-20	-30	-40
Reactants	54 Cr($^{(H_2^0)}_6$	at UPD lead	

D. Discussion

The overall impression that is conveyed by the rate comparisons in Figures 7.2 and 7.3 is that the theory of weak-overlap electron transfer is remarkably successful in describing the energetics of such reactions. The experimental rate constants do tend to be smaller than the calculated values. This might be taken as an indication that nonadiabaticity prevails in most reactions even at the closest approach distance. Nevertheless, it is worthwhile to search further for explanations of rate disparities.

A useful approach is to examine the reactivity of metal complexes as a function of ligand and electronic structure. Reactions of aquo, ammine and electrode co-reactants are examined in Figure 7.6 by plotting the difference between log k_{corr} and log k(T) against a normalized free energy driving force coordinate. Although the data for the homogeneous reactions are scattered, the overall indication is that the reaction rates increasingly deviate from theory as the driving force increases. This trend is reminiscent of earlier observations based on relative rate comparisons via the Marcus cross relation. 310,311 (See Section VI. B). However, explanations in terms of the shortcomings of the cross relation are inapplicable here, since the various approximations inherent in that approach (cancellation of electrostatic work terms, additivity of outer-shell reorganization energies, etc.) are not made in the present analysis.

The driving force dependence of the breakdown of theory suggests that the explanation lies in the calculation of Franck-Condon barriers, rather than in neglect of work terms, nonadiabaticity or other pre-

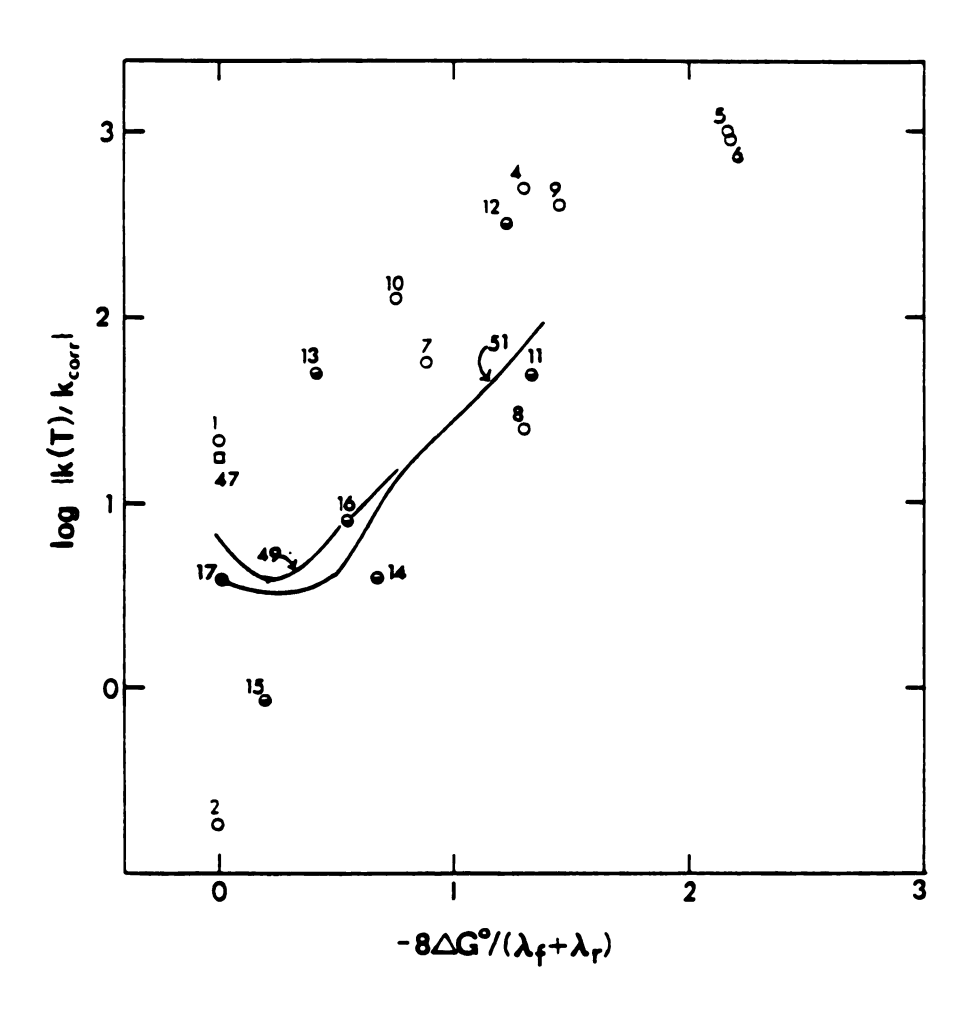


Figure 7.6. Log $\left[k(T)/k_{corr}\right]$ for reactions involving aquo complexes plotted against the reduced driving force $\Delta C^0/(\lambda_f^{+\lambda}_r)$. Key to reaction type as in Figures 7.3 and 7.4.

exponential factors. Interestingly, the apparent breakdowns for homogeneous reactions are paralleled in the electrochemical oxidations of $V(H_20)_6^{2+}$ and $Cr(H_20)_6^{2+}$, but not in the corresponding electrochemical reductions. Nearly all of the homogeneous reactions included in Figure 7.6 also involve aquo oxidations. A reasonable hypothesis is that the driving force dependent rate discrepancies for both the homogeneous and electrochemical reactions arise because the rate calculations overestimate the extent to which the activation free energy for the aquo complex is diminished by increasing the driving force. A speculative explanation for this centers on hydrogen bonding between aquo ligands and the surrounding solvent. It is usually assumed that $\lambda_{\mbox{out}}$ possesses the same value for forward and reverse reactions. Nevertheless there is ample evidence of enhanced hydrogen bonding in the $M(H_2^0)_6^{3+}$ state compared with the M(H₂0)₆²⁺ state. 55,222 This suggests that λ out out exceed λ_{out}^{2+} , which in turn would yield an even greater asymmetry between aquo oxidation and reduction reactions than is expected from inner-shell considerations alone.

A possibility which cannot be dismissed is that the driving force dependence of $\log \left[(k_{corr}/k(T)) \right]$ represents merely a coincidental ordering of experimental and calculational errors, at least for the homogeneous rate data. Indeed, the calculated rate constants could be in error by as much as a factor of twenty in some cases due to errors in estimating λ_n and therefore λ_{in} . Such uncertainties emphasize the need for accurate measures of symmetrical metal-ligand stretching frequencies in addition to data concerning metal-ligand bond lengths.

The cross reactions involving $\mathrm{Co}(\mathrm{H}_20)_6^{3+/2+}$ are of special interest since it has often been suggested that these are somehow anomalous. The rate comparisons summarized in Figures 7.2, 7.3 and 7.6 indicate that while such cross-reaction rates do indeed deviate from the predictions of theory, these deviations are comparable to those found for other reactions. The $\mathrm{Co}(\mathrm{H}_20)_6^{3+/2+}$ self-exchange rate however, exhibits enormous deviations from theory. Endicott and coworkers have suggested that the hexaquo cobalt (III)/(II) self-exchange follows a catalytic inner-sphere pathway, a conclusion which is strongly supported by the present calculations of outer-sphere rates. ³⁸⁴ Curiously, the activation entropy for this reaction is typical of that found for genuine outer-sphere reactions (Figure 7.4), suggesting that the magnitude of ΔS^* is not particularly diagnostic of the reaction mechanism.

Reactions between aquo and polypyridine complexes form an interesting group. On average the cross reactions involving low-spin polypyridine complexes with aquos are nearly four orders of magnitude slower than predicted (Figure 7.7) while the rates of corresponding reactions of pairs of aquo complexes and pairs of polypyridine complexes evidently agree more closely with theory. The discrepancies between k_{corr} and k(T) appear to be independent (or nearly so) of the reduced driving force for the reaction. These observations suggest that some type of barrier to precursor formation, perhaps arising from an energetically unfavorable interaction between aquo and polypyridine ligands, might be the source of the rate discrepancies.

Alternative explanations of rate disparities in terms of miscalculation or neglect of factors contributing to nuclear reorgani-

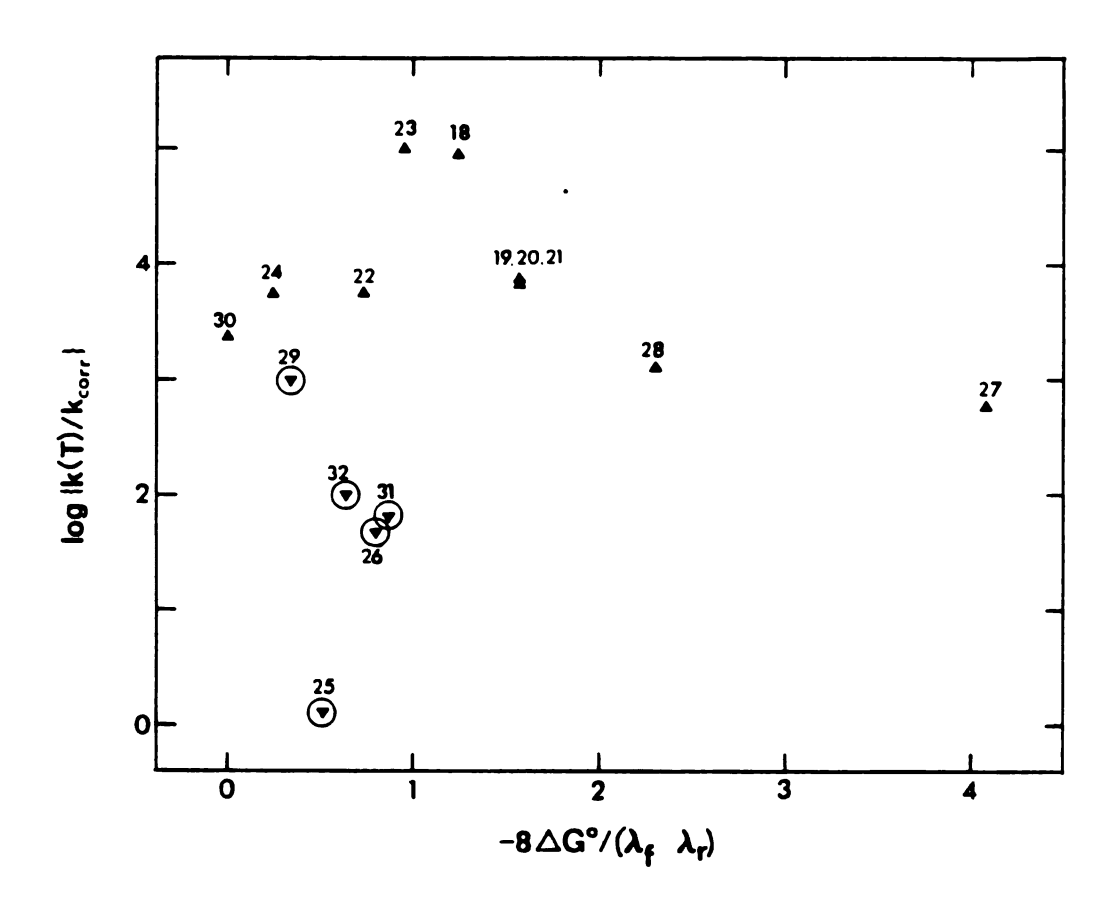


Figure 7.7. Log $\left[k(T)/k_{corr}\right]$ for reactions between polypyridine and aquo complexes plotted against the reduced driving force $\Delta G^{0}/(\lambda_{f}+\lambda_{r})$. Key:

(A) low-spin polypyridines with aquos; \bigcirc high-spin polypyridines with aquos.

zation energies appear to be untenable. The effects of such errors should be attenuated with increasing excergonicity, yet rate discrepancies persist even in the $\text{Ru}(\text{H}_2\text{O})_6^{2+}$ - $\text{Ru}(\text{bpy})_3^{3+}$ cross reaction for which ΔG_0 approaches λ_f .

The behavior of aquo complexes with polypyridine reactants contrasts with the behavior of aquo complexes with other coreactants. One might speculate that some of the pecularities of $M(H_20)_6^{3+/2+}$ reactivity, which are tentatively attributed here to hydrogen bonding interactions with the solvent, are somehow circumvented when the aquo reactant is placed in close proximity to a polypyridine coreactant. Interestingly solvent "structure breaking" capabilities have often been attributed to the latter. 306

The activation parameters for the aquo-polypyridine reactions are characterized by ΔS^* values which differ from theory by some 85 J deg⁻¹ mol⁻¹, a discrepancy similar to that found for a variety of other cross reactions (Figure 7.4). In contrast, ΔH_{corr}^* values are quite similar to the predicted values. Such enthalpic behavior distinguishes these cross reactions from most others, which instead exhibit ΔH_{corr}^* values that are smaller than expected (Figure 7.5). Evidently, ΔH^* rather than ΔS^* is the parameter signaling a typical rate behavior. It is perhaps not useful to speculate concerning the details of the postulated work term for aquo-polypyridine reactions, beyond suggesting that it is partly enthalpic.

Since cross reactions between aquo couples and either $Co(bpy)_3^{3+/2+}$ or $Co(phen)_3^{3+/2+}$ agree more closely with theory than do the corresponding reactions involving low-spin polypyridine couples, it is worth-

while to ask whether these differences are related to the differences in electronic structure between the cobalt couples and the others. Although this is an intriguing possibility, the most likely explanation is that the reactivity differences are due to miscalculations of metal-ligand bond reorganization energies for the $Co(phen)_3^{3+/2+}$ and $Co(bpy)_3^{3+/2+}$ Substantial calculational errors are certainly possible for couples. these couples given the tentative nature of the force constant estimates and the large uncertainties $(\frac{1}{2}0.027 \text{ Å})$ in the EXAFS estimate of Ad. For reactions requiring very large adjustments of bond lengths even small uncertainties in $\wedge d$ become significant in the rate calculations. This suggestion also accounts for the otherwise puzzling result that k exceeds k(T) for the $Co(bpy)_3^{3+/2+}$ and $Co(phen)_3^{3+/2+}$ self-exchanges. Note that catalytic inner-sphere pathways which might cause k to exceed the calculated outer-sphere rate constant are not available since both the Co(III) and Co(II) centers are substitutionally inert.

"Cross reactions" between metal complexes and electrode surfaces form a distinctive set of electron-transfer reactions, one in which the thermodynamic driving force can be varied without altering the chemical identity of the reactants. Complexes exhibit different degrees of outer-sphere reactivity with different electrode co-reactants, even after correcting rate constants for electrostatic double-layer effects. Such differences are intriguing since they are unexpected from electron transfer theory. Despite the differences in $k_{\rm corr}$ values, the variations of rate constants with driving force are essentially the same for the reduction of ${\rm Cr}({\rm H_20})_6^{3+}$ (and other reactants) at different surfaces. Liu has suggested that differences in $k_{\rm corr}$ can be understood in terms

of the degree of hydrophilicity and corresponding interfacial solvent ordering that is exhibited by each metal surface. 136 The least hydrophilic surface, mercury, appears to correspond most closely to an ideal "weakly interacting" coreactant, while the most hydrophilic surface, gallium, strays furthest from ideal behavior. Activation parameters are markedly more sensitive to electrode composition that are the kcorr values. The electrostatic effects of double-layer structure on electrochemical kinetics parameters are better understood than the corresponding salt effects on homogeneous kinetics. Thus it can be claimed fairly confidently that the variations in activation parameters, as well as rates, represent something other than uncertainties in electrostatic work terms. The apparent importance of electrode-solvent interactions suggests that specific solvent interactions with homogeneous co-reactants, most notably polypyridine complexes, may also bear some relation to electron-transfer reactivity.

There are too few examples of each of the other groups of cross reactions to be able to isolate ligand-specific reactivity patterns. A general observation however is that a rather less optimistic view of the success of electron-transfer theory emerges when cross reactions are included in rate comparisons.

Comparisons between calculated and experimental activation parameters, which have been alluded to in the foregoing discussion, form a more demanding test of theory than do the rate comparisons. Overall the results summarized in Figures 7.4 and 7.5 are nothing short of remarkable. Clearly, it is possible to account quite adequately for

variations in ΔH^* and especially, ΔS^* as the thermodynamic and structural properties of the reactant are varied.

On an absolute level however, the agreement between experiment and theory is less satisfactory. We noted above that a discrepancy of 85 \pm 25 J deg \pm mol \pm is observed between \pm and \pm and \pm for nearly all the homogeneous reactions. One explanation is that outer-sphere electron transfer reactions are in most cases strongly nonadiabatic, such that the value of \pm is about \pm 10 \pm 8. Besides being inconsistent with the few ab initio studies of electronic coupling between outer-sphere reactants, \pm 14,15 such a value is simply too small to account for the observed rate constants.

Various other possibilities were considered in a recent examination of the effects of reactant-solvent hydrogen bonding on activation entropies (Section V. A). There it was concluded that the differences between ΔS_{corr}^* and ΔS_{calc}^* almost certainly cannot arise from the temperature dependence of the Franck-Condon barrier, i.e. $\Delta G^*(T)$, but instead must represent a work term associated with precursor formation. Friedman has arrived at a similar conclusion on the basis of his studies of ion-pair correlation functions for aquo complexes. The Specifically, the negative activation entropy for the $Fe(H_20)_{6}^{3+/2+}$ self-exchange is assigned in his work to coulombic repulsion between the charged reactants. A significant finding is that the entropic component of such electrostatic interactions is expected to be nearly independent of ionic strength. The common feature of the set of homogeneous reactions examined here is that each involves a reactant of charge 2+ and another of charge 3+. Provided that electrostatic interactions are controlled

essentially entirely by the charges of the reactants, with the reactant size and ligand composition being of little importance, such interactions provide a very plausible explanation. Various other factors such as steric requirements, marginal nonadiabiticity, variations of κ_{el} with temperature, etc. likely contribute, at least to a minor extent, to the observed discrepancies between experiment and theory.

Returning to the adiabaticity question, an unexpected finding is that the AS* values for reactions involving cobalt centers are no more discrepant than for other reactions. For the cobalt couples electron transfer is a formally spin-forbidden process. Jortner and coworkers have noted that the spin restriction an be partially overcome through spin-orbit coupling, leading to an electron transfer probability in the case of Co(NH₃)^{3+/2+}₆ self-exchange that is 10⁻⁴ smaller than expected in the absence of spin restrictions. Since evidence for such spin-related nonadiabaticity is wholly lacking in the rate and activation entropy comparisons (note also the conclusions for Section VI. C), one suspects either that spin-orbit coupling is a more successful reaction scheme than previously believed or that another mechanism is available to circumvent the spin restriction.

Offsetting the unfavorable experimental activation entropies are activation enthalpies which tend to be more favorable than predicted. Overall, the differences between $\Delta H_{\text{corr}}^{*}$ and $\Delta H_{\text{corr}}^{*}$ and $\Delta H_{\text{corr}}^{*}$ and $\Delta H_{\text{corr}}^{*}$ and $\Delta H_{\text{corr}}^{*}$ differences, namely, electrostatic interactions that differ from those assumed in making work term corrections. The larger scatter in $\Delta H_{\text{corr}}^{*}$ values compared with $\Delta S_{\text{corr}}^{*}$ values is not unexpected, since calculations of activation enthalpies are more sensi-

tive to errors in estimates of reactant structural parameters. However, scatter in the Δ H* data could additionally result if breakdowns in theory arising from inter-reactant and reactant-solvent interactions, as well as departures from purely outer-sphere reaction pathways, are manifested chiefly as enthalpic effects, as has been suggested above.

E. Conclusions

In a global sense electron-transfer theory is reasonably successful in predicting the rates of self-exchange and cross reactions as well as those for electrochemical reactions. The lingering discrepancies of 10 to 104 -fold seem to arise chiefly from specific, nonelectrostatic reactant-reactant and reactant-solvent interactions. Cross reactions between aquo and polypyridine couples are the best example of the former, while electrochemical reactions are the strongest example of the latter. Nonadiabaticity evidently is not exceptionally important in reactions requiring formally spin-forbidden electronic transitions, although in general nonadiabaticity certainly could be significant. The variations of activation parameters with thermodynamic and structural factors generally are well described by theory. However, the theoretical estimates of $\triangle H^*$ and $\triangle S^*$ are substantially different to the experimental values. Such errors, at least in homogeneous reactions, probably represent mainly miscalculations of electrostatic work terms rather than failures of electron-transfer theory itself.

CHAPTER VIII

CONCLUSIONS AND SUGGESTIONS FOR FURTHER WORK

A. Conclusions

Differential capacitance experiments indicate that silver is capable of adsorbing several simple inorganic anions to the extent of a monolayer at the most positive accessible potentials. Electrochemical roughening which is required in order to observe SERS signals from adsorbed ions was found to produce only minor changes in the average surface concentrations of such anions at silver.

Underpotential deposition of a single atomic layer of lead on to a silver electrode was sufficient to transform the double-layer structure and adsorption properties of the surface essentially to those of a bulk lead electrode. Thus, adsorption is greatly diminished at the UPD lead/silver, as well as UPD thallium/silver surfaces in comparison to unmodified silver. The differences in anionic adsorption properties between these three surfaces as well as mercury appear to be related to differences in the degree hydrophilicity of the metal electrodes.

In order to evaluate electrochemical kinetics at a molecular level and to correlate electron-transfer reactivity in different environments an "encounter preequilibrium" treatment was refined and further developed. This treatment provides a more satisfactory theoretical description of redox processes than is obtained from the conventional colli-

sional model. In particular, a clearer picture of the physical signifiance of the frequency factor emerges from the former.

The preequilibrium treatment was applied to the problem of the influence of the metal surface composition on redox reactivity. Rates of inner-sphere electron transfer reactions at silver are diminished by three to five orders of magnitude when the surface is modified by underpotentially depositing a monolayer of lead or thallium on silver. An analysis on the basis of the encounter pre-equilibrium model indicates that the reactivity differences are associated with a change in reaction mechanism from inner- to outer-sphere and an accompanying decrease in the precursor stability constant. Surprisingly, rate constants for the elementary electron-transfer step for several chromium(III) reductions are closely similar at four different electrode surfaces.

A careful consideration of entropic driving forces for intramolecular electron-transfer indicates that, contrary to common belief,
such reactions typically involve a significant Franck-Condon activation
entropy. This complicates the analysis of frequency factors from the
point of view of monitoring nonadiabaticy. Nevertheless when carried
through, such an analysis can account for peculiarities such as positive
activation entropies and the marked sensitivity of apparent frequency
factors to non-bridging ligands.

From an evaluation of rate responses to systematic alterations of double-layer structure together with rate comparisons for parallel inner- and outer-sphere reaction pathways it is concluded that chromium(III) aquo reductions are mildly nonadiabatic at the mercury-

aqueous interface. The corresponding ammine reductions are decidely adiabatic.

A generalized comparison of electrochemical and homogeneous redox reactions of aquo complexes provides good evidence that driving force dependent breakdowns of the relative electron-transfer theory for the two data sets have a common origin. Subsequent absolute calculations indicated that such breakdowns result in part from differences in force constants for inner-shell reorganization between different oxidation states.

Comparisons between self-exchange and cross reactions as well as between homogeneous and electrochemical exchange reactions provide substantial evidence that the homogeneous self-exchange reaction of the hexasquo iron(III)/(II) couple probably follows an extraordinary reaction pathway in comparison to other reactions involving aquo complexes. It was speculated that this pathway might involve water as a bridging ligand. Since the $\text{Fe}(\text{H}_20)_6^{3+/2+}$ self exchange has served as the prototype reaction for evaluating outer-sphere electron-transfer theories, information concerning the reaction mechanism should be of considerable interest.

Absolute theoretical estimates of rate constants for nearly sixty outer-sphere homogeneous and electrochemical reactions exhibit tolerably good agreement with the experimental rate constants. However, the agreement between theoretical and experimental activation enthalpies and entropies is considerably worse. Nevertheless, this poor agreement appears to be due to the inadequecies of the treatment of electrostatic work terms rather than the electron-transfer theory itself.

B. Suggestions for Further Work

There are a number of experiments involving ionic adsorption which might be expected to yield interesting surface chemistry. Because of the enormous range of positive electrode charge available at silver in adsorbing electrolytes diffuse-layer potentials should be an important factor in anionic specific adsorption. The influence of the diffuse layer could be investigated by examining specific adsorption over a range of ionic strengths. One suspects that diffuse-layer effects at very large electrode charges might be coupled to electrosorption valencies, Frumkin g parameters and other isotherm parameters in peculiar and interesting ways.

The simultaneous ionic adsorption analysis scheme outlined in Section III. G could be tested by monitoring specific adsorption from chloride-bromide-perchlorate or chloride-azide-perchlorate mixed electrolytes at silver. If successful, such experiments would be useful for establishing more satisfactorily the connections between SERS intensities and average surface concentrations of Raman scatterers. A fault of the experiments described in Section III. A is that the electrode was roughened in one electrolyte, soaked in a second solution and subjected to capacitance measurements in a third electrolyte. All of these steps could be performed with a single electrolyte solution, thereby paralleling more closely the experimental protocol employed in SERS experiments, if the proposed analysis scheme were used in place of the conventional Rurwitz-Parsons method.

Another sequence of experiments might focus on the thermodynamic properties of metal electrodes which are covered only partially by an

underpotentially deposited metal. A nonlinear relationship was found between the degree of surface coverage of silver by UPD lead, and the magnitude of the differential double-layer capacitance. Such nonlinear relationships might be observed with regard to the ionic adsorption properties of such surfaces as well and would have interesting consequences in connection with theories of adsorption.

Additional insights concerning electron-transfer energetics at underpotentially deposited lead and thallium electrode surfaces might be gained if suitable inner-sphere reactions could be found. Chromium(III) thiophene reductions represent one possibility. An investigation of solvent isotope effects on outer-sphere reductions at UPD lead/silver and UPD thallium/silver might provide clues as to the importance of specific interactions between reactants and the solvent inner-layer since hydrogen-bonding interactions generally are stronger in D₂0 than H₂0.

The relative electron-transfer theory could be used to elucidate various features of the electrochemical reduction kinetics of chromium(III) complexes if corresponding data could be gathered for homogeneous outer-sphere reactions of such complexes with a common reductant such as $Os(NH_3)_6^{2+}$ or $Co(bpy)_3^{-+}$.

An improtant conclusion from the study of absolute electrontransfer reactivity (Chapter VII) is that the usual treatment of electrostatic work terms is inadequate for homogeneous redox reactions. In order to develop a more satisfactory treatment it would be useful to measure activation parameters over a range of ionic strengths for a set of reactions involving a number of different reactant charge combinations. An improved description of electrostatic effects on kinetics parameters would be extremely valuable if it enabled such effects to be separated from additional subtle factors (e.g. nonadiabaticity) which may well be masked in many circumstances by the current (inadequate) treatment.

Finally, it was noted that the absolute theory of electron transfer predicts that negative activation enthalpies will be observed under certain conditions. Indeed negative values have been found for the $Fe(H_20)_6^{2+}$ -Fe(bpy) $_3^{3+}$ and other cross reactions. It would be worthwhile to search out electrochemical rections which might exhibit such behavior. The chief requirement according to theory is that the entropy driving force $(-T\Delta S^0)$ for electron transfer must exceed in absolute value the intrinsic reorganization energy (λ_f). Oxidations of sumine complexes in nonaqueous solvents such as acetonitrile involve enormous entropy changes (circa 200 J deg⁻¹ mol⁻¹) or more; (see Section V. C). The entropy driving force effects might be sufficiently large to reveal not only negative ideal activation enthalpies, but also an "inverted" enthalpy region where AH* increases with increasing exothermicity. An enthalpic inverted region is expected under extreme circumstances from theoretical considerations. Rate behavior in this region might be influenced by anomalous nuclear tunneling effects or other unusual fac-In any case this problem appears to be worthy of additional cogitation, as well as experimental investigation.

APPENDIX I

Reaction Entropies for Transition-Metal Redox Couples in Various Solvents

This appendix consists of a listing of previously unreported $\Delta S_{\rm rc}^{\rm o}$ data which were obtained in connection with the work described in Section V. C.

Table A.1. Reaction Entropies (J deg⁻¹ mol⁻¹) for Transition-Metal Redox Couples in Various Solvents.

Redox Couple	Solvent ^a	∆S°rc
Ru(NH ₃) ^{3+/2+}	acetonitrile	185
$Ru(NH_3)_6^{3+/2+}$	acetone	200
Ru(en) ₃ +/2+	formamide	90
Ru(NH ₃) ₅ pz ^{3+/2+}	nitromethane	165
Ru(NH ₃) ₅ pz ^{3+/2+}	propylene carbonate	155
Ru(NH ₃) ₄ bpy ^{3+/2+}	acetonitrile	155
Ru(NH ₃) ₄ phen ^{3+/2+}	nitromethane	120
Ru(NH ₃) ₄ phen ^{3+/2+}	dimethylsulfoxide	125
Ru(NH ₃) ₄ phen ^{3+/2+}	propylene carbonate	150
Ru(NH ₃) ₂ (bpy) ₂ ^{3+/2+}	nitromethane	115
Ru(NH ₃) ₂ (bpy) ₂ ^{3+/2+}	acetonitrile	130
Ru(NH ₃) ₂ (bpy) ₂ ^{3+/2+}	dimethylsulfoxide	110
Ru(NH ₃) ₂ (bpy) ₂ ^{3+/2+}	propylene carbonate	135
Ru(bpy)3+/2+	acetonitrile	115
Ru(bpy)32+/+	acetonitrile	70
Ru(bpy)3+/0	acetonitrile	25
Cr(bpy)3+/2+	acetonitrile	105
Cr(bpy) ₃ ^{2+/+}	acetonitrile	65
Cr(bpy)3+/0	acetonitrile	20
Cr(bpy) ₃ ^{2+/+} Cr(bpy) ₃ ^{+/0} Co(bpy) ₃ ^{3+/2+}	acetonitrile	190

Table A.1 (continued)

Redox couple	Solvent	ΔS ^o rc
Co(bpy) ₃ ^{2+/+}	acetonitrile	60
Co(sep) ^{3+/2+}	acetonitrile	210
Co(EFME-Oxosar-H) ^{2+/+}	water	30
Co(EFME-Oxosar-H) ^{2+/+}	N-methylformamide	90
11	acetonitrile	165
п	formamide	75
и -	dimethylformamide	175
11	dimethylsulfoxide	160 ^b
11	propylene carbonate	150 ^b
11	me than o l	165 ^b
H ·	nitromethane	140 ^b
11	ethanol	105 ^b

- a. 0.1 $\underline{\mathbf{M}}$ KPF₆ supporting electrolyte
- b. measured by Dr. Peter Lay

APPENDIX II

Negative Activation Enthalpies

In comparing experimental and theoretically calculated activation parameters (Chapter VII) it was noticed that in a few instances negative activation enthalpies have been observed for homogeneous outer-sphere reactions. Marcus and Sutin have pointed out that this peculiar result is actually expected under certain conditions from the relative electron-transfer theory. In connection with the work described in Chapter VII it was of interest to ascertain under what conditions the absolute electron-transfer theory would predict negative values of ΔH^* .

The problem is somewhat simplified by assuming equal inner-shell force constants for the oxidized and reduced states of each reactant, and a value of the intrinsic activation entropy equal to zero. It is found that negative ΔH^* values can be expected within the so-called "normal" free energy region $(\Delta G^0 < \lambda)$, provided that the value of the thermodynamic factor $T\Delta S^0$ exceeds the intrinsic free energy barrier ΔG^*_{int} (= $\lambda/4$). This requirement is fulfilled, for example in the cross reaction of $Fe(H_2 0)_3^{2+}$ with $Ru(bpy)_3^{3+}$. Furthermore it is found that the range of free energy driving force over which ΔH^* should be negative extends from $\Delta G^0 = -\lambda - 2T\Delta S^0$ to $\Delta G^0 = -\lambda$. Under all circumstances ΔH^* as well as ΔG^* and ΔS^* are expected to equal zero at $\Delta G^0 = 0$.

Figure A.1 illustrates a sample calculation for a hypothetical reaction involving an intrinsic free energy barrier of 44 kJ mol⁻¹ and a

thermodynamic entropy change of 180 J deg⁻¹ mol⁻¹. The most interesting result of the calculation is the appearance within the "normal" free energy region of an enthalpic "inverted" region where ΔH^{*} increases with increasing free energy or enthalpy driving force. The threshhold of the inverted enthalpy region is at $\Delta G^{\circ} = -\lambda - T\Delta S^{\circ}$.

The <u>free energy</u> inverted region has been the subject of much experimentation and speculation. $^{391-393}$ Part of the interest stems from the possibility that nuclear tunneling phenomena may be of greater importance in inverted reactions. 393 One difficulty in probing reactivity in this region is that reactions are usually extremely fast since ΔG^{*} is small in the vicinity involving sufficiently large thermodynamic entropy changes it appears that the analogous enthalpic inverted region may be more easily studied, since ΔG^{*} will be significantly greater than zero through most of the region. We note also that the free energy inverted region is expected to be inaccessible in electrochemical reactions at metal electrodes for reasons outlined by Marcus. 394 Nevertheless the enthalpic inverted region should be observable. Currently experimental results along these lines for the electrochemical oxidations of $Cr(H_2O)^{2+}_{6}$ ($\Delta S^{0}_{rc} = 205$ J deg $^{-1}$ mol $^{-1}$) and $V(H_2O)^{2+}_{6}$ ($\Delta S^{0}_{rc} = 155$ J deg $^{-1}$ mol $^{-1}$) are being compared with theoretical predictions.

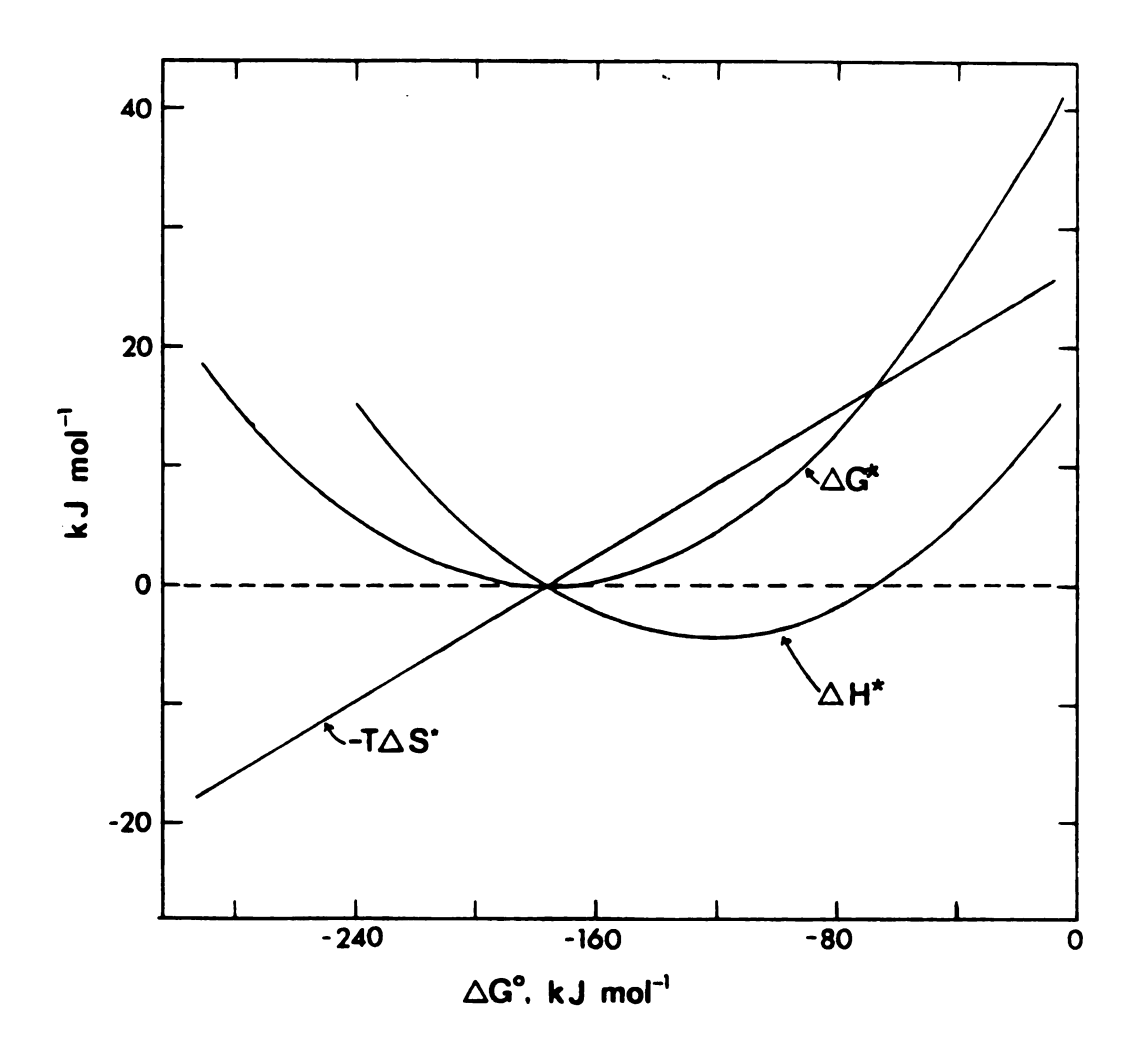


Figure A.1. Variation of calculated activation parameters with free energy driving force, ΔG° , for a reaction for which $\Delta G^{\star}_{int} = 44 \text{ kJ mol}^{-1}$, $\Delta S^{\star}_{int} = 0 \text{ J deg}^{-1} \text{ mol}^{-1}$ and $\Delta S^{\circ} = -180 \text{ J deg}^{-1} \text{ mol}^{-1}$.

REFERENCES

- 1. A. Hamelin, T. Vitanov and E. Sevastyanov, J. Electroanal. Chem., 145, 225 (1983).
- 2. A. Bewick and B. Thomas, J. Electroanal. Chem., <u>70</u>, 239 (1976); <u>84</u>, 127 (1977).
- 3. A. Bewick and B. Thomas, J. Electroanal. Chem., 65, 911 (1975).
- 4. H. Siegenthaler, K. Juttner, E. Schmidt and W. J. Lorenz, Electrochemica Acta, 23, 1009 (1978).
- 5. See, for example: R. R. Adzic', Israel J. Chem., 18, 166 (1979).
- 6. For a review, see: D. M. Kolb in "Advances in Electrochemisry and Electrochemical Engineering," H. Gerischer and C. Tobias, Eds.; J. Wiley and sons, New York, 1978, Vol. 11, p. 125.
- 7. D. M. Kolb and H. Gerischer, Surface Sci., 51, 323 (1975).
- 8. For reviews see: (a) R. P. Van Duyne in "Chemical and Biochemical Applications of Lasers", C. B. Moore, Ed.; Academic Press, New York, 1979, Vol. 4, Chapter 5. (b) T. E. Furtak and J. Reyes, Surface Sci., 93, 382 (1980). (c) R. L. Birke, J. R. Lombardi and L. A. Sanchez, Adv. Chem. Ser., in press.
- 9. See, for example: (a) N. Sutin, Acc. Chem. Res., <u>15</u>, 275 (1982). (b) N. Sutin, Prog. Inorg. Chem., <u>30</u>, 292 (1983).
- 10. B. S. Brunschwig, C. Creutz, D. H. Macartney, T-K. Sham and N. Sutin, Faraday Dis., 74, 113 (1982).
- 11. P. Bernhard, H. B. Burgi, J. Hauser, H. Lehmann and A. Ludi, Inorg. Chem., 21, 3936 (1982).
- 12. J. K. Beattie, cited in reference 10.
- 13. R. A. Marcus, J. Chem. Phys., 43, 679 (1965).
- 14. M. D. Newton, Int. J. Quant. Chem., Symp., 14, 363 (1980).
- 15. M. D. Newton, ACS Symp. Ser., 198, 255 (1982).

- 16. See, for example: J. F. Endicott, T. Ramasami, D. C. Gaswick, R. Tamilarasan, M. J. Heeg, G. R. Brubaker and S. C. Pyke, J. Am. Chem. Soc., 105, 5301 (1983).
- 17. B. L. Tembe, H. L. Friedman and M. D. Newton, J. Chem. Phys., <u>76</u>, 1490 (1982).
- 18. R. A. Marcus, Int. J. Chem. Kin., 13, 865 (1981).
- 19. T. Holstein, Ann. Phys. (Liepzig), 8, 343 (1959).
- 20. T. Holstein, Philos. Mag., 37, 49 (1978).
- 21. R. N. Kestner, J. Logan and J. Jortner, J. Phys. Chem., <u>78</u>, 2148 (1974).
- 22. P. P. Schmidt in Specialist Periodical Reports on Electrochemistry, H. R. Thirsk, Senior Reporter, Vol. 6, The Chemical Society, London, 1978, Chapter 4.
- 23. B. S. Brunschwig, J. Logan, M. D. Newton and N. Sutin, J. Am. Chem. Soc., 102, 5798 (1980).
- 24. H. L. Friedman and M. D. Newton, Faraday Dis., 74, 73 (1982).
- 25. J. Jortner, Philos. Mag., 40, 317 (1979).
- 26. See, for example: J. F. Endicott, K. Kumer, T. Ramasami and F. P. Rotinger, Prog. Inorg. Chem., 30, 142 (1983).
- 27. N. Sutin, Inorganic Biochemistry, G. L. Eichorn, Ed., Vol. 2, American Elsevier, New York, 1973, p. 611.
- 28. G. M. Brown and N. Sutin, J. Am. Chem. Soc., <u>101</u>, 883 (1979).
- 29. A. M. North, "The Collision Theory of Chemical Reactions in Liquids", Methuen, London, 1964.
- 30. M. J. Weaver, Inorg. Chem., <u>18</u>, 402 (1979).
- 31. M. J. Weaver in "Inorganic Reactions and Methods", Verlag Chemie, Berlin, in press.
- 32. D. M. Mohilner, Electroanal. Chem., 1, 241 (1966).
- 33. A. J. Bard and L. R. Faulkner, "Electrochemical Methods", John Wiley and Sons, New York, 1980, Chapter 12.
- 34. D. C. Grahame and B. A. Soderberg, J. Chem. Phys., <u>22</u>, 449 (1954).

- 35. H. D. Hurwitz, J. Electroanal. Chem., 10, 35 (1965).
- 36. E. Dutkiewicz and R. Parsons, J. Electroanal. Chem., 11, 100 (1966).
- 37. K. F. Lin and T. R. Beck, J. Electrochem. Soc., <u>123</u>, 1145 (1976); 126, 252 (1979).
- 38. D. C. Grahame, Chem. Rev., 41, 441 (1947).
- 39. J. P. Badiali, M. L. Rosinberg and J. Goodisman, J. Electroanal. Chem., 143, 73 (1983).
- 40. R. Parsons, J. Electroanal. Chem., <u>118</u>, 3 (1981).
- 41. N. B. Grigoryev, Dokl. Akad. Nauk SSSR, 229, 647 (1976).
- 42. L. A. Bagotskaya, B. B. Damaskin and M. D. Levi, J. Electroanal. Chem., 115, 189 (1980).
- 43. U. V. Palm, M. P. Pyarnoya and N. B. Grigorev, Sov. Electrochem., 13, 913 (1977).
- 44. G. Valette and A. Hamelin, J. Electroanal. Chem., 45, 301 (1973).
- 45. See, for example: P. Delahay, "Double Layer and Electrode Kinetics", Interscience Publishers, New York, 1965.
- 46. W. J. Albery, "Electrode Kinetics", Oxford University Press, London, 1975.
- 47. A. N. Frumkin, O. A. Petry and N. Nikolayeva-Fedorovich, Electrochimica Acta, 8, 177 (1963), and references cited therein.
- 48. W. R. Fawcett, Can. J. Chem., 59, 1844 (1981).
- 49. V. S. Krylov and I. F. Fishtik, Can. J. Chem., <u>59</u>, 2026 (1981).
- 50. B. E. Conway, "Theory and Principles of Electrode Processes," Ronald Press, New York, 1965, Chapter 6.
- 51. S. Kang, K. Matsuda and R. Tamamushi, Coll. Czech. Chem. Comm., 47, 1433 (1983).
- 52. J.E.B. Randles, Trans. Faraday Soc., 48, 828 (1952).
- 53. M. J. Weaver, J. Phys. Chem., 80, 2645 (1976).
- 54. M. J. Weaver, J. Phys. Chem., 83, 1748 (1979).
- 55. E. L. Yee, R. J. Cave, K. L. Guyer, P. D. Tyma and M. J. Weaver, J. Am. Chem. Soc., <u>101</u>, 1131 (1979).

- 56. For recent reviews see: (a) reference 9; (b) J. Ulstrup, "Charge Transfer Processes in Condensed Media", Springer, West Berlin, 1979; (c) R. R. Dogonadze, A. M. Kuznetsov and T. A. Marsagishvili, Electrochem. Acta, 25, 1 (1980); (d) R. D. Cannon, "Electron Transfer Reactions," Butterworths, London, 1980.
- 57. For insightful reviews of earlier work see: (a) R. A. Marcus, Ann. Reviews Phys. Chem., 15, 155 (1964); (b) V. G. Levich in "Advances in Electrochemistry and Electrochemical Engineering," P. Delahay, Ed.; Interscience, New York, Vol. 4, p. 249.
- 58. J. J. Hopfield, Proc. Natl. Acad. Sci. USA, 71, 3640 (1974).
- 59. B. Chance, D. C. DeVault, H. Frauenfelder, R. A. Marcus, J. B. Schrieffer and N. Sutin, Eds., "Tunneling in Biological Systems", Academic Press. New York, 1979.
- 60. M. Bixon and J. Jortner, Faraday Disc., 74, 17 (1982).
- 61. H. Taube, "Electron Transfer Reactions of Complex Ions in Solution", Academic Press, New York, 1970.
- 62. R. A. Marcus, J. Chem. Phys., 26, 867, 872 (1957).
- 63. P. Siders and R. A. Marcus, J. Am. Chem. Soc., 103, 748 (1981).
- 64. D. C. Devault and B. Chance, Biophys. J., 6, 825 (1966).
- 65. E. Buhks, M. Bixon and J. Jortner, J. Phys. Chem., <u>85</u>, 3763 (1981).
- 66. T. Guarr, E. Buhks and G. McLendon, J. Am. Chem. Soc., <u>105</u>, 3763 (1983).
- 67. E. U. Condon, Phys. Rev., 32, 858 (1928).
- 68. S. E. Schwartz, J. Chem. Ed., <u>50</u>, 608 (1973).
- 69. W. Kauzmann, "Quantum Chemistry", Academic Press, New York, 1957, p. 535.
- 70. M. Sharp, M. Petersson and K. Edstrom, 95, 123 (1979).
- 71. R. S. Rodgers and F. C. Anson, J. Electroanal. Chem., <u>42</u>, 381 (1973).
- 72. M. J. Weaver and F. C. Anson, J. Electroanal. Chem., <u>65</u>, 711 (1975).
- 73. M. J. Weaver and F. C. Anson, Inorg. Chem., <u>71</u>, 1871 (1976).
- 74. T. W. Swaddle and E. L. King, Inorg. Chem., 4, 532 (1965).

- 75. N. Fogel, J. Tai and J. Yarborough, J. Am. Chem. Soc., <u>74</u>, 1674 (1952).
- 76. T. W. Swaddle and E. L. King, Inorg. Chem., 3, 234 (1964).
- 77. E. L. King and E. B. Dismukes, J. Am. Chem. Soc., <u>74</u>, 1674 (1952).
- 78. C. L. Robinson and J. C. Bailer, Inorg. Syn., 2, 200 (1946).
- 79. M. Linhard and W. Berthold, Z. Anorg. Chem., 279, 173 (1955).
- 80. D. L. Gay and G. C. Lalor, J. Chem. Soc. A, 1179 (1966).
- 81. R. R. Baker and B. D. Mehta, Inorg. Chem., 4, 848 (1965).
- 82. S. Sahami and M. J. Weaver, J. Electroanal. Chem., <u>124</u>, 35 (1981).
- 83. F. H. Burstall and R. S. Nyholm, J. Chem. Soc., 3570 (1952).
- 84. E. L. Yee and M. J. Weaver, Inorg. Chem., 19, 1077 (1980).
- 85. K. L. Guyer, Ph.D. Dissertation, Michigan State University, 1981.
- 86. J. T. Hupp, D. Larkin and M. J. Weaver, Surface Sci., <u>125</u>, 429 (1983).
- 87. D. Larkin, K. L. Guyer, J. T. Hupp and M. J. Weaver, J. Electroanal. Chem., <u>138</u>, 401 (1982).
- 88. M. J. Weaver, unpublished observations.
- 89. Saeed Sahami, Ph.D. Dissertation, Michigan State University, 1981.
- 90. W. R. Fawcett and R. O. Loutfy, J. Electroanal. Chem., <u>39</u>, 185 (1972).
- 91. D. J. Myers, R. A. Osteryoung and J. Osteryoung, Anal. Chem., <u>46</u>, 2089 (1974).
- 92. S. W. Barr, Ph.D. Dissertation, Michigan State University, 1981.
- 93. K. B. Oldham and E. P. Parry, Anal. Chem., 40, 65 (1968).
- 94. Z. Galus, "Fundamentals of Electrochemical Analysis", Ellis Horwood (pub.), New York, 1976.
- 95. G. Valette, A. Hamelin and R. Parsons, Z. Phys. Chem. N.F., <u>113</u>, 71 (1978).

- 96. See for example, B. Pettinger, H. Wetzel, Ber. Bunseng. Phys. Chem. 85, 473 (1981).
- 97. M. J. Weaver, F. Barz, J. G. Gordon II, M. R. Philpott, Surface Sci., <u>125</u>, 409 (1983).
- 98. M. Fleischmann, J. Robinson, R. Waser, J. Electroanal. Chem. 117, 257 (1981).
- 99. G. Valette, J. Electroanal. Chem., 122 (1981).
- 100. A. Vashkyalis, O. Demontaite, Sov. Electrochem. 14, 1050 (1978).
- 101. J. T. Hupp, D. Larkin, H. Y. Liu and M. J. Weaver, J. Electroanal. Chem., 131, 299 (1982).
- 102. M. J. Weaver, F. Barz, J. G. Gordon II, J. T. Hupp and M. R. Philpott, J. Electroanal. Chem., in press.
- 103. M. J. Weaver and F. C. Anson, J. Electroanal. Chem., <u>65</u>, 737 (1975).
- 104. Analogous methods to I and II, but involving analyses carried out at constant of rather than E have been commonly utilized to determine specific ionic adsorption at mercury electrodes.
- 105. Reference 45, p. 103.
- 106. J. W. Schultze and K. J. Vetter, J. Electroanal. Chem., 44, 63 (1973).
- 107. M. J. Weaver and F. C. Anson, J. Electroanal. Chem., <u>58</u>, 95 (1975).
- 108. B. B. Damaskin, Sov. Electrochem. 7, 776 (1971).
- 109. K. L. Guyer, S. W. Barr and M. J. Weaver, in "Proc. 3rd Symp. on Electrode Processes", S. Bruckenstein, J.D.E. McIntyre, B. Miller (eds), Electrochemical Society, Princeton, New Jersey, 1980, p. 390.
- 110. S. W. Barr, K. L. Guyer and M. J. Weaver, J. Electroanal. Chem. 111, 41 (1980).
- 111. G. Valette, J. Electroanal. Chem., 146, 439 (1983).
- 112. G. Valette, J. Electroanal. Chem., 132, 311 (1982).
- 113. J. F. Evans, M. G. Albrecht, D. M. Ullevig and R. M. Hexter, J. Electroanal. Chem. 106, 209 (1980).
- 114. S. G. Schultz, M. Janick-Czachor and R. P. Van Duyne, Surface Sci. 104, 419 (1981).

- 115. H. Wetzel, H. Gerischer and B. Pettinger, Chem. Phys. Lett. 78, 392 (1981).
- 116. H. Wetzel, H. Gerischer and B. Pettinger, Chem. Phys. Lett. <u>80</u>, 159 (1981).
- 117. R. E. Kunz, J. G. Gordon II, M. R. Philpott and A. Girlando, J. Electroanal. Chem. 112, 391 (1980).
- 118. W. J. Plieth, J. Phys. Chem. 86, 3166 (1982).
- 119. J. W. Owen, T. T. Chen, R. K. Chang and B. L. Laube, paper presented at the International Conference on Electronic and Molecular Structure of Electrode-Electrolyte Interfaces, Logan, Utah, July 1982; submitted to Surface Sci.
- 120. Note that the electrode potentials in reference 97 are quoted versus Ag/AgC1 (saturated KC1) which has a potential of about -45 mV on the s.c.e. scale employed here.
- 121. C. S. Allen and R. P. Van Duyne, Chem. Phys. Lett. <u>63</u>, 455 (1979); G. C. Schatz and R. P. Van Duyne, Surf. Sci. <u>101</u>, 425 (1980).
- 122. F. Barz, J. G. Gordon II, M. R. Philpott and M. J. Weaver, Chem. Phys. Lett., <u>91</u>, 291 (1982).
- 123. S. H. Macomber, T. E. Furtak and T. M. Devine, Chem. Phys. Lett., 90, 439 (1982).
- 124. S. Farquharson, J. T. Hupp, M. J. Weaver, unpublished observations.
- 125. T. Watanabe, N. Yanagihara, K. Honda, B. Pettinger and L. Moerl, Chem. Phys. Lett., 96, 649 (1983).
- 126. J. J. Kester, J. Chem. Phys., 78, 7466 (1983).
- 127. R. L. Birke, J. R. Lombardi and L. A. Sanchez, Adv. Chem. Ser., 201, 69 (1982).
- · 128. B. Pettinger and H. Wetzel, Bev. Bunsenges Phys. Chem., 85, 473 (1981).
- 129. B. Pettinger, M. R. Philpott and J. G. Gordon III, J. Phys. Chem., 85, 2746 (1981).
- 130. K. L. Guyer, S. W. Barr and M. J. Weaver in "Proc. Symp. on Electrocatalysis", W. E. O'Grady, P. N. Ross, Jr., F. G. Will (Eds.), Electrochemical Society, Pennington, NJ, 1982, p. 377.
- 131. S. Farquharson, K. L. Guyer, P. A. "Bruce" Lay, R. H. Magnuson and M. J. Weaver, J. Am. Chem. Soc., manuscript submitted.

- 132. S. Farquharson, M. J. Weaver, P. A. Lay, R. H. Magnuson and H. Taube, J. Am. Chem. Soc., <u>105</u>, 3350 (1983).
- 133. For reviews, see: (a) A. N. Frumkin, O. A. Petrii and B. B. Damaaskin, in "Comprehensive Treatise of Electrochemistry", J. O'M. Bockris, B. E. Conway., E. Yeager (eds), Vol. I, Plenum, New York, 1980, chapter 5; (b) S. Trassati, in "Advances in Electrochemistry and Electrochemical Engineering", H. Gerischer, C. W. Tobias (eds), J. Wiley, New York, 1977, p. 213; and (c) S. Trassati in "Modern Aspects of Electrochemistry", B. E. Conway, J. O. 'M. Bockris (eds), Vol. 13, Plenum, New York, 1979, chapter 2.
- 134. D. M. Kolb, M. Przasnyski and H. Gerischer, J. Electroanal. Chem. 54, 25 (1974).
- 135. S. Swathirajan and S. Bruckenstein, Electrochimica Acta, 28, 865 (1983).
- 136. H. Y. Liu, Ph.D. Dissertation, Michigan State University, 1982.
- 137. H. Bort, K. Juttner, W. J. Lorenz and E. Schmidt, J. Electroanal. Chem., 90, 413 (1978).
- 138. M. Bratoeva, Sov. Electrochem., 16, 19 (1980).
- 139. R. Salin and B. G. Cooksey, J. Electroanal. Chem. <u>106</u>, 251 (1980).
- 140. E. S. Sevastyanov, M. N. Terakopyan and V. K. Chubarova, Sov. Electrochem. 16, 368 (1980).
- 141. V. F. Ivanov and Z. N. Ushakova, Sov. Electrochem. 9, 753 (1973).
- 142. G. Valette, J. Electroanal. Chem., <u>139</u>, 285 (1982).
- 143. L. Pauling, "The Nature of the Chemical Bond", 3rd edition, Cornell University Press, Ithaca, 1960, p. 402.
- 144. J. E. Huheey, "Inorganic Chemistry", 2nd edition, Harper and Row, New York, 1978, p. 74.
- 145. R. Parsons and P. C. Symons, <u>64</u>, 1077 (1968).
- 146. E. Schmit and S. Stucki, Ber. Bunseng, Ges., 77, 913 (1973).
- 147. K. V. Rybalka, Sov. Electrochem., 8, 400 (1972).
- 148. R. Payne, Trans. Far. Soc., 64, 1638 (1968).
- 149. N. B. Grigorev, V. A. Bulavka and Y. M. Loshkarev, Sov. Electrochem., 11, 1318 (1975).

- 150. V. A. Bulavka, N. B. Grigorev and Y. M. Loshkarev, Sov. Electrochem., 14, 899 (1978).
- 151. R. Payne, J. Phys. Chem., 70, 204 (1966).
- 152. A. R. Sears and P. A. Lyons, J. Electroanal. Chem., <u>42</u>, 69 (1973).
- 153. E. R. Gonzalez, J. Electroanal. Chem., 90, 431 (1978).
- 154. S. Trassatti, J. Electroanal. Chem., 65, 815 (1975).
- 155. A. K. Vijh, J. Phys. Chem., 78, 2240 (1974).
- 156. S. Levine, G. M. Bell and D. Calvert, Can. J. Chem., <u>40</u>, 518 (1964).
- 157. D. J. Barclay, J. Electroanal. Chem., 19, 318 (1968).
- 158. D. J. Barclay, Croat. Chim. Acta, 43, 221 (1970).
- 159. B. E. Conway, Z. Phys. Chem. N. F., 98, 61 (1975).
- 160. R. G. Pearson, J. Am. Chem. Soc., 85, 3533 (1963).
- 161. 8. Trassatti in Mod. Aspects Electrochem., B. E. Conway and J. O' M. Bockris, Eds., Vol. 13, Plenum Press, New York, 1979, chapter 2.
- R. H. Hauge, J. W. Kauffman and J. L. Margrave, J. Am. Chem. Soc., <u>102</u>, 6005 (1980).
- 163. J. W. Kauffman, R. H. Hauge and J. L. Margrave, ACS Symp. Ser., 179, 355 (1982).
- 164. R. H. Hauge, J. W. Kauffman, L. Fredin and J. L. Margrave, ACS Symp. Ser., <u>179</u>, 363 (1982).
- 165. "CRC Handbook of Chemistry and Physics", 56th edition, R. C. Weast, Ed.; CRC Press, Cleveland, 1975.
- 166. L. A. Avaca, E. A. Gonzales and R. C. Rocha Filho, J. Electroanal. Chem., 147, 345 (1983).
- 167. S. Lakshmanan and S. K. Rangarajan, J. Electroanal. Chem., 27, 127 (1970).
- 168. B. Damaskin, U. Palm and M. Vaartnou, J. Electroanal. Chem., 70, 103 (1976).
- 169. B. Baron, P. Delahay and D. J. Kelsh, J. Electroanal. Chem., <u>18</u>, 187 (1968).

- 170. B. B. Damaskin, Sov. Electrochem., 7, 776 (1971).
- 171. See for example, S. W. Benson, "The Foundation of Chemical Kinetics", McGraw-Hill, New York, N.Y., 1960, Chapter 15; J. W. Moore, R. G. Pearson, "Kinetics and Mechanism" 3rd. edn., Wiley, New York, N.Y., 1981, Chapter 7.
- 172. J. Reiss, J. Chem. Phys. 18, 996 (1950).
- 173. Reference 29, pp. 37-9.
- 174. T. T-T Li, M. J. Weaver and C. H. Brubaker, J. Am. Chem. Soc. 104, 2381 (1982).
- 175. N. B. Slater, "Theory of Unimolecular Reactions", Cornell University Press, Ithaca, N.Y., 1959, pp. 57-9.
- 176. E. Buhks, M. Bixon and J. Jortner, J. Phys. Chem. <u>85</u>, 3763 (1981).
- 177. J. M. Hale, J. Electroanal. Chem. 19, 315 (1968).
- 178. M. J. Weaver and T. L. Satterberg, J. Phys. Chem. <u>81</u>, 1772 (1977).
- 179. L. I. Krishtalik, Sov. Electrochem. 11, 174 (1975).
- 180. R. A. Marcus, J. Phys. Chem. 67, 853 (1963).
- 181. M. J. Weaver, J. Phys. Chem. 84, 568 (1980).
- 182. J. T. Hupp and M. J. Weaver, Inorg. Chem., 22, 2557 (1983).
- 183. Reference 46, Chapter 4.
- 184. V. Srinivasan, S. W. Barr and M. J. Weaver, Inorg. Chem. <u>21</u>, 3154 (1982).
- 185. J. E. B. Randles and K. W. Somerton, Trans. Far. Soc. <u>48</u>, 937 (1952).
- 186. J. T. Hupp and M. J. Weaver, J. Electroanal. Chem., <u>143</u>, 43 (1983).
- 187. H. Y. Liu, J. T. Hupp and M. J. Weaver, to be published.
- 188. J. K. Farmer and M. J. Weaver, to be published.
- 189. See for example, G. M. Torrie and J. P. Valleau, J. Phys. Chem. 86, 3251 (1982); G. M. Torri, J. P. Valleau and G. N. Patey, J. Chem. Phys. 76, 4615 (1982); D. Henderson and L. Blum, Can. J. Chem. 59, 1906 (1981).

- 190. D. Henderson and L. Blum, J. Electroanal. Chem. 132, 1 (1982).
- 191. See for example, B. W. Ninham, Pure Appl. Chem. 53, 2135 (1981).
- 192. R. W. Murray, Accts. Chem. Res., 13, 135 (1980).
- 193. A. P. Brown and F. C. Anson, Anal. Chem., 49, 1589 (1977).
- 194. R. F. Lane and A. T. Hubbard, J. Phys. Chem., <u>77</u>, 1401, 1411 (1973).
- 195. N. Oyama, T. Ohsaka, M. Kaneko, K. Sato and H. Matsuda, J. Am. Chem. Soc., 105, 6003 (1983).
- 196. A. P. Brown and F. C. Anson, J. Electroanal. Chem., <u>92</u>, 133 (1978).
- 197. M. Sharp, M. Petersson and K. Edstrom, J. Electroanal. Chem., 109, 271 (1980).
- 198. M. Sharp and M. Petersson , J. Electroanal. Chem., <u>122</u>, 409 (1981).
- 199. K. L. Guyer and M. J. Weaver, J. Phys. Chem., in press.
- 200. S. W. Barr and M. J. Weaver, J. Phys. Chem., in press.
- 201. M. J. Weaver, J. Israel Chem., <u>18</u>, 35 (1979).
- 202. R. A. Marcus, Electrochim. Acta, 13, 995 (1968).
- 203. W. L. Reynolds and R. W. Lumry, "Mechanisms of Electron Transfer", Ronald Press, New York, 1966,, p. 129.
- 204. S. W. Barr, K. L. Guyer and M. J. Weaver, J. Phys. Chem., manuscript submitted for publication.
- 205. W. H. Reinmuth, J. Electroanal. Chem., 21, 425 (1969).
- 206. H. Taube in reference 59 p. 173.
- 207. E. L. Yee, Ph.D. Dissertation, Michigan State University, 1981.
- 208. J. A. Riddick and W. B. Bunger, "Organic Solvents", Wiley, New York, 1970.
- 209. G. J. Janz and R. P. T. Tomkins, "Nonaqueous Electrolyte Handbook", Vol. I, Academic Press, New York, 1972.
- 210. J. W. Vaughan and C. F. Hawkins, J. Chem. Eng. Data, 9, 140 (1964).

- 211. J. T. Hupp and M. J. Weaver, J. Electroanal. Chem., <u>152</u>, 1 (1983).
- 212. T. T-T. Li and M. J. Weaver, manuscript in preparation.
- 213. N. Sutin and B. S. Brunschwig, ACS Symp. Ser., 198, 105 (1982).
- 214. T. T-T. Li, M. J. Weaver and C. H. Brubaker, Jr., J. Am. Chem. Soc., <u>104</u>, 2381 (1982).
- 215. J. Logan and M. D. Newton, J. Chem. Phys., <u>78</u> (Part II), 4086 (1983).
- 216. T. L. Satterberg and M. J. Weaver, J. Phys. Chem., <u>81</u>, 1772 (1977).
- 217. K. L. Guyer, T. L. Satterberg and M. J. Weaver, unpublished experimental results.
- 218. S. W. Barr, K. L. Guyer, T. T-T. Li, H. Y. Liu and M. J. Weaver in "The Chemistry and Physics of Electrocatalysis", J. D. E. McIntyre, E. Yeager and M. J. Weaver (Eds.), The Electrochemical Society, Pennington, N.J., in press.
- 219. On the basis of crystallographic data for bridging azide and thiocyanate (Wells, A. F. "Structural Inorganic Chemistry", Clarendon Press, Oxford, 4th ed., 1975, pp. 746, 648) Cr(II)-surface bond distances of 6.5 7 Å are obtained. However, the N₃-Hg and NCS -Hg bond angles are likely to be less than 180°, thereby decreasing somewhat the Cr(II) surface separation.
- 220. M. J. Weaver, J. Phys. Chem., 84, 568 (1980).
- 221. M. J. Weaver, H. Y. Liu and Y. Kim, Can. J. Chem., <u>59</u>, 1944 (1981).
- 222. M. J. Weaver and S. M. Nettles, Inorg. Chem., 19, 1641 (1980).
- 223. Γ was calculated from the nuclear tunneling factor, Γ h, for the Cr(OH₂)^{3+/2+} self-exchange reaction (6.0) given in reference 10 using contact (1) (reference 211); equals the corresponding value for the self-exchange reaction.
- 224. Equivalently, A can be determined by evaluating the so-called "real" activation enthalpy from the temperature dependence of k^{OS} measured at a fixed overpotential, and assuming that the "corr activation entropy (i.e. the activation entropy corrected for the entropic driving force ΔS^O_{rc}) equals ΔS_{int}.

- 225. The major component of ΔS is associated with the temperature dependence of n; a value of ca. -15 J deg. mol is obtained from the corresponding quantity determined for self-exchange reactions. ΔS , using the relations in reference 23, given that ΔS = 0.5ΔS int.h. (The factor 0.5 arises because only one redox center has to be activated for the electrochemical reaction, rather than two as in the homogeneous case.)
- 226. The effective value of ΔH_{i}^{*} is slightly (0.3 kcal. mol⁻¹) larger than the values given in reference 54 since these were determined by assuming that the frequency factor is slightly temperature dependent as expected from the collision model utilized in reference 54.
- 227. Evidence supporting such differences in the reactant solvation at mercury electrodes and in homogeneous solution is provided by the markedly different solvent deuterium isotope effects observed for aquo complexes in these reaction environments (references 228 and 229).
- 228. M. J. Weaver, P. D. Tyma and S. M. Nettles, J. Electroanal. Chem., 114, 53 (1980).
- 229. M. J. Weaver and T. T-T. Li, J. Phys. Chem., 87, 1153 (1983).
- 230. J. F. Endicott and J. Ramasami, J. Am. Chem. Soc., <u>104</u>, 5252 (1982).
- 231. J. M. Hale in "Reactions of Molecules at Electrodes", N. S. Hush (Ed.), Interscience, New York, 1971, Chapter 4.
- 232. J. M. Hale, J. Electroanal. Chem., 19, 315 (1968).
- 233. T. T-T. Li, H. Y. Liu and M. J. Weaver, manuscript submitted for publication.
- 234. A. Capon and R. Parsons, J. Electroanal. Chem., 46 215 (1973).
- 235. A. N. Frumkin, N. V. Fedorovich, N. P. Berezina and K. E. Kies, J. Electroanal. Chem., 58 189 (1975).
- 236. N. V. Fedorovich, A. N. Frumkin and H. E. Case, Collect. Czech. Chem. Commun., 36 722 (1971).
- 237. A. N. Frumkin, N. V. Fedorovich and S. I. Kulakovskaya, Sov. Electrochem., 10 313 (1973).
- 238. M. D. Levi, N. V. Fedorovich and B. B. Damaskin, Can. J. Chem., 59, 2019 (1981).
- 239. A. N. Frumkin, J. Electroanal. Chem., 9 173 (1965).

- 240. M. J. Weaver and F. C. Anson, J. Electroanal. Chem., <u>58</u>, 81 (1975).
- 241. M. J. Weaver and F. C. Anson, J. Electroanal. Chem., <u>97</u>, 4403 (1975).
- 242. M. J. Weaver and T. L. Satterberg, J. Phys. Chem., <u>82</u>, 1784 (1978).
- 243. R. V. James and E. L. King, Inorg. Chem., 9, 1301 (1970).
- 244. R. Lumry and S. Rajender, Biopolymers, 9, 1125 (1970).
- 245. R. A. Marcus, J. Phys. Chem., 72, 891 (1968).
- 246. R. A. Marcus and N. Sutin, Inorg. Chem., 14, 213 (1975).
- 247. The value of β is related to both the magnitude of the entropic and free energy driving forces (see reference 246). However, for reactions having small or moderate values of ΔG^0 , $\beta = 0.5 \stackrel{-}{-} 0.05$.
- 248. M. J. Weaver, Israel J. Chem., <u>18</u>, 35 (1979).
- 249. J. T. Hupp and M. J. Weaver, ACS Symp. Ser., 198, 181 (1982).
- 250. P. P. Schmidt in "Electrochemistry A Specialist Periodical Report", Vol. 5, Chemical Society, London, 1975, Chapter 2.
- 251. R. A. Marcus in "Special Topics in Electrochemistry", P. A. Rock (Ed.), Elsevier, New York, 1977.
- 252. See, for example: R. M. Noyes, J. Am. Chem. Soc., <u>84</u>, 513 (1962).
- 253. S. Sahami and M. J. Weaver, J. Electroanal. Chem., <u>122</u>, 155 (1981).
- 254. S. Sahami and M. J. Weaver, J. Electroanal. Chem., <u>122</u>, 171 (1981).
- 255. S. Sahami and M. J. Weaver, J. Sol. Chem., 10, 199 (1981).
- 256. C. M. Criss, J. Phys. Chem., <u>78</u>, 1000 (1974).
- 257. N. Sailsuta, F. C. Anson and H. B. Gray, J. Am. Chem. Soc., <u>101</u>, 455 (1979).
- 258. In reference 23 the temperature dependence of Γ is formally considered to be a constituent of ΔS int. Since n decreases with temperature, this yields a significant negative contribution to ΔS int. For the present purposes, we prefer to correct for the nuclear tunneling factor separately since this forms part of the inner-shell, rather than the solvent, contribution to ΔS int.

- 259. J. W. Cobble, J. Chem. Phys., 21, 1446 (1953).
- 260. K. J. Laidler, Can. J. Chem., 34, 1107 (1956).
- 261. E. L. King, J. Phys. Chem., 63, 1070 (1959).
- 262. J. T. Hupp and M. J. Weaver, manuscript in preparation.
- 263. P. G. Sears, R. R. Holmes and L. R. Dawson, J. Electrochem. Soc., 102, 145 (1955).
- 264. J. A. Riddick and W. B. Bunger, "Organic Solvents", Wiley-Interscience, New York, 1970.
- 265. C. P. Smith and W. S. Walls, J. Chem. Phys., 3, 557 (1935).
- 266. J. Silverman and R. W. Dodson, J. Phys. Chem., 56, 846 (1952).
- 267. K. V. Krishnamurty and A. C. Wahl, J. Am. Chem. Soc., <u>80</u>, 5921 (1958).
- 268. T. J. Meyer and H. Taube, Inorg. Chem., 7, 2369 (1968).
- 269. F. P. Dwyer and A. M. Sargeson, J. Phys. Chem., 65, 1892 (1961).
- 270. E. S. Yang, M. S. Chan and A. C. Wahl, J. Phys. Chem., <u>84</u>, 3094 (1980).
- 271. J. T. Hupp, P. A. Lay, H. Y. Liu, W. H. F. Petri, A. M. Sargeson and M. J. Weaver, J. Electroanal. Chem., in press.
- 272. Reference 45, Chapters 7 and 9.
- 273. P. Zuman, "Substituent Effects in Organic Polarography", Plenum Press, New York, 1967, p. 76.
- 274. D. R. Stranks, Disc. Faraday Soc., 29, 73 (1960).
- 275. C. M. Criss, R. P. Held and E. Luksha, J. Phys. Chem., <u>72</u>, 2970 (1968).
- 276. C. M. Criss, J. Phys. Chem., 78, 1000 (1974).
- 277. V. Gutmann, "The Donor-Acceptor Approach to Molecular Interactions," Plenum Press, New York, 1978; Electrochimica Acta, 21, 661 (19760.
- 278. G. J. Janz and R. P. T. Tomkins, "Nonaqueous Electrolyte Handbook", Vol. I, Academic Press, New York, 1972.
- 279. J. W. Vaughan and C. F. Hawkin, J. Chem. Eng. Data, 9, 140 (1964).

- 280. P. Dobos, "Electrochemical Data", Elsevier Scientific Publishing Company, Amsterdam, 1975, p. 105.
- 281. P. George, G. I. H. Hansnia and D. H. Irvine, J. Chem. Phys., <u>22</u>, 1616 (1954).
- 282. P. George, G. I. H. Hanania and D. H. Irvine, Recl. Trav. Chim. Pays-Bas, 75, 759 (1956).
- 283. P. George, G. I. H. Hanania and D. H. Irvine, J. Chem. Soc., 2448 (1959).
- 284. P. George, W. A. Eaton and M. Trachman, Federation Proc., 27, 526 (1968).
- 285. P. George., G. I. H. Hanania and W. A. Eaton in "Hemes and Hemoproteins", B. Chance, R. W. Estabrook and T. Yonetani, Eds., Academic Press, New York, 1966, p. 267.
- 286. G. I. H. Hanania and D. H. Irvine, W. A. Eaton and P. George, J. Phys. Chem., <u>71</u>, 2022 (1967).
- 287. J. Lin and W. G. Breck, Can. J. Chem., 43, 766 (1965).
- 288. N. Sutin, M. J. Weaver and E. L. Yee, Inorg. Chem., <u>19</u>, 1096 (1980).
- 289. E. L. Yee, O. A. Gansow and M. J. Weaver, J. Am. Chem. Soc., <u>102</u>, 2278 (1980).
- 290. J. T. Hupp and M. J. Weaver, Inorg. Chem., in press.
- 291. J. T. Hupp and M. J. Weaver, J. Electrochem. Soc., in press.
- 292. Y-M. Tsou and F. C. Anson, J. Electrochem. Soc., in press.
- 293. J. E. J. Schmitz and J. J. Steggerda, manuscripts submitted for publication.
- 294. K. M. Kadish, K. Das, D. Schaeper, C. L. Merill and B. R. Welch, Inorg. Chem., <u>19</u>, 2816 (1980).
- 295. K. M. Kadish and D. Schaeper, JCS Chem. Com., 1273 (1980).
- 296. H. Ogino and K. Ogino, Inorg. Chem., 22, 2208 (1983).
- 297. J. T. Hupp and M. J. Weaver, J. Phys. Chem., in press.
- 298. M. P. Youngblood and D. W. Margerum, Inorg. Chem., <u>19</u>, 2816 (1983).
- 299. J. M. Anast, A. W. Hamburg and D. W. Margerum, Inorg. Chem., <u>22</u>, 2139 (1983).

- 300. V. T. Taniguchi, B. G. Malmstrom, F. C. Anson and H. B. Gray., Proc. Natl. Acad. Sci., USA, 79, 3387 (1982).
- 301. V. T. Taniguchi, N. Salisuta-Scott, F. C. Anson and H. B. Gray, Pure and Appl. Chem., <u>52</u>, 2275 (1980).
- 302. V. T. Taniguchi, W. R. Ellis, Jr., V. Cammarata., J. Webb, F. C. Anson and H. B. Gray, Adv. Chem. Ser.
- 303. E. F. Wawrousek and J. V. Mcardle, J. Inorg. Biochem., <u>17</u>, 169 (1982).
- 304. W. Bottcher, G. M. Brown and N. Sutin, Inorg. Chem., <u>18</u>, 1447 (1979).
- 305. T. Curtis, B. P. Sullivan and T. J. Meyer, Inorg. Chem. 22, 224 (1983).
- 306. N. Sailasuta, F. C. Anson and H. B. Gray, J. Am. Chem. Soc., <u>99</u>, 2786 (1977).
- 307. L. E. Bennett, Prog. Inorg. Chem., 18, 1 (1973).
- 308. P. Siders and R. A. Marcus, J. Am. Chem. Soc. 103, 741 (1981).
- 309. See for example, R. G. Linck, in "Homogeneous Catalysis", G. N. Schrauzer, ed., Marcel Dekker, New York, 1971, Chapter 7.
- 310. M. Chou, C. Creutz and N. Sutin, J. Am. Chem. Soc. <u>99</u>, 5615 (1977).
- 311. M. J. Weaver and E. L. Yee, Inorg. Chem. 19, 1936 (1980).
- 312. M. J. Weaver, J. Phys. Chem. 84, 568 (1980).
- 313. P. D. Tyma and M. J. Weaver, J. Electroanal. Chem. <u>111</u>, 195 (1980).
- 314. M. J. Weaver, J. Electroanal. Chem. 93, 231 (1978).
- 315. J. Lipkowski, A. Czerwinski, E. Cieszynska, Z. Galus and J. Sobkowski, J. Electroanal. Chem. 119, 261 (1981).
- 316. (a) For example, see D. H. Angell and T. Dickinson, J. Electroanal. Chem. 35, 55 (1972). (b) D. C. Johnson and E. W. Resnick, Anal. Chem. 49, 1918; J. Weber, Z. Samec, V. Marecek, J. Electroanal. Chem. 87, 271 (1978).
- 317. R. C. Young, F. R. Keene and T. J. Meyer, J. Am. Chem. Soc. <u>99</u>, 2468 (1977).

- 318. Under these conditions it is likely that any residual work terms will affect each value of kh to an essentially equal extent. In addition, the predominant reaction channel for cross reactions having similarly small driving forces will involve transition—state structures that closely resemble those for the parent self-exchange reactions (reference 249).
- 319. The estimate of k^h, 60 M⁻¹ sec⁻¹, for Ru^{3+/2+} given in reference 304 refers to an ionic strength of 1 M, and is therefore uncorrected for work terms. Application of this correction yields k^h 200 M sec⁻¹. (reference 311)
- 320. J. F. Endicott, B. Durham and K. Kumar, Inorg. Chem. <u>21</u>, 2437 (1982).
- 321. G. M. Brown, H. J. Krentzien, M. Abe and H. Taube, Inorg. Chem. 18, 3374 (1979).
- 322. Admittedly, the self-exchange rates for $0s(bpy)_3^{3+/2+}$ and $Cr(bpy)_3^{3+/2+}$ may differ somewhat. However, if anything the former reaction should have faster self-exchange kinetics as a result of greater delocalization of the transferred electron, which would yield an even smaller value of k from Equation 6.6.
- 323. Although a frequency factor formulation based on the simple gasphase collision model has conventionally been employed to estimate A_h and A_e (reference 13), the use of an "encounter preequilibrium" model where activation is considered to occur chiefly via unimolecular activation within a statistical distribution of encounter complexes appears to be physically more appropriate for both homogeneous (references 10,18,28) and electrochemical (reference 186) electron-transfer processes.
- 324. Since it is likely that the outer-sphere transition state for electrochemical reactions is separated from the electrode by a layer of water molecules (reference 312), R_e is estimated to be twice the sum of the reactant radius (3.5 % and the effective diameter of a water molecule (3 %).
- 325. J. Strouse, S. W. Layten and C. E. Strouse, J. Am. Chem. Soc., 99, 562 (1978).
- 326. N. J. Hair and J. K. Beattie, Inorg. Chem. <u>16</u>, 245 (1977); J. K. Beattie, S. P. Best, B. W. Skelton and A. H. White, J. Chem. Soc. Dalton, 2105 (1981).
- 327. J. A. Jafri, J. Logan and M. D. Newton, Israel J. Chem. 19, 340 (1980).

- 328. T. D. Hand, M. R. Hyde and A. G. Sykes, Inorg. Chem. 14, 1720 (1975).
- 329. J. N. Braddock and T. J. Meyer, J. Am. Chem. Soc. <u>95</u>, 3158 (1973).
- 330. J. F. Endicott, C.-L. Wong, J. M. Ciskowski and K. P. Balakrishman, J. Am. Chem. Soc. <u>102</u>, 2100 (1980).
- 331. Footnote 54, reference 320.
- 332. It was asserted (reference 330) that the Co³⁺ Fe²⁺ reaction follows an outer-sphere pathway on the basis of the age ment with the rates of other cross reactions involving Co³⁺ and outer-sphere reductants using Equation 6.1 and utilizing the measured value of k¹. However, using the present estimate of k¹ for outer-sphere Fe self exchange instead yields a Co³⁺ Fe reaction rate ca. 10 -fold larger than predicted from Equation 6.1, indicative of a water-bridged pathway for this reaction as well.
- 333. For example, see S. Trassati, J. Electroanal. Chem. 123, 121 (1981).
- 334. B. M. Gordon, L. L. Williams and N. Sutin, J. Am. Chem. Soc., <u>83</u>, 2061 (1961).
- 335. M. H. Ford-Smith and N. Sutin, J. Am. Chem. Soc., <u>83</u>, 1830 (1961).
- 336. N. Sutin and B. M. Gordon , J. Am. Chem. Soc., <u>83</u>, 70 (1961).
- 337. T. J. Przystas and N. Sutin, J. Am. Chem. Soc., 95, 5545 (1973).
- 338. Y. Ohsawa, T. Sajiand and S. Aoyagi, J. Electroanal. Chem., <u>106</u>, 327 (1980).
- 339. C. T. Lin, W. Bottcher, M. Chou., C. Creutz and N. Sutin, J. Am. Chem. Soc., 98, 6536 (1976).
- 340. N. Sutin, Acc. Chem. Res. 1, 225 (1968).
- 341. R. Parsons, Croat, Chim. Acta 42, 281 (1970).
- 342. N. Sutin and B. Brunschwig, ACS Symp. Ser., 198, 106 (1982).
- 343. T. W. Newton, J. Chem. Educ. <u>45</u>, 571 (1968).

- 344. In the Appendix to reference Equation 6.20 was claimed to be generally applicable in the "weak overlap" limit when ΔG_{-1} and ΔG_{-2} exhibit a quadratic dependence upon (E-E¹) as predicted by the harmonic oscillator model. In fact, the proof given is not entirely correct inasmuch as the energy minimization condition [$[(\Delta G_{-1}^{-1} + \Delta G_{-2}^{-2})/\partial \beta = 0]$ employed in reference 182 leads to Equation 6.21, Equation 6.22 only being obtained as a special case when the slopes of the ΔG_{-1}^{-1} E and ΔG_{-2}^{-1} E plots are equal and of opposite sign at the intersection point.
- 345. J. F. Endicott, R. R. Schroeder, D. H. Chidester and D. R. Ferrier, J. Phys. Chem. 77, 2579 (1973).
- 346. T. Saji, T. Yamada and S. Aoyagui, J. Electroanal. Chem. <u>61</u>, 147 (1975); T. Saji and Y. Mariyama, S. Aoyagui, ibid, <u>86</u>, 219 (1978).
- 347. M. J. Weaver and F. C. Anson, J. Phys. Chem. 80, 1861 (1976).
- 348. M. J. Weaver, Inorg. Chem., 15, 1733 (1976).
- 349. See reference 313 for references to earlier work.
- 350. V. Balzani, F. Scandola, G. Orlandi, N. Sabbatini and M. T. Indelli, J. Am. Chem. Soc. 103, 3370 (1981).
- 351. J. F. Endicott, B. Durham, M. D. Glick, T. J. Anderson, J. M. Kuszaj, W. G. Schmonsees and K. P. Balakishnan, J. Am. Chem. Soc. 103, 1431 (1981).
- 352. J. F. Endicott, B. Durham and K. Kumar, Inorg. Chem. in press.
- 353. (a) S. S. Isied and H. Taube, J. Am. Chem. Soc., 95, 8198 (1973); (b) H. Fischer, G. M. Tom and H. Taube, <u>ibid.</u>, 98, 5512 (1976); (c) K. Rieder and H. Taube, <u>ibid.</u>, 99, 789 (1977). (d) S. K. S. Zawacky and H. Taube, ibid., 103, 3379 (1981).
- 354. (a) J.-J. Juro, P. L. Gaus and A. Haim, J. Am. Chem. Soc., <u>101</u>, 6189 (1979); (b) A. P. Szecsy, and A. Haim, <u>ibid.</u>, <u>103</u>, 1679 (1981); (c) A. P. Szecsy and A. Haim, <u>104</u>, 3063 (1982).
- 355. For reviews, see: (a) A. Haim, Acc. Chem. Res., 8, 264 (1975);
 (b) H. Taube, Adv. Chem. Ser., 162, 217 (1977);
 (c) T. J. Meyer, ACS Symp. Ser., 198, 137 (1982).
- 356. R. A. Marcus and N. Sutin, Inorg. Chem., 14, 213 (1975).

- 357. The nonzero, albeit small, values of Sint that are obtained using the dielectric continuum model arise from the prediction that the polarization entropy will depend on the square of the ionic charge Z. Since Sint = 0 when the transition-state entropy is exactly midway between that for the reactants and products, any such nonlinearity between the entropy and Z will yield Sint = 0. However, the entropy difference between reactants and products is commonly found to be substantially larger than predicted from the Born model, yielding more positive values of Sint. For the systems considered here, we estimate that this contributes ca. 12-16 J deg mol to Sint, although partly compensated by the influence of nuclear tunneling (reference 5), yielding ΔSint = 4-9 J deg-1 mol-1.
- 358. The values of $\Delta S_{\text{exp}}^{*}$ were extracted from literature experimental data using the proper bimolecular frequency factor K_{pv_n} , where K_{pv_n} is the precursor equilibrium constant, rather than the unimolecular frequency factor kT/h. (Note that the compilation given in reference 311 contains values of $\Delta S_{\text{exp}}^{*}$ that are ca. 10 e.u. less negative resulting from the use of a collisional, rather than a preequilibrium, model for the frequency factor).
- 359. J. L. Cramer and T. J. Meyer, Inorg. Chem., 13, 1250 (1974).
- 360. R. G. Gaunder and H. Taube, Inorg. Chem., 9, 2627 (1970).
- 361. J. K. Beattie, R. A. Binstead, and M. Broccardo, Inorg. Chem. <u>17</u>, 1822 (1978).
- 362. J. V. Beitz, J. R. Miller, H. Cohen, K. Wieghardt and D. Meyerstein, Inorg. Chem., 19, 966 (1980).
- 363. J. E. Schmitz, P. J. Koonen, J. G. M. van der Linden, and J. J. Steggarda, Extended Abstracts, Electrochemical Society meeting, Washington, D. C., October 1983; J. J. Steggarda, personal communication.
- 364. An attempt to evaluate ΔS^O for Ru(III)/(II) in the binuclear complex H₂0 Ru(NH₃)₄(bpy) Co(NH₃)₅ was thwarted by minor distortions in the cyclic voltammograms, most likely caused by small amounts of the mononuclear ruthenium complex as an impurity.
- 365. S. S. Isied, ACS Symp. Ser., 198, 221 (1982).
- 366. For reviews of experimental work see: R. D. Cannon in "Inorganic Reaction Mechanisms-Specialist Periodical Reports", Vol. 7, Royal Society of Chemistry, 1981, Chapter 1 and chapters in previous volumes.
- 367. R. A. Marcus, J. Chem. Phys., 24, 966 (1956).
- 368. H. C. Stynes and J. A. Ibers, Inorg. Chem., 10, 2304 (1971).

- 369. J. K. Beattie and C. J. Moore, Inorg. Chem., 21, 1292 (1982).
- 370. A. Wheeler, C. Brouty, P. Spinat and P. Herpin, Acta Crystallogr. Sect. B., 31, 2069 (1975).
- 371. D. J. Szalda, C. Creutz, D. Mahajan and N. Sutin, Inorg. Chem., <u>22</u>, 2372 (1983).
- 372. In a number of recent publications (e.g. reference 9) K_A^O is underestimated by a factor of two, evidently because the coefficient describing the distance dependence of the electronic-coupling matrix element H_{AB} has been mistakenly identified with a related factor describing the variation of k_{e1} with distance.
- 373. E. L. Yee, J. T. Hupp, and M. J. Weaver, Inorg. Chem., in press.
- 374. R. D. Cannon, Chem. Phys. Lett., 49, 299 (1977).
- 375. Solvent reorganization models are reviewed in: E. D. German and A. M. Kuznetsov, Electrochim. Acta, 26, 1595 (1981).
- 376. (a) A. Zalkin, D. H. Templeton and T. Ukei, Inorg. Chem., <u>12</u>, 1641 (1973); (b) J. Baker, L. M. Englehardt, B. N. Figgis and A. H. White, J. Chem. Soc., Dalton Trans., 2105 (1981).
- 377. T. Holstein in reference 59, p. 129.
- 378. T. Holstein and H. Scher, Philos. Mag. B, 44, 343 (1981).
- 379. A. Ekstrom, A. B. McLaren and L. E. Smythe, Inorg. Chem., <u>15</u>, 2853 (1976).
- 380. A. Ekstrom, A. B. McLaren and L. E. Smythe, Inorg. Chem., <u>14</u>, 2899 (1975).
- 381. M. J. Burkhart and T. W. Newton, J. Phys. Chem., 73, 1741 (1969).
- 382. Bruce Bockris and S. U. M. Khan, "Quantum Electrochemistry", Plenum Press, New York, 1979.
- 383. S. U. M. Khan and J. O'M. Bockris, J. Phys. Chem., <u>87</u>, 2599 (1983).
- 384. J. F. Endicott, B. Durham and K. Kumar, Inorg. Chem., <u>21</u>, 2437 (1982).
- 385. E. Buhks, M. Bixon, J. Jortner and G. Navon, Inorg. Chem., <u>18</u>, 2014 (1979).
- 386. C. Creutz, M. Chou, T. L. Netzel, M. Okumura and N. Sutin, J. Am. Chem. Soc., <u>102</u>, 1309 (1980).
- 387. C.-T. Lin, W. Bottcher, G. M. Brown, C. Creutz and N. Sutin, J. Am. Chem. Soc., <u>98</u>, 6536 (1976).

- 388. C. Creutz, Inorg. Chem., 17, 1056 (1978).
- 389. R. X. Ewall and L. E. Bennett, J. Am. Chem. Soc., 96, 940 (1974).
- 390. J. V. McArdle, H. B. Gray, C. Creutz and N. Sutin, J. Am. Chem. Soc., 96, 5737 (1974).
- 391. F. P. Dwyer, N. A. Gibson and E. C. Gyarfas, J. Proc. R. Soc., N. S. W., 84, 80 (1950).
- 392. D. N. Huchital, N. Sutin and B. Warnquist, Inorg. Chem., $\underline{6}$, 838 (1967).
- 393. A. A. Schilt, "Analytical Applications of 1,10-Phenanthroline and Related Compounds," Pergamon Press, New York, 1969, p. 120.
- 394. F. P. Dwyer and E. C. Gyarfas, J. Am. Chem. Soc., <u>76</u>, 6320 (1954).
- 395. P. J. Smoelnars, J. K. Beattie and N. D. Hutchinson, Inorg. Chem., 20, 2202 (1981).
- 396. K. Nakamoto, "Infrared and Raman Spectra of Inorganic and Coordination Compounds," 3rd ed., Wiley-Interscience, New York, 1978.
- 397. K. H. Schmidt and A. Muller, Inorg. Chem., 14, 2183 (1975).
- 398. A. A. Noyes and T. J. Deahl, J. Am. Chem. Soc., 59, 1337 (1937).
- 399. H. S. Habib and J. P. Hunt, J. Am. Chem. Soc., 88, 1668 (1966).
- 400. L. E. Bennett and J. L. Shepherd, J. Phys. Chem., <u>66</u>, 1275 (1962).
- 401. M. R. Hyde, R. Davies and A. G. Sykes, J. Chem. Soc., Dalton Trans., 1838 (1972).
- 402. G. Dulz and N. Sutin, J. Am. Chem. Soc., 86, 829 (1964).
- 403. J. F. Endicott and H. Taube, J. Am. Chem. Soc., 86, 1686 (1964).
- 404. K. Ohashi, T. Amano and K. Yamamoto, Inorg. Chem., 16, 3364 (1977).
- 405. C. A. Jacks and L. E. Bennett, Inorg. Chem., 13, 2035 (1974).
- 406. R. J. Campion, N. Purdie and N. Sutin, Inorg. Chem., 3, 1091 (1964).
- 407. R. Davies, M. Green and A. G. Sykes, J. Chem.Soc., Dalton Trans., 1171 (1972).
- 408. R. Berkoff, K. Krist and H. D. Gafney, Inorg. Chem., 19, 1 (1980).
- 409. H. M. Neumann, quoted in R. Farina and R. G. Wilkens, Inorg Chem., <u>7</u>, 514 (1968).

410. T. Gennett and M. J. Weaver, Anal. Chem., in press.

3.3A	Differential capacitance versus electrode potential for	
	electropolished polycrystalline silver (RF 1.2) in NaClO4-	
	NaCl mixtures at ionic strength 0.5. Keys to chloride	
	concentrations: 1, 0 mm; 2, 1 mm; 3, 2.5 mm; 4, 6 mm;	
	5, 15 m <u>M</u> ; 7, 100 m <u>M</u> ; 8, 200 m <u>M</u>	58
3.3B	As in Figure 3.3A, but for electrochemically roughened	
	silver (RF 1.9)	59
3.4	Surface concentration of specifically adsorbed chloride	
	(per cm ² real area) at electropolished (solid curves) and	
	roughened silver (dashed curves) versus electrode potential	
	for bulk chloride concentrations of 0.015 \underline{M} and 0.10 \underline{M} ,	
	analyzed from Figures 3A and B as outlined in text	60
3.5A	Differential capacitance vesus electrode potential for	
	electropolished polycrystalline silver in NaClO4-NaBr mix-	
	tures of ionic strength 0.5. Key to bromide concentration	
	(solid curves): 1, 0 mM; 2, 0.6 mM; 3, 2 mM; 4, 5 mM;	
	5, 15 mm; 6, 40 mm; 7, 100 mm. The dashed curve is the	
	cell resistance for 100 mM bromide plotted on the same	
	potential scale	61
3.5B	As in Figure 3.5A, but for roughened silver (RF=1.9)	62
3.5C	As in Figure 3.5A, but for roughened silver (RF=4.2)	63

3.6A	Surface concentration of specifically adsorbed bromide (per
	cm ² real area) at electropolished (solid curve) and rough-
	ened silver (dashed, dotted-dashed curves) for bulk concen-
	tration x at 15 mm obtained from Figures 3.5A and B 64
3.6B	As in Figure 3.6A but for x=100 mM
3.7A	Differential capacitance versus electrode potential for
	electropolished silver in NaClO ₄ -NaI mixtures of ionic
	strength 0.5. Key to iodide concentrations: 1,0 mm; 2,
	0.2 mM; 3, 0.5 mM; 4, 1.2 mM; 5, 2.2 mM; 6, 5 mM; 7, 10 mM. 70
3.7B	As in Figure 3.7A but for roughened silver (RF 4.6) 71
3.8A	Differential capacitance versus electrode potential for
	electropolished silver in NaClO4-NaNCS mixtures of ionic
	strength 0.5. Key to thiocyanate concentrations: 1, 0 mm;
	2, 0.3 m <u>M;</u> 3, 1 m <u>M;</u> 4, 3 m <u>M;</u> 5, 10 m <u>M;</u> 6, 30 m <u>M;</u> 7, 100 m <u>M</u> . 72
3.8B	As in Figure 3.8A but for roughened silver (RF=2.1) 73
3.9	Differential capacitance versus electrode potential for
	roughened silver in KC1-KSCN mixtures of ionic strength
	0.1. Key to thiocyanate concentrations: 1, 0 mM; 2, 5 mM;
	3, 10 mM; 4, 23 mM; 5, 50 mM

3.10A	Differential capacitance versus electrode potential for
	electropolished silver in NaClO4-NaN3 mixtures of ionic
	strength 0.5. Key to azide concentrations: 1, 0 mm; 2,
	1 m <u>M;</u> 3, 3 m <u>M;</u> 4, 10 m <u>M;</u> 5, 30 m <u>M;</u> 6, 100 m <u>M</u>
3.10B	As in Figure 3.10A, but for roughened silver (RF=2.3) 78
3.11	Surface concentration of specifically adsorbed azide
	(per cm ² real area) at electropolished (solid curves) and
	roughened silver (dashed curves) versus electrode potential
	for bulk azide concentrations of 0.01 M and 0.1 M analyzed
	from Figures 3.10A, 3.10B as outlined in the text 79
3.12	Atomic positions of the (100), (110), and (111) faces in
	the fcc structure (after Hamelin, et al., reference 1) 85
3.13	Fractional coverage, θ , of chloride anions (solid curve)
	and normalized Raman peak intensity (dashed curve) for
	Ag-Cl stretching mode, both plotted against electrode
	potential. Electrolyte is 0.4 M NaClO ₄ + 0.1 M NaCl. Raman
	data from reference 102 89
3.14	Fractional coverage, θ , of bromide anions (solid curve) and
	normalized Raman peak intensity (dashed curve) for Ag-Br

stretching m	ode, both	plotted	against	electr	ode po	tenti	al.	
Electrolyte	is 0.45 <u>M</u>	NaC104	+ 0.05 <u>M</u>	NaBr.	Raman	data	from	
reference 10)2							90

- 3.17 Linear sweep current-potential curves for anodic removal of lead layer deposited on silver. Sweep rate was 5 mV sec⁻¹, electrode rotated at 600 r.p.m. Electrolyte was 0.5 M/2 NaClO₄ adjusted to pH 3.5 with HClO₄, containing 0.6 μM/2 Pb²⁺. Lead deposits corresponding to anodic stripping curves (a)-(c) formed as follows: (a) Electrode rotated at

600 r.p.m., held at -0.585 V for 10 mins. (b) As (a), but	•
held at -1.20 V for additional 20 mins. with no rotation.	(c)
Electrode rotated at 600 r.p.m., held at -0.65 v for 10	
minutes 101	101

- Differential electrode capacitance C versus electrode

 potential E for a monolayer of UPD lead on polycrystalline

 silver (curves a-d) and for polycrystalline bulk lead

 (curves a'-d') as a function of ionic strength of sodium

 perchlorate, adjusted to pH 3.5. Concentrations of NaClO₄:

 (a,a') 0.5 M; (b) 0.1 M; (c) 0.05 M; (d,d') 0.01 M......105
- 3.20 Differential electrode capacitance C versus electrode potential E for UPD lead layer on polycrystalline silver having various coverages of lead. Electrolyte was 0.5 M

	NaClO ₄ , pH 3.5, with 0.6 م <u>M</u> Pb ²⁺ . Lead coverages
	(percentage of monolayer): (a) 0%; (b) 22%; (c) 35%;
	(d) 61%; (e) 93%; (f) 100%107
3.21	Differential capacitance vs. electrode potential for UPD
	lead/silver in NaCl + NaF mixed electrolytes at an ionic
	strength of 0.5 M. Key to chloride concentrations: (O)
	0 m <u>M;</u> (♠) 8 m <u>M;</u> (♥) 20 m <u>M;</u> (♠) 60 m <u>M;</u> (■) 200 m <u>M</u>
3.22	Differential capacitance vs. electrode potential for UPD
	lead/silver in NaBr + NaF mixed electrolytes at an ionic
	strength of 0.5 M. Key to bromide concentrations: (O)
	0 m <u>M;</u> (♠) 3 m <u>M;</u> (▲) 10 m <u>M;</u> (♥) 30 m <u>M</u>
3.23	Differential capacitance vs. electrode potential for UPD
	lead/silver in NaI + NaF mixed electrolytes at an ionic
	strength of 0.5 M. Key to iodide concentrations: () 0 mM;
	(O) 0.3 \underline{m} ; (∇) 1 \underline{m} ; (Δ) 3 \underline{m} ; (Δ) 10 \underline{m} ; (\Box) 30 \underline{m} ;
	(■) 100 m <u>M</u>
3.24	Surface concentration of chloride vs. electrode potential
	for UPD lead/silver. Conditions as in Figure 3.21116
3.25	Surface concentration of bromide vs. electrode potential
	for HPD lead/silver. Conditions as in Figure 3.22117

3.26	Surface concentration of iodide vs. electrode potential for
	UPD lead/silver. Solid line: NaI + NaF. Dashed line:
	NaI + NaClO ₄ . Concentrations as in Figure 3.23118
3.27	Surface concentration of chloride vs. electrode charge
	density for UPD lead/silver. Conditions as in Figure
	3.21119
3.28	Surface concentration of bromide vs. electrode charge
	density for UPD lead/silver. Conditions as in Figure
	3.22 122
3.29	Surface concentration of iodide vs. electrode charge
	density for UPD lead/silver. Conditions as in Figure
	3.26121
3.30	Differential capacitance vs. electrode potential for UPD
	lead/silver in NaBr + NaClO mixed electrolytes at an
	ionic strength of 0.5 M. Key to bromide concentrations:
	(O) 0 mM, (●) 1 mM, (◆) 3 mM, (▲) 10 mM, (▼) 30 mM, (□) 100
	m <u>M</u> 120
3.31	Surface concentration of thiocyanate vs. electrode potential
	for UPD lead/silver in NaNCS + NaF mixed electrolytes at an
	ionic strength of 0.5 M. Key to thiocyanate concentrations:
	(\triangle) 1 mM, (\blacksquare) 3 mM, (\bigcirc) 10 mM, (\blacksquare) 30 mM, (\square) 100 mM124

- 3.34 Surface concentration of thiocyanate vs. electrode charge density for UPD lead/silver. Conditions as in Figure 3.31..127
- 3.35 Surface concentration of azide vs. electrode charge density for UPD lead/silver. Conditions as in Figure 3.32...........128
- 3.36 Surface concentration of perchlorate vs. electrode charge density for UPD lead/silver. Conditions as in Figure 3.33..129
- 3.37 Linear sweep current-potential curves for anodic of thallium layer deposited on silver. Sweep rate was 20 mV/s. Electrolyte was 0.5 $\underline{\text{M}}$ NaF, containing 0.8 $\mu\underline{\text{M}}$ TlClO_{$\underline{\Lambda}$}. Curve (a):

	600 RPM; (b) electrode held at -960 mV for 12 minutes at
	600 RPM and then held for 15 minutes at -1300 mV without
	rotation137
3.38	Differential capacitance versus electrode potential for: (a)
	a monolayer of underpotentially deposited thallium on poly-
	crystalline silver in 0.05 \underline{M} NaClO ₄ ; (b) the equivalent of
	circa. 3 monolayers of thallium on polycrystalline silver in
	0.05 M NaClO ₄ ; (c) as in (a), except in 0.2 M NaClO ₄ 139
3.39	Differential capacitance vs. electrode potential for UPD
	thallium/silver in NaCl+NaF mixed electrolytes at an ionic
	strength of 0.5 M. Key to chloride concentrations:
	(●) 0 mM; (○) 1 mM; (▲) 10 mM; (▽) 50 mM (■) 100 mM; (◇) 200
	<u>m</u> 141
3.40	Differential capacitance vs. electrode potential for UPD
	thallium/silver in NaBr + NaF mixed electrolytes at an ionic
	strength of 0.5 M. Key to bromide concentrations: () 0 mM;
	(■) 20 m <u>M;</u> (▲) 50 m <u>M;</u> (▼) 100 m <u>M;</u> (♦) 200 m <u>M</u> 142
3.41	Differential capacitance vs. electrode potential for UPD
	thallium/silver in NaI + NaF mixed electrolytes at an ionic
	strength of 0.5 \underline{M} . Key to iodide concentrations: (\triangle) 0 \underline{M} ;
	(●) 1 m <u>M</u> ; (○) 5 m <u>M</u> ; (■) 10 m <u>M</u> ; (□) 20 m <u>M</u> (◆) 50 m <u>M</u> 143

electrode held at -960 mV for 12 minutes while rotating at

3.42	Surface concentration of chloride vs. electrode potential for
	UPD thallium/silver. Conditions as in Figure 3.38144
3.43	Surface concentration of bromide vs. electrode potential for
	UPD thallium/silver. Conditions as in Figure 3.39145
3.44	Surface concentration of iodide vs. electrode potential for
	UPD thallium/silver. Conditions as in Figure 3.40146
3.45	Surface concentration of chloride vs. electrode charge density
	for UPD thallium/silver. Conditions as in Figure 3.38147
3.46	Surface concentration of bromide vs. electrode charge density
	for UPD thallium/silver. Conditions as in Figure 3.39148
3.47	Surface concentration of iodide vs. electrode charge density
	for UPD thallium/silver. Conditions as in Figure 3.40149
3.48	Surface concentration of perchlorate vs. electrode potential
	for UPD thallium/silver in NaClO ₄ + NaF mixed electrolytes at
	an ionic strength of 0.5 M. Key to perchlorate concentra-
	tions: (O) 10 m <u>M;</u> (△) 60 m <u>M;</u> (□) 200 m <u>M</u>
3.49	Surface concentration of thiocyanate vs. electrode potential
	for UPD thallium/silver in NaNCS + NaF mixed electrolytes at
	an ionic strength of 0.5 \underline{M} . Key to thiocyanate concentra-
	tions: (O) 1 mM, (■) 5 mM, (△) 20 mM, (●) 50 mM, (□) 100 mM151